Cyclodextrin Assisted Self-Assembly of Stimuli-Sensitive Block Copolymers in Aqueous Media

by

Fanny Yuen

A thesis

presented to the University of Waterloo

in fulfillment of the

thesis requirement for the degree of

Master of Applied Science

in

Chemical Engineering

Waterloo, Ontario, Canada, 2010

©Fanny Yuen 2010

AUTHOR'S DECLARATION

I hereby declare that I am the sole author of this thesis. This is a true copy of the thesis, including any required final revisions, as accepted by my examiners.

I understand that my thesis may be made electronically available to the public.

Abstract

Structures with well-defined architectures and tailored physical properties can be produced by supramolecular self-assembly of stimuli-sensitive polymeric inclusion complexes consisting of cyclodextrins. Recently, there has been significant interest in the use of double hydrophilic block copolymers to design novel supramolecular nanostructures as these polymers micellize under external stimuli, such as temperature, pH, and complexation. Cyclodextrins (CDs) have the ability to spontaneously complex with water-soluble guest molecules. The complexation of the polymer with CD induces self-assembly of the polymers.

In this research, two systems were studied, a PEO-b-PNIPAM/α-CD system and a PPO-b-PMAA/β-CD system. First, the block copolymers were synthesized by ATRP to achieve well-defined monodisperse polymers. The chemical composition of the polymer was determined by NMR and gel permeation chromatography. Then, the microstructure and aggregation behaviour in aqueous solutions were studied using a combination of static and dynamic light scattering, and isothermal titration and differential scanning calorimetric techniques.

The PEO-b-PNIPAM/α-CD system

Below the lower critical solution temperature (LCST) of PNIPAM, PEO-b-PNIPAM was highly soluble. Above the LCST, the thermo-sensitive PNIPAM block precipitated, and the copolymer self-assembled into micelles with a PNIPAM core and a hydrophilic PEO shell. As α-CD was titrated to the polymer, the CDs threaded onto the PEO segments and induced micellization, forming rod-shaped nanostructures comprising of a PEO/α-CD condensed phase and a PNIPAM shell. Increasing the temperature of the system above the LCST caused the PNIPAM segments to collapse, resulting the de-threading of the CD.

The PPO-b-PMAA/β-CD system

At high pH, the PPO-b-PMAA was highly soluble. As acid was titrated into the sample, the MAA segments became protonated, and aggregation occurred due to hydrogen bonding with the PPO segments. At low pH, the addition of β-CD was shown to aid in polymer dissolution. At high pH, α-CD did not thread onto the polymer due to a smaller cavity size, but as β-CD was titrated to the polymer, the CDs threaded onto the PPO segments and induced micellization, producing vesicle nanostructures comprising of a PPO/β-CD condensed phase and a PMAA shell. Increasing the temperature of the PPO-b-PMAA/β-CD system above the LCST of PPO showed no change to the system's morphology.

Acknowledgements

It is my pleasure to thank all of the people who helped make this thesis possible.

Foremost, I would like to express my sincerest gratitude to my thesis supervisor, Professor Tam Kam Chiu for his guidance throughout my work. Our discussions were extremely insightful, and when I had difficulty, he was always able to offer helpful suggestions.

I would also like to extend my gratitude to those who offered me advice and technical support. I would like to acknowledge Dr. Palaniswamy Ravi for his synthesis advice, Dr. Neil McManus and Dr. Firmin Moingeon for their guidance in GPC analysis, Jannet Venne for sharing her NMR expertise, and Salim Kouri and my lab mates for always offering their help. I would like to mention Albert Lam and Kate Brockman who helped me conduct some preliminary experiments. In addition, I would like to thank Mrs. Carrie Baumken at the Writing Center for her efforts to teach me to be a better technical writer.

On this occasion, I wish to thank my family, friends, and sorority sisters for their support in my life as a graduate student. Special thanks to Ben Turnbull for encouraging me to reach my full potential.

Lastly, I would also like to thank the following organizations for their financial support, the University of Waterloo, the Ontario Government, the Waterloo Institute of Nanotechnology, and NSERC.

Table of Contents

List of Figures

List of Tables

Chapter 1

Introduction

1.1 Overview

Supramolecular self-assembly of stimuli-sensitive cyclodextrin (CD) polymeric inclusion complexes are capable of forming a multitude of sophisticated superstructures. Systems of these novel complexes can have applications in areas such as drug delivery, sensors, separations, and membranes. Polyethylene oxide-poly(*N*-isopropylacrylamide) (PEO-b-PNIPAM) and polypropylene oxide-poly(methacrylic acid) (PPO-b-PMAA) are double hydrophilic block copolymers that exist as free chains in aqueous solutions at room temperature. However, PNIPAM and PPO are temperature sensitive, PMAA is pH sensitive, and PEO and PPO may be encapsulated by α-CD and β-CD, respectively. When these properties are activated, either separately or together, the hydrophilic/hydrophobic balance of the systems is altered and can cause the polymer chains to self-assemble. The investigation of the morphological changes of these self-assembled nanostructures over temperature, pH and complexation is the focus of this thesis.

1.2 Research Objectives

In studying PEO-b-PNIPAM and PPO-b-PMAA polymer systems, there were two main objectives. The first was to characterize the self-assembly behavior of the two polymer systems with respect to temperature and pH in aqueous solutions. By performing quantitative studies on the systems' morphological transitions with changes in temperature and/or pH, the mechanism of self-assembly could be elucidated. The second was to investigate the effects of complexation of the block copolymer with CD and its impact on the self-assembly. Molecular-level understanding of the CD binding and of complex formation can be achieved through quantitative monitoring of the systems

while CD is added. Studies on the morphological transitions of polymers induced by changes in temperature in the presence and absence of CD can be compared. A description of the mechanisms of the stimuli-responsiveness and self-assembly of the block copolymer can be useful for future studies in the area of stimuli-responsive polymer inclusion complexes.

Experimental techniques used in these studies include Surface Tensiometry, Isothermal Titration Calorimetry (ITC), Laser Light Scattering (LLS), and Differential Scanning Calorimetry (DSC). Surface Tensiometry provides information on the critical micelle concentration (CMC). ITC can be used to measure the thermodynamic parameters, such as binding constant (K), enthalpy (ΔH), entropy (ΔS), heat capacity (C_p), and reaction stoichiometry (n). LLS is a technique used to determine the hydrodynamic radius (R_h) and radius of gyration (R_g), where the conformational and morphology of the nanostructure can be elucidated. The DSC can be used to measure additional thermodynamic parameters of the samples, such as enthalpy (ΔH), heat capacity (C_p), and transition temperature (T_m) of the system when subjected to a thermal scan.

1.3 Outline of Thesis

The work presented herein describes the synthesis and behaviour of two stimuli-sensitive polymer inclusion complex systems: PEO-b-PNIPAM/α-CD and PPO-b-PMAA/β-CD. Chapter 2 provides an overview of the current literature in the field of stimuli-sensitive polymer inclusion complexes. Information regarding the common experimental techniques used in self-assembly characterizations is reviewed in Chapter 2. Chapter 3 provides an in depth discussion on the theory and equipment used in the characterization of the two inclusion complex systems selected. Chapter 4 examines the synthesis and characterization of the PEO-b-PNIPAM/α-CD system. The synthesis procedure of the PEO-b-PNIPAM black copolymer and the various physical characterization techniques are described.

Chapter 4 also presents a detailed mechanism on the self-assembly of the system and the impact of temperature and CD on its morphology. Chapter 5 discusses the organization of the PPO-b-PMAA system with changes in temperature and pH. Information regarding the PPO-b-PMAA system and the PPO-b-PMAA/β-CD system is compared. Finally Chapter 6 concludes the report and recommends future studies.

Chapter 2

Literature Review

2.1 Introduction

Stimuli-responsive polymers have been used for numerous applications, such as biomaterials[1], drug delivery systems[2-6], and chemical separations[7]. These polymers allow external stimuli to alter their conformation and solubility and modify the hydrophobic/hydrophilic balance of the system. Supramolecular self-assemblies have the ability to produce well-defined architectures with tailored physical properties[8-10]. Self-assemblies consist of reversible non-covalent interactions and, thus, are considered dynamic processes[11]. Multi-component self-assemblies have attracted significant interest in the scientific community as these interactions may be controlled by external stimuli. Dynamic self-assembly may be induced by either changing the external environment or by transforming the physical characteristics of one or more building blocks. Strategies adopted include changes in pH, temperature and electro-potential, or induced mechanical motion. Inclusion complexation with various types of cyclodextrins (CDs) can induce self-assembly of polymer/CD complexes and result in the formation of systems with different morphologies[12] and physical properties[13]. By complexing stimuli-responsive polymers with CD, a wide variety of polymer/CD complexes with amphiphilic properties may be produced. In this review, the effect of pH, temperature, light, and redox potential on the self-organization behaviour of various polymer/CD complexes will be discussed.

2.2 Amphiphilic Polymers

Amphiphilic block copolymers spontaneously self-assemble into ordered structures (such as micelles, spheres, vesicles or rods) in polar solvents at concentrations exceeding the critical micelle

concentration (CMC). The hydrophobic segments associate to form a hydrophobic inner core, while the hydrophilic segments shield the core from the solvent by forming the corona.

PEO is a water soluble and biocompatible polymer with numerous applications in personal homecare, pharmaceuticals and industrial products. Due to its widespread applications, there has been significant interest in studying the solution properties of PEO, and the development of PEO derivatives. Amphiphilic characteristics have been imparted to PEO polymers by the grafting of hydrophobic blocks. The grafting of hydrophobic blocks to polyethylene oxide (PEO or PEG) has been widely studied and applied to a variety of potential applications in biomedical and specialty chemicals sectors. Poly(ethylene oxide)-block-polystyrene (PEO-b-PS) is one of the most widely studied amphiphilic polymeric systems[14, 15]. The CMC is very low because PS is extremely hydrophobic[16]. In dilute solutions, regular core-shell micelles coexist with polymeric clusters. Yu and Eisenberg[17, 18] tailored the block compositions and preparation methods to achieve a variety of morphologies. Due to the hydrophobicity and high glass transition temperature (T_g) of the PS core, the system was unsuitable for use in drug delivery as a more permeable and lower T_g core is required. For use in drug delivery systems, Dai et al.[19] combined poly(ethyl acrylate) (PEA) with PEO to form a polymer with more moderate hydrophobic characteristics, lower T_g, and more dynamic and permeable cores.

Phase transition of polymers may be induced by external stimuli, such as temperature[1, 6], pH[20], light[21], electric field [22], and solvent composition[23]. Alexandridis and Hatton[24] studied Pluronic triblock copolymers composed of alternating blocks of PEO and poly(propylene oxide) (PPO/PPG) that were used as polymeric surfactants. At concentrations exceeding the CMC, micelles composed of a hydrophobic PPO core and a hydrophilic PEO corona formed in aqueous solution. At very high

concentrations, a thermo-responsive hydrogel was produced. By varying the composition of ethylene oxide and propylene oxide blocks, the solution and phase behaviours could be manipulated.

Poly(N-isopropylacrylamide) (PNIPAM) is a thermo-responsive polymer that exhibits a coil-globule transition in aqueous solution at its lower critical solution temperature (LCST) of approximately 32^{o}C[25-28]. Below the LCST, PNIPAM is soluble in water. Above the LCST, PNIPAM undergoes a reversible phase transition from a swollen hydrated state to a shrunken dehydrated state, losing approximately 90 % of its volume. PNIPAM has been used in a variety of applications[29] related to temperature-dependent controlled release systems[30-34], surface modifications[5, 35-40], and microfluidics[41]. Amphiphilic properties can be acquired by adding a hydrophobic end-functional group. Bontempo et al.[42] used controlled radical polymerization with a biotinylated initiator to synthesize a mono-dispersed PNIPAM that possessed a biotin end-group. The polymer was then complexed with streptavidin to generate a thermo-sensitive polymer-protein conjugate. Unlike many temperature sensitive polymers, such as poly(N-(3-ethoxypropyl) acrylamide[43], that exhibit LCST, poly(N,N-dimethyl-N-(3'sulfopropyl)-3-methacrylotlaminopropanaminium salt)[44] exhibited an upper critical solution temperature behaviour (UCST).

Various polymeric hydrogels have been found to be responsive to a variety of external factors[22, 26, 45-47]. Thermal-sensitive microporous hydrogels were synthesized by cross-linking PNIPAM, and, with increasing temperature, the hydrogels rapidly shrank due to changes in the affinity of the polymer chains with the aqueous medium[48]. In addition, various types of hydrogels composed of PNIPAM graft chains showed fast and reversible phase transitions in response to changes in temperature[26, 49, 50]. There have been many studies on the use of polymers in controlled drug delivery. Smart hydrogels that exhibit large volume changes with external stimuli can be used to control the diffusion and

permeation of drugs, making them superior drug carriers[51-61]. Intelligent hydrogel systems have found many applications in medicine[62], biotechnology[63], and environmental systems[64].

Recently, there has been significant interest from the scientific research community in using double hydrophilic block copolymers to design novel supramolecular nanostructures because the polymer blocks, under normal conditions are both soluble in aqueous solutions. However, these copolymers will self-assemble into various types of nanostructures when subjected to external stimuli, such as pH and temperature. Below the LCST, PEO-b-PNIPAM is highly soluble. Above the LCST, the thermo-sensitive PNIPAM block phase separates, and the copolymer self-assembles into micelles comprising of a PNIPAM core and a hydrophilic PEO shell. Qin et al.[65] discussed the use of PEO-b-PNIPAM self-assembled structures as drug delivery vehicles since the polymer was biocompatible. PEO-b-PNIPAM was found to be amphiphilic in water at body temperature (37 ^{o}C) and formed vesicles. However, if the temperature is decreased, the vesicles disassembled and released its encapsulants.

2.3 Cyclodextrin

Cyclodextrins (CDs) are a family of cyclic oligosaccharides comprised of α-1,4-linked glucopyranose subunits. The three most common naturally occurring CDs, α-, β-, and γ-CD, consist of 6, 7, and 8 glucose units, respectively, and are produced by enzymatic conversion of starch. These CDs are rigid and possess shallow truncated cone shaped structures with hydrophilic exteriors and comparably more hydrophobic cavities. The diameters of α-, β-, and γ-CD are 4.5 Å, 7.0 Å, and 8.5 Å, respectively, and each have the height of ca. 7.8 Å[66]. The cavity of the torus-shaped CD allows it to spontaneously complex with a variety of guest molecules to form inclusion complexes (ICs)[67, 68]. The driving forces of IC formation between the CD cavity and the guest molecule include geometric compatibility, Van der Waals forces and hydrophobic interactions[69, 70]. To stabilize the IC, hydrogen

bonding may occur between the CD and the guest molecule and between the hydroxyl groups on the rims of neighbouring CDs[71, 72]. The formation of these ICs greatly modifies the physical and chemical properties of the guest molecules. Due to their highly polar exteriors and less polar interiors, CDs are best known for their ability to increase the solubility of low polarity guest molecules in water as the encapsulated compound is shielded from the aqueous solvent. CDs are used to encapsulate hydrophobic drugs in drug delivery systems, to enhance the scrubbing efficiency of low polarity volatile organic compounds, and to mask toxic substances by converting them into non-toxic ICs[73]. The recommended wastewater treatment for tributylphosphate (TBH) in nuclear reprocessing plants is the complexation of TBH with β-CD[73].

Research on ICs extends to a wide range of applications in organic and polymer synthesis[74-77], catalysis[78], pharmaceuticals[79-84], biotechnology[85], supramolecular chemistry[86, 87], chromatography[88], and environmental mediation[89]. A natural antibacterial agent, allylisothiocyanate, was encapsulated in α- and β-CD to be slowly released in cheese packaging films for the control of mold[90, 91]. As a solid phase extraction adsorbent, β-CD was used to extract brilliant blue (a common food colourant) from samples[92]. CD was also used in the separation of enantiomers through capillary zone electrophoresis[93-98]. Beads of epichlorohydrin-crosslinked β-CD polymers were used in a column to trap polycyclic aromatic hydrocarbon contaminants in water for use in municipal waste water mediation[89], and CD was used to encapsulate glutathione drugs for oral administration[99] . Phenolphthalein-modified CDs were used as colour changing molecular sensors/indicators, where in alkaline solution, the β-CD complexed with phenolphthalein, and the sample changed from colourless to purple[100].

2.4 Polymer Inclusion Complex

Polymer inclusion complexes (PICs) are a result of non-covalent host-guest interactions between CDs and polymers. These PICs are useful building blocks for constructing supramolecular structures. Due to their interesting properties and varied applications, topics such as inclusion complexes of CDs with linear polymers[67, 101, 102], random and block copolymers[103-107], and selective polymers[108-112] have captured the interest of scientists.

Harada and Kamchi[113] were the first to report the complexation of CD with water-soluble polymers. In their study of α-CD and PEO, they determined that hydrogen bonding was the main factor for the inclusion complex formation. Through molecular models, they showed that PEO chains were able to penetrate the α-CD cavities while bulkier polymers were not able to. Huang et al.[114] confirmed these results using a double hydrophilic block copolymer, PEO-b-PDMA. They found that multiple α-CDs threaded onto the PEO chains to form pesudopolyrotaxanes which then aggregated into novel supramolecular nanostructures. Such aggregation was the driving force for the block copolymer assembly into micellar-like particles comprising of an α-CD/PEO core and a PDMA shell. The samples were freeze dried and characterized using X-ray diffraction to investigate the microstructure of the aggregates. The α-CD/PEO complex showed characteristic peaks at 19.7^{o} of 2θ, which reveals the existence of packed columns and the existence of "channel-type" microcrystalline structures. 1D nuclear overhauser effect (NOE) was used to determine the proximity of EO proton and α-CD proton pairs. This information was used to confirm threading of the PEO chain into the CD cavity. Dynamic light scattering (DLS) measurements showed a large hydrodynamic radius that confirmed the existence of supramolecular aggregates. Finally, transmission electron microscopy (TEM) images showed spherical particles which correspond to micellar particles.

The Harada group also found that tubular polymeric structures may be formed by threading α-CDs[102, 108, 115] onto a PEG chain and capping the ends with organic groups. Rotaxanes were also used in the synthesis of capillary electrochromatography beads[116] and nanoscale devices, such as molecular shuttles, switches, and information storage systems[117].

The self-assembled threading of CD onto linear polymer chains depends on electrostatic, hydrophobic and hydrogen bonding interactions. The thermodynamics of these threading interactions showed negative ΔH and ΔS. Threading yield was found to be statistically dependent on polymer and CD concentrations[116].

Supramolecular structures ranging from aggregates to reversible networks could be formed simply by mixing amphiphilic polymers with CD in water[118-120]. CD forms PICs with hydrophobic moieties; the hydrophobic tails of polymeric chains are encapsulated within the CD cavity to reduce hydrophobic interactions[121, 122]. The intensity of these hydrophobic interactions can be tuned by adding different amounts of CD[122, 123-131]. Using dynamic light scattering, it was found that, when β-CD derivatives were added to hydrophobically-modified hydroxyethyl-cellulose, the hydrophobic interactions could be modulated[129].

Li et al. conducted extensive studies on polypseudorotaxanes of PEG and CD. They observed that stable hydrogels were produced at high concentrations of high molecular-weight PEGs[66, 103, 105, 132]. It was reported that copolymers consisting of a dextran (Dex) backbone and PPG/PEG linear side chains improved the stability of PICs with CD[133, 134]. Harada's group synthesized nanotubes based on the assembly and cross-linking of CD polyrotaxanes on PEO chains[135]. Okmura and Ito[136] reported the formation of a 3D gel structure consisting of α-CD and PEG polyrotaxanes that comprised of

covalently cross-linked CD rings. CDs with pendant groups have also been shown to form self-inclusion complexes[137, 138].

Tu et al.[139] synthesized a well-defined PEO-b-PNIPAM block copolymer using ATRP. α-CD was added for selective threading of PEO block to transform the system from a random coil to a rod/coil-like structure. They used a variety of spectroscopic methods to characterize the supramolecular structures of the self-assembled complexes in solid state. The α-CD threaded only onto the PEO segments to form a column-like structure. In the solid state, the ICs self-assembled into hexagonally packed plates, and the uncomplexed PEO and PNIPAM chains formed a brush conformation. The system phase separated into alternating long-range-ordered lamellar and amorphous phases.

The formation of supramolecular structures consisting of amphiphilic polymers in water has found applications ranging from drug delivery to associative thickeners. In drug delivery, these systems combine the polymer's aggregation properties with drug affinity. The drug may be loaded via polymeric chain absorption to the hydrophobic segment, and the hydrophilic block aids in the biological interactions[140]. IC systems form superior associative thickeners as their complementary components are of low viscosity, and aggregation only occurs when the separate components are mixed together[141].

Liu et al.[12] used α-CD as "artificial chaperones" to facilitate the self-assembly of a double hydrophilic block copolymer, poly(ethylene oxide)-*b*-poly(4-vinylpyridine) (PEO-*b*-P4VP), in the synthesis of polymeric vesicles. At a pH of 4, the polymer was first complexed with α-CD and allowed to self-assemble into meta-stable micelles. The P4VP corona was then ionically cross-linked with poly(ethylene oxide)-*b*-poly(acrylic acid) (PEO-*b*-PAA). Through dialysis, the α-CD was removed from the system to produce vesicles, and, when no α-CD was used, the system formed cross-

linked micelles. A schematic comparison of the two processes is shown in Figure 2.1. To characterize their nanostructures, they employed a variety of techniques. 2D NOE was used to confirm the formation of the PEO/α-CD complexes. The solution was freeze dried and dissolved in DMSO-d_6. The NOESY spectra showed correlation peaks between the protons on the inside of the α-CD cavity and protons of the EO units. DLS measurements were used to determine the number averaged diameter of the PEO-b-P4VP/α-CD solutions. The large diameter sizes confirmed the formation of micelles. TEM images also showed well-defined spherical morphologies. From nuclear magnetic resonance (NMR), it was also shown that the intensity ratios of PEO to P4VP decreased significantly with the addition of CD. This result is due to a decrease in PEO chain mobility resulting from the less soluble pseudorotanes.

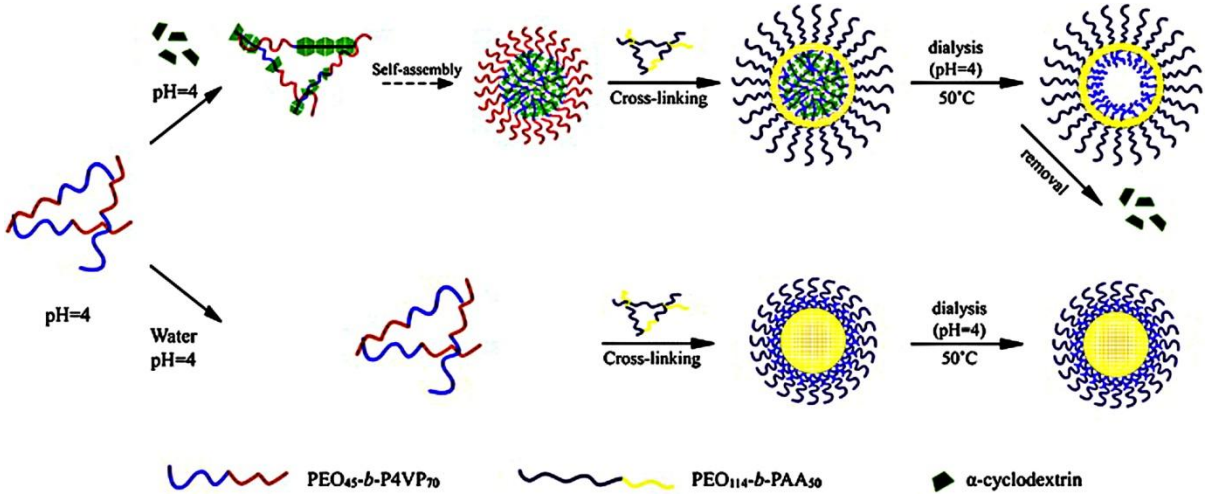

Figure 2.1: Schematic comparison of self-assembly processes for a PEO-b-P4VP and PEO-b-PAA system with and without the use of α-CD as molecular chaperones. (ref. 12)

2.5 pH-Responsive Inclusion Complexes

Stimuli-responsive polymers have the ability to modulate interactions between the CD cavity and its guest, and they play a key role in controlling the assembly and disassembly processes[142]. Becuwe et al. introduced pyridine-4-yl indolizin β-CD as a pH-dependent molecular switch. At neutral pH values, the molecule displayed a stable self-included conformation of the aromatic groups and the hydrophobic cavity. In acidic pH conditions, the pyridyl group became protonated, causing a conformational change in the structure[143]. For pH-responsive polymeric systems, CD is often complexed with a polyelectrolyte. For example, Wenz et al.[67, 102, 144] prepared a variety of polypseudorotaxanes consisting of α-CD and a polycation guest, such as poly(iminooligomethylene), in acidic pH conditions. They found that the inclusion process was largely dependent on the degree of protonation of amino groups along the polymer chain.

Variations of pH-responsive system, such as polyethyleneimine (PEI) polymer IC systems, have been studied. It was found that the complexation ratios, at high pH values, of PEI units to α-CD were 2:1 and 4:1 for γ-CD. Single linear PEI chains threaded onto α-CD, while two linear PEI chains threaded onto γ-CD in the parallel and antiparallel directions. At lower pH values (<8), the secondary amine on the PEI chains became protonated, and the ionization of these groups led to dethreading. The cationic nature of PEI chains did not favour the complexation of CD onto the polymer chains[142]. PEG-b-PEI, PEG-b-PEI-b-PEG, PEI-b-PEG-b-PEI, PEG-b-PEI-g-dex, and dex-g-(PEG-b-PEI) copolymers were found to complex with CD at both high and low pH values. However, comparing

the complexation ratios, it could be seen that at high pH values, α-CD threaded onto both PEG and PEI blocks, but, at lower pH values, CD only threaded onto the neutral PEG block. At high pH values, it was evident that the viscoelastic properties of the system increased, and at low pH values, the viscosity of the system decreased. Again, the key to threading and dethreading is directly related to the ionization of the secondary amines[145-148]. A schematic is shown in Figure 2.2. 2-sulfonato-6-napthyl competing pendant groups were also investigated and were found to have little effect on the encapsulation[148]. Furthermore, Karaky et al.[149] investigated pH-switchable supramolecular sliding gels composed of α-CD and PEI-b-PEG-b-PEI. At basic pH, the CD rings were homogeneously distributed along the polymer chains and at acidic pH, the EI units of the microgel deprotonated leading to an increase in swelling. Due to the unfavourable electrostatic interactions, the α-CD molecules moved from the PEI block to the central PEG block.

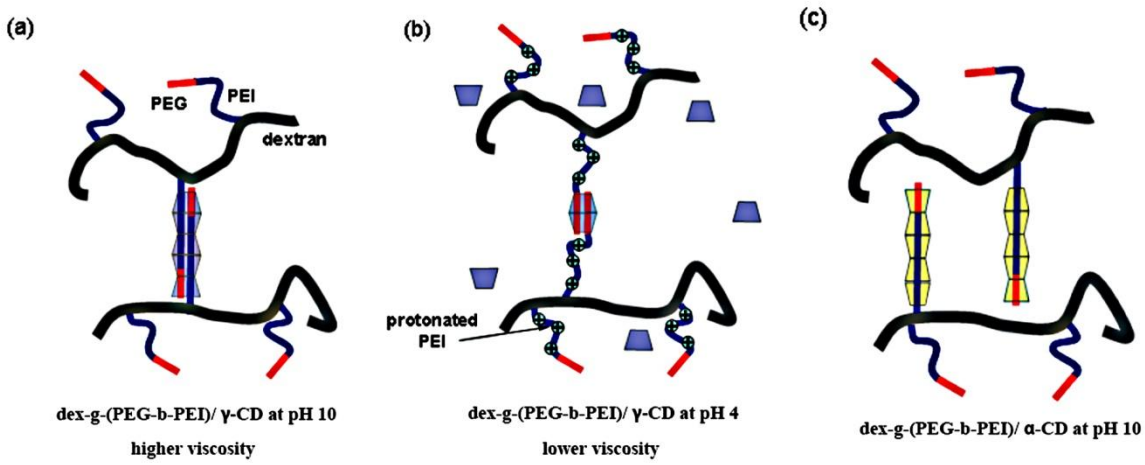

Figure 2.2: Supramolecular networks of dex-g-(PEG-b-PEI)/CD at different conditions. (a) PEG and PEI complexation with γ-CD in parallel and anti-parallel directions at pH 10. (b) PEI segments are protonated at pH 4 and γ-CD only complexes with the PEG block. (c) PEG and PEI complexation with α-CD at pH 10. (ref 145)

In a microgel comprising of β-CD, epichlorohydrin (EPI), and poly(vinyl alcohol) (PVA), the association constant of the methyl orange (MO) guest molecule was found to be thirteen times greater at pH 7.4 than at 1.4. At low pH values, the protonation of MO molecules produced ammonium and azonium tautomers that greatly weakened the hydrophobic interactions between MO and β-CD. Due to the low complexation at low pH values, it was found that MO readily diffused out of the microgel, resulting in a higher release rate[150]. An illustration of the pH dependence of the microgel is shown in Figure 2.3.

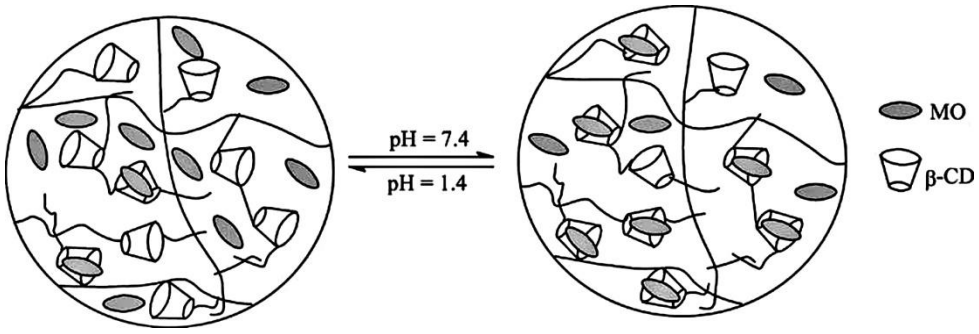

Figure 2.3: pH-dependent complexation in a EPI-PVA-CD microgel system. (ref. 150)

A variety of polymer-CD systems have been synthesized and they have been shown to exhibit self-threading or associative properties[118, 151-153]. In a poly[(methyl vinyl ether)-alt-(maleic acid)]-g- β-CD (P(MVE-AM)-g- β-CD) and PEO-Adamantyl (Ad_3) system, strong inter-chain associations due to the complexation between PEO-Ad_3 and CDs were reported. At low pH values, where all COOH groups were protonated, additional hydrogen bonding between the PEO backbone of PEO-Ad_3 and the COOH groups of P(MVE-AM)-g-β-CD contributed to the associative properties[154]. Studies on associative thickeners have shown that, by introducing charged groups onto hydrophobically-modified copolymers, the solubility of the system could be enhanced, and pH-responsive characteristics could be introduced[161-163]. These synthetic polyelectrolytes exhibited less associative

behaviour and microdomain organization than non-ionic systems[164]. The conformation of the polymers depended on the degree of ionization of the polymeric chains. At low pH values, compact polymer coils were formed, and at high pH values, the repulsion of ionized groups produced extended structures. Moine et al.[141] reported the use of β-CD polymers in thickening applications, and by mixing aqueous solutions of poly(β-malic acid-co- β-ethyladamantyl malate) (PMLA-Ad) and a β-CD polymer, the viscosity of the solution changed with pH. As a result of the COOH groups on the polyester backbone, the degree of ionization could be modified by changing pH. Due to the lipophilicity of the hydrophobic moieties (i.e. adamantine groups), there was a high degree of complexation between the guest and the apolar cavities of β-CD. At pH values of 2.1-2.5, most of the carboxylic acid groups were protonated, causing the polymer to exhibit a compact conformation with hydrophobic microdomains. Hence, the mobility and accessibility of the adamantyl groups decreased and the probability of complexation was lowered. The lowered association was found to be independent of polymer concentration. At pH values greater than 5, the COOH groups dissociated, allowing the copolyester to swell. The swelling increased the connectivity of the system, and induced better accessibility for the adamantine groups, and the formation of the complex increased the viscosity of the system.

α-CD was found to produce pseudo-rotaxanes with poly(ε-lysine) (PL) in aqueous solutions at high pH values. At pH values ranging from 8.5 to 11.5, stable crystalline precipitates, comprising of deprotonated PL and α-CD, were obtained[156]. At low pH values, the PL amino side groups protonated and led to decomplexation[157]. CD-PL polymers were also studied for pH dependence[158]. It was found that 6-(p-toluidino)-2-naphthalenesulfonate (TNS) complexed with α-CDs and β-CDs at ratios of 1:1 and 2:1, respectively. At neutral pH values, the attractive interactions between cationic groups of PL

and the included TNS within the CD cavity of another chain were dominant. At alkaline conditions, only repulsive interactions existed due to the deprotonation of the amino DL groups, causing a decrease in intermolecular aggregation.

Pyrene labeled poly(acrylic acid) (PAAMePy) was found to complex with γ-CD at a 2:1 ratio of pyrene to γ-CD. At a pH of 3, the PAA polymer existed in a compact conformation, and free pyrenes formed ICs with γ-CD due to the hydrophobic interactions. When pyrene was encapsulated by γ-CD, the pyrene units were capable of arranging in parallel and anti-parallel stacking patterns. At a pH of 8, the COOH groups of PAA became deprotonated, the repulsive interactions between the PAA polymers decreased the proximity of pyrene units, and dimer formation was not observed[159].

Liu et al.[155] studied a double hydrophilic block copolymer of poly(ethylene oxide)-b-poly(acrylic acid) (PEO-b-PAA). At basic pH values, the PAA groups were ionized. As α-CD was added, encapsulation of the PEO blocks occurred. The ICs then induced self-assembly into spherical nanostructures. The radii of these structures were found to be much larger than a single stretched polymer chain, and the ratio of R_g/R_h was closed to unity, suggesting that the stable nanostructures were vesicles. At low pH, the PAA groups protonated, and the polymer/CD complexes aggregated to produce a turbid solution. A schematic of the PEO-b-PAA/CD self-assembly is shown in Figure 2.4, and a summary of polymer pH-responsive CD systems is documented in Table 2-1.

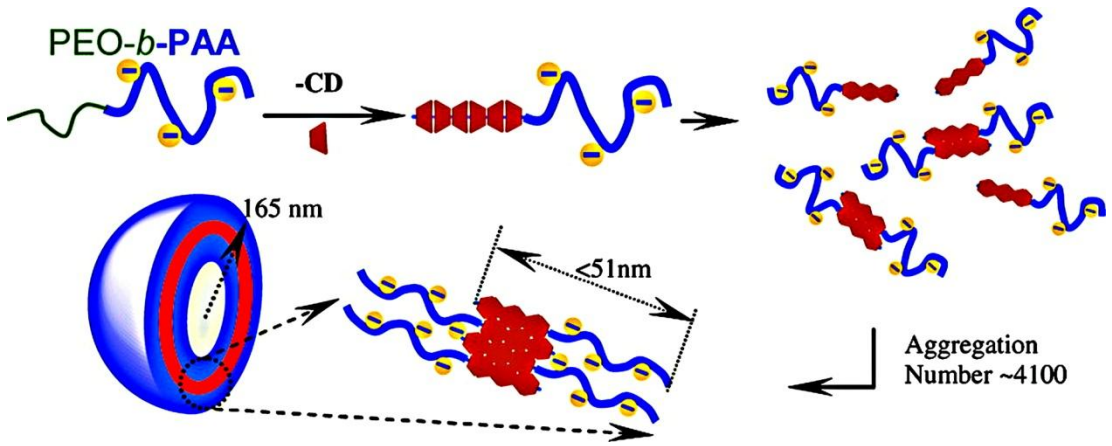

Figure 2.4: Vesicle self-assembly of PEO-b-PAA induced by the complexation with α-CD. (ref. 155)

Table 2-1: pH-Responsive Cyclodextrin Systems

CD Type	Encapsulant	Polymer	Results	Noted Applications	Reference
α-CD	PEO	PEO-PAA	High pH: PAA ionizes, vesicle formation Low pH: PAA protonation, aggregation		155
α-CD	PL	PL	High pH: Pseudorotaxane formation Low pH: Protonation of PL amino side groups, decomplexation		156, 157
α-CD/ β-CD	TNS	PL	Neutral pH: Cationic PL amino group, stabilized complexes High pH: PL amino groups deprotonation, no aggregation	Drug delivery, targeting, emobilization, sensors, bioseparations	158
α-CD/ β-CD	Py	PAAMePy	Low pH: Compact formation, IC forces dominate High pH: Repulsive interactions between COO-, decrease in complexation		159
β-CD	PEO-AD3	PEO-AD3	Neutral pH: COOH group as polyacid Low pH: COOH has neutral properties, Complexation		154
β-CD	Adamantyl	PMLA-Ad	Low pH: COOH protonation, hydrophobic microdomains, low complexation Higher pH: COOH dissociation, polymer swelling, accessibility increase, complexation, polymer aggregation, high viscosity	Thickener	141
β-CD	MO	β-CD cross-linked between EPI and PVA	Neutral pH: Complexation Low pH: Protonation of MO, decomplexation	Controlled delivery systems	150
β-CD	Heavy Metals	Cross-linked β-CD Polymer	Retention of heavy metal increased with pH increase Due to acidic dissociation of pyrometallic group CD stronger than OH^-	Environmental, Pharmaceutical	160
γ-CD/ α-CD	PEI	PEI	High pH: CD binds to PEI Low pH: Protonation of PEI, decomplexation	Drug delivery, tissue engineering, artificial gene delivery carrier	142, 147, 149
γ-CD/ α-CD	PEI/PEG	PEG-b-PEI	High pH: CD binds to both PEI and PEG Low pH: Protonation of PEI, threading only on PEG		145, 146, 148

2.6 Temperature-Responsive Inclusion Complexes

Temperature-dependent complexations with CDs have been extensively studied[101, 165-167] due to their ability to produce supramolecular structures of desired architectures [58-61, 168-171]. In general, the rate of complexation of polymer with CD increased significantly with increasing temperatures. The rheological effects of the temperature-dependent complexations were also studied.

Temperature-responsive ICs of PNIPAM have been extensively studied due to the polymer's rapid and dramatic phase transition at its LCST. PNIPAM chains have been found to influence the

association of CD with guest molecules due to steric hinderance[168, 169, 172]. With 8-anilino-1-napthalene sulfonic acid ammonium salt (ANS) or 2-anilino-6-napthalene sulfonic acid (2.6-ANS) as a guest, the PNIPAM-β-CD polymeric system showed correlations between complexation and phase transition. It was found that the complexation between CD and ANS induced phase transition of the PNIPAM chains, and the phase transition of the NIPAM chains impacted CD/ANS complex formation. An illustration of this correlation is shown in Figure 2.5. When complexation between CD and ANS occurred, a hydrophobic environment was produced, resulting in the reduction of the LCST. Due to the decrease in LCST, the polymer chain shrank and became insoluble. The steric hindrance due to shrinkage and crowding of the polymer chains destabilized the CD/ANS complex, resulting in a reduction in complex formation. When ANS was decomplexed from CD, the LCST of PNIPAM was increased due to the hydrophilic environment. The hydrophilic environment caused the polymer to swell, and the polymer resolublized. When the polymer swelled, there was an increase in CD/ANS complexation due to a decrease in steric hindrance around the CD/ANS complex[168, 170, 173]. The molecular-recognition-induced phase transition of poly(N-isopropylacrylamide-co-glycidyl methacrylate) (P(NIPAM-co-GMA)) and mono-6-deoxy-6-ethylene diamino- β-CD (ECD) or mono-6-deoxy-6-hexane diamino-β-CD (HCD) systems were investigated. It was found that the LCST of the system with the ANS guest was lower than the LCST of the polymer in water. As more ANS was encapsulated, the LCST decreased. The hydrophobic phenyl groups of the ANS were found outside the CD cavity after encapsulation, which induced a sudden phase transition with increasing temperature. In systems using NS (2-napthalenesulfonic acid) as the guest molecule, the opposite LCST effects were observed. The complexation between CD and NS enlarged the hydrophilic moiety of the polymers[174].

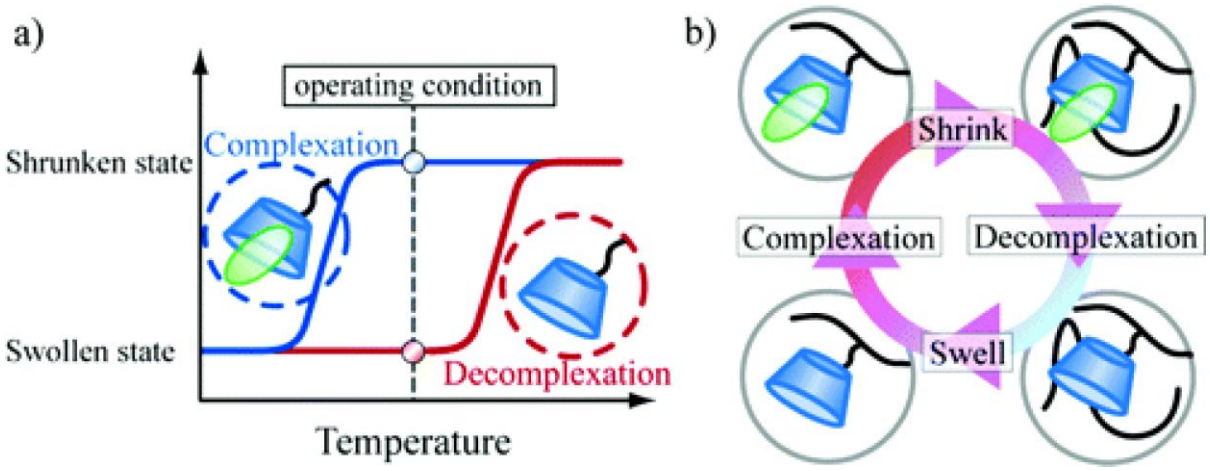

Figure 2.5: Schematic of poly(NIPAM-co-CD)/ANS system detailing the correlations between complexation and swelling. (ref. 173)

Duan et al.[175] used ATRP to synthesize a PNIPAM polymer with an insoluble pyrene end group. At low temperatures, the solution was clear due to the formation of micelles. At high temperatures, the solution became turbid as the PNIPAM chains collapsed and agglomerated due to the increased hydrophobicity. β-CD is known to form ICs with pyrene. It was found that β-CD with pyrene functional groups disturbed the formation of PNIPAM aggregates, resulting in an increase in the system's LCST. Duan et al. also found that for polymers of the same molecular weight, the LCST of the py-PNIPAM functionalized polymer was much lower than the LCST of the PNIPAM homopolymer, showing that the hydrophobic pyrene group affected the polymer's liquid phase transition. In addition, they also investigated the polymer's LCST with respect to molecular weight. The LCST of PNIPAM decreased with increasing molecular weight. However, the LCST of py-PNIPAM increased with increasing MW, where the impact of pyrene end group was reduced for the longer PNIPAM chain. Pluronics systems comprising of PEO-b-PPO-b-PEO and heptakis (2,6-di-O-methyl)-β-CD (hβ-CD) were investigated over a temperature range of 5-70 °C. At low temperatures,

the Pluronics dispersed as unimers, and at ambient temperatures, the increased hydrophobicity caused the PPO segments to aggregate, forming spherical micelles. The aggregation number was found to increase with increasing temperature. hβ-CD formed pseudo-polyrotaxanes with the polymers in their unimeric or micellar form by preferentially threading onto the PPO segment of the polymer backbone. This threading improved the water solubility of the block and disrupted aggregate formation. However, at temperatures above 50 °C, the solubility decreased, the aggregation became irreversible, and large scale aggregation of the system occurred[176].

Poly(N-isopropylacrylamide-co-2-hydroxyethylacrylate) (PNIPAM-PHEAc-β-CD) colloidal crystals exhibited a variety of brilliant colours as the content of β-CD was varied. These crystals could be reversibly transformed from invisible to visible materials with changes in temperature. Since the system possessed a LCST above body temperature, was biocompatible, and exhibited good water stability and solubility, it was evaluated as a possible drug delivery carrier. Using 5-florouacil (5-FU), a model anti-tumour cancer drug, the time release behaviour of the system was investigated[180].

A temperature responsive poly(N-isopropylacrylamide-co- glycidylmethacrylate/cyclodextrin)-grafted-polyethylene terephthalate (P(NIPAM-co-GMA/ β-CD)-g-PET) membrane showed an increase in contact angle from 65 to 76.9^0 when the temperature was increased from 25 to 45 ^{0}C. In contrast, the substrate membrane's contact angles decreased with increasing temperature. The guest, ANS, was found to adsorb at 25 °C and desorbed at 40 °C due to the swollen-shrunken configurational variations and changes in the ability of β-CD to recognize ANS[177].

Most thermal-responsive hydrogels exhibit a negative volume transition as the temperature is increased. A pseudo-interpenetrating network was formed by interpenetrating water-soluble epichlorohydrin- β-CD (EP-β-CD) into a PNIPAM hydrogel. This system showed a lower LCST due

to the fact that the EP-β-CD chains interpenetrated into the PNIPAM network and did not directly link to a PNIPAM backbone. The release of the ibuprofen (IBU) guest was prolonged due to the inclusion complex between CD and the drug[178]. Polymeric systems possessing UCST properties are less common than those exhibiting a LCST. However, in some applications, it may be necessary to utilise polymers that possess a UCST. An interpenetrating polymer network of poly(acrylic acid)-graft-β-CD (PAAc-g-β-CD) and polyacrylamide (PAAM) was shown to exhibit a UCST of approximately 35 °C. The IBU drug guest was found to diffuse at a faster rate at 37 °C than at 25 °C[179].

Pseudorotaxanes comprising of poly[(methoxy diethylene glycol methacrylate)-g-PEG] (PDMPaM) with hexasodium calyx[6]arenehexasulfonic acid (SCX_6), DM-β-CD, and α-CD were reported. It was observed that the encapsulation by SCX_6, DM-β-CD, and α-CD caused a large increase, a slight increase, and a decrease in the LCST, respectively. The size of the sulphate groups of SCX_6 increased the hydrophilicity of the polymer, and the bulky nature of SCX_6 obstructed the coil-globule transition. DM-β-CD slightly increased the hydrophilicity of the polymer due to its high solubility (388g/dL). The lower solubility of α-CD (14.5g/dL) decreased the hydrophilicity, and neighbouring α-CD formed hydrogen bonds[44] . Table 2-2 summarizes the polymer temperature-responsive CD systems discussed in this section.

Table 2-2: Temperature-Responsive Cyclodextrin Systems

CD Type	Encapsulant	Polymer	Results	Noted Applications	Reference
α-CD/ β-CD	PEG	PDMPaM	SCX_6: LCST increase β-CD: Slight LCST increase α-CD: LCST decrease		44
β-CD	py	py-PNIPAM	CD/py IC disturbs PNIPAM aggregation LCST increase with CD addition		175
β-CD	ANS	PNIPAM-β-CD	Complexation and phase transition properties are interrelated CD/ANS ICs LCST decrease Below LCST: CD/ANS complexation Above LCST: Decomplexation		170, 173
β-CD	ANS	β-CD-EDA-PNIPAM	LCST at 35 ^{o}C Temperature increase disrupts IC		168
β-CD	ANS/ NS	PNG/ ECD/HCD	Molecular-recognition-induced phase transition LCST decrease with ANS LCST increase with NS	Molecular separations	174
β-CD	ANS	P(NIPAM-co-GMA/β-CD)-g-PET	Increase of contact angle with increase in temperature 25 ^{o}C: Adsorption 40 ^{o}C: Desorption Due to swollen-shrunken configuration	Membrane	177
β-CD	IBU	PNIPAM hydrogels with β-CD	Lowered LCST Prolonged release of drug	Drug Delivery	178
β-CD	IBU	PAAc-g-β-CD	UCST at 35 ^{o}C Faster release of IBU at higher temperatures	Drug Delivery	179
β-CD	5-Fu	P(NIPAM-HEAc)	Colour colloidal crystals Visible/invisible due to temperature	Drug Delivery	180

2.7 Photo-responsive Inclusion Complexes

Photo-induced mechanical motion is a popular strategy to control supramolecular self-assemblies through external stimuli[181]. It requires two photoisomers that absorb different wavelengths of light and exhibit different properties. Some benefits of using photoisomerization include no waste, no addition of chemicals, low cost, fast response, high sensitivity, and reversibility and repeatability. Photo-responsive polymers have found useful application in photo-functional systems, photonics, and photo-switchable materials.

Azobenzene (Azo) and azo derivatives, such as stilbene and 4,4’-azodibenzoic acid (ADA), are popular compounds used in photoisomerization systems. The molecule’s trans state is the most stable

due to a better configuration and more electron delocalization. Therefore, in dark or visible light, the molecule exists mainly in the trans state. However, with the irradiation of ultraviolet (UV) light, the azobenzene molecule will isomerize to the cis state. This photoisomerization resulted in changes to the physical and chemical properties of the system, and these changes are reversible and do not depend on the polarity of the solvent[182] . Systems of azobenzene-modified polymers and proteins with surfactants and systems of hydrophobically modified polymers with azobenzene tails have been studied as photo-viscosifiers[183]. Lee et al.[184] mixed amphiphilic polymers (n-alkyl-modified polyacrylates) with azobenzene surfactants to show a 100-fold swing in viscosity as the system formed photochromic micelles. The system was reversibly dispersed into its molecular components on exposure to UV light. Azo dyes have been used in commercially available opto-electronic thin-films[182] .

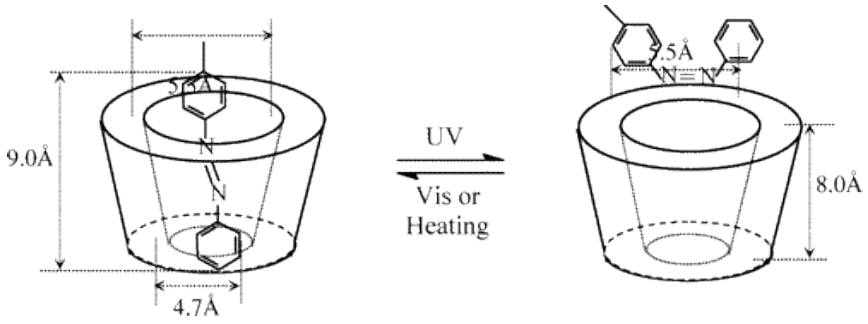

Figure 2.6: Illustration of the dimensions of azobenzene groups compared to the α-CD cavity. (ref. 187).

These photosensitive molecules are also known to form favourable ICs with CDs. However, as shown in Figure 2.6, due to the size and shape of the α-CD cavity, only the trans state molecules can fit, and the cis state molecules are excluded from complexation. Wang et al.[185] developed a lockable light-driven molecular shuttle of α-CD on a NPSI track, which is shown in Figure 2.7. The NSPI track consisted of two binding sites, a biphenyl unit (P) and a stilbene unit (S), and two stoppers, amino

disulfonic napthalimide disodium salt (N) and isopthalic acid (I). While the stilbene unit was in the trans state, the CD preferred to rest over the S unit. In contrast to the studies by Stanier et al.[186], when the α-CD/NPSI samples were UV irradiated, the track did not successfully push the α-CD from the S unit to the P unit. The reason for this is that the carboxylic acid groups from the I stopper hydrogen bonded to the hydroxyl groups of the α-CD, which locked the α-CD to the stilbene unit. To unlock the system, a base was added to convert the COOH groups of I to COO^- groups. This freed the CD and allowed it to be pushed from S to P when S was transformed from trans to cis state. The α-CD could be shifted back to the S unit by radiating the sample with visible light. The sample could then be re-locked with the addition of an acid. It was noted that, although the UV irradiated experiments were operated at the photostationary state, only 63 % of the stilbene units were actually converted to the cis state.

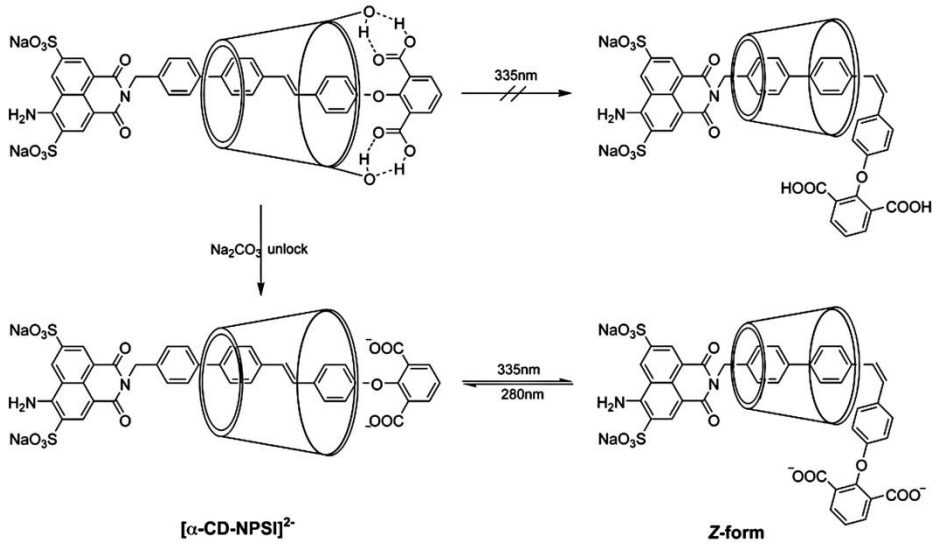

Figure 2.7: Lockable photosensitive NPSI molecular shuttle. (ref. 185)

Zheng et al.[187] used the ITC to study the inclusion complexation between CDs and azopolymers. They titrated α-CD into water, a methylcellulose polymer, and an azobenzene functionalized cellulose polymer. They found that there were only negligible differences in the differential enthalpic binding

curves for the titrations into water and methylcellulose polymer. However, the ITC data showed a highly exothermic reaction for the azobenzene functionalized methylcellulose. They concluded that α-CD formed complexes with the less polar azobenzene groups. Other relevant observations were that complexation took place instantly at the first injection, and as titration continued, the binding curve progressively merged with the dilution curve when all the azobenzenes were encapsulated by the α-CD. The derived thermodynamic parameters from the enthalpic binding curves, shown in Figure 2.8, indicated that the complexation with CD was enthalpy driven and entropy opposed, with Van der Waals interactions as the main driving force. They also concluded that polymers with higher azobenzene content were less favoured to form ICs due to the strong H-aggregation of the azobenzene groups. The azobenzene groups had to dissociate from each other to allow CD to bind; therefore, making complexation more difficult as azobenzene content increased. Using the nonlinear one-site binding model, they were able to show that α-CD formed a 1:1 inclusion complex with azobenzene. Zheng et al.[187] also continued their study by UV irradiating azobenzene-polymer samples before titration. It was found that the UV irradiated samples did not fully convert to the cis state, even though a photostationary state was reached; however, the lower saturation concentration was apparent. The reaction stoichiometry was found to be 0.41 compared to 1.17 for the non-irradiated sample. They concluded that azobenzene in the trans state readily formed ICs with α-CD, and those in the cis state did not.

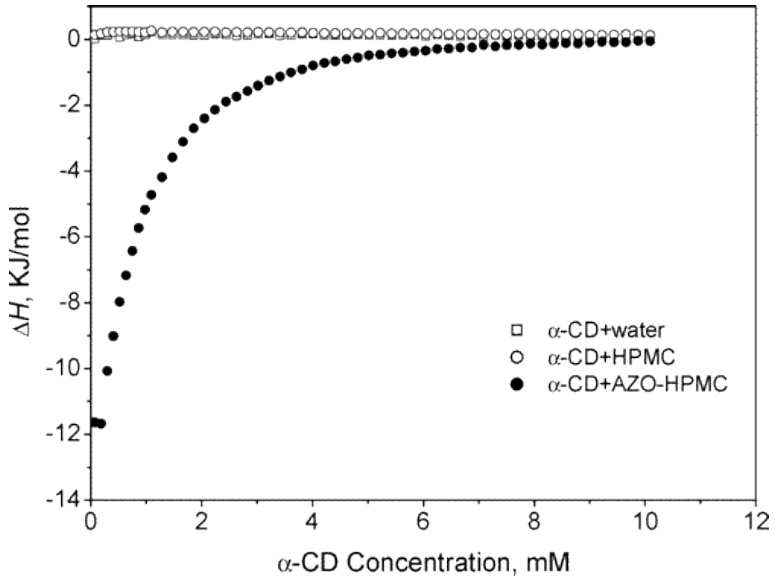

Figure 2.8: Differential enthalpic binding curves for α-CD titrations into water, HPMC, and Azo-HPMC. (ref. 187)

Films on quartz slides were prepared using layer-by-layer deposition of azobenzene-modified poly(allylamine hydrochloride) (Azo-PAH) and sulfonated CDs. Azo-PAH was found to complex with α-CD, but not β-CD. The Azo-PAH transformed from the trans to the cis state with UV irradiation. In contrast to the dry state, where there was no change in the responsiveness when the slide was swelled in the solvent, the inclusion complexation with CD allowed an increase in the photoresponsive behavior. This system may be implemented in the application of photoresponsive azobenzene-containing polyelectrolyte films[188]. Systems of azobenzene-modified polyacrylate (AMP) and β-CD or epichlorohydrin-containing β-CD (poly-CD) were shown to act as photo-sensitive viscosity switches. The photo-response of dilute samples was found to be dependent on the density of the photochrome and the interactions of the polymer chains[182].

Tomatsu et al.[152, 189] controlled gel-to-sol and sol-to-gel transitions of poly(acrylic acid) (PAA) with dodecyl (C_{12}) side chains, P(AA/C_{12}), with the addition of α-CD and ADA. P(AA/C_{12}) alone formed a gel due to the C_{12} side chain networks formed by hydrophobic interactions. When α-CD was added to the solution, complexation occurred between α-CD and C_{12} side chains. This event caused a reduction in hydrophobic interactions and dissociation of the network structure, which resulted in the sol behaviour. Trans ADA was added to the P(AA/C_{12})/α-CD mixture, and the sample reverted back to a gel. The CD preferentially complexed with ADA and left the C_{12} chains free to re-establish the hydrophobic network structure. When the sample was irradiated with UV light, the ADA molecules transformed into the cis state. ADA complexation was no longer favourable, the α-CD returned to binding with the C_{12} side groups, and the mixture returned to sol behaviour. By irradiating the sample with visible and UV light, the mixture's gel-sol behaviour could be altered repeatedly. However, it was noted that the percentage of ADA in cis state started at 5 %, increased to 89 % after UV irradiation, but only returned to 15 % after visible radiation. Therefore, the results appeared not to be fully reversible, even though the viscosity data appeared to be fully reversible.

Zheng et al.[13] studied the sol-gel transition temperatures of azobenzene hydroxypropyl methyl cellulose (HMC). Due to the hydrophobic interactions of azobenzene groups, the sol-gel transition temperature of the dark adapted polymer was only 26.5 ^{o}C. When the sample was irradiated with UV light, the trans azobenzene groups isomerised to the cis form. The azobenzene groups no longer exhibited the same hydrophobic interactions, causing the sol-gel transition temperature to rise to 36.5 ^{o}C. By irradiating the sample with visible light, the transition temperature could be returned to the original state. An alternative method to raise the sol-gel transition temperature was to add α-CD to the trans state polymer. By encapsulating the azobenzene groups, the side groups became more hydrophilic, thereby raising the transition temperature to 57 ^{o}C. With the irradiation of UV light, the

transition temperature increased to 49 ^{o}C since, in the cis conformation, the azobenzene groups could not be encapsulated by CD, thus, they no longer exhibited strong hydrophobic interactions. Although not noted in the paper, it is likely that the transition temperatures of the two cis conformation samples should not differ by 12.5 ^{o}C solely due to the addition of uncomplexed CD. An explanation may be that the samples, although at a photostationary state, did not fully convert from trans to cis state. This artificially depressed the sol-gel transition temperature of the no-CD sample and increased the transition temperature of the sample with CD. The azobenzene conformations are shown in Figure 2.9.

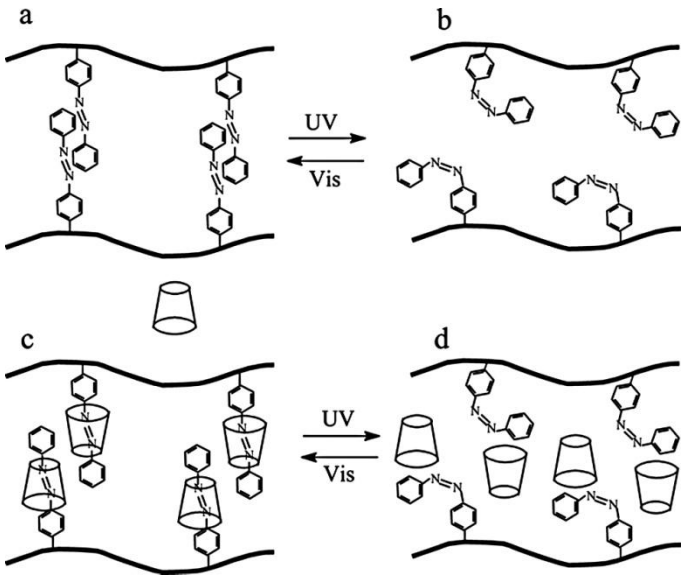

Figure 2.9: Conformation of an Azo-HMC polymer at a) trans state, b) cis state, c) trans state with CD and d) cis state with CD. (ref. 13)

Tomatsu et al.[190] studied photo-responsive hydrogel systems consisting of water-soluble PAA polymers, P6αCD or P3αCD, and a photo-responsive polymer, PC_{12}Azo. The difference between P6αCD and P3αCD was the direction in which the CDs were attached. The CDs of P6αCD were bonded to the polymer on the primary side, and the CDs of P3αCD were bonded on the secondary

side. When mixing the water-soluble polymers with $PC_{12}Azo$, it was found that P3αCD/$PC_{12}Azo$ mixtures possessed a lower viscosity than that of P6αCD/$PC_{12}Azo$. It was reasoned that, due to the direction of the α-CD, the azobenzene group was able to thread further into the CD cavity of the P6αCD than that of the P3αCD. When the P3αCD/$PC_{12}Azo$ mixture was irradiated with UV light, the viscosity decreased. Through ^{1}H NMR it was shown that the azobenzene completely dissociated from the CD cavity. With the irradiation of visible light, the viscosity increased as the azobenzene groups rethreaded into the CD cavity. When the P6αCD/$PC_{12}Azo$ samples were irradiated with UV light, the viscosity increased. Through NMR characterization techniques, it was shown that the CD shifted from encapsulating the azobenzene group to complexation of the C_{12} side chain on the $PC_{12}Azo$ polymer, forming an interlocking complex. The results could be reversed with visible light as shown schematically in Figure 2.10.

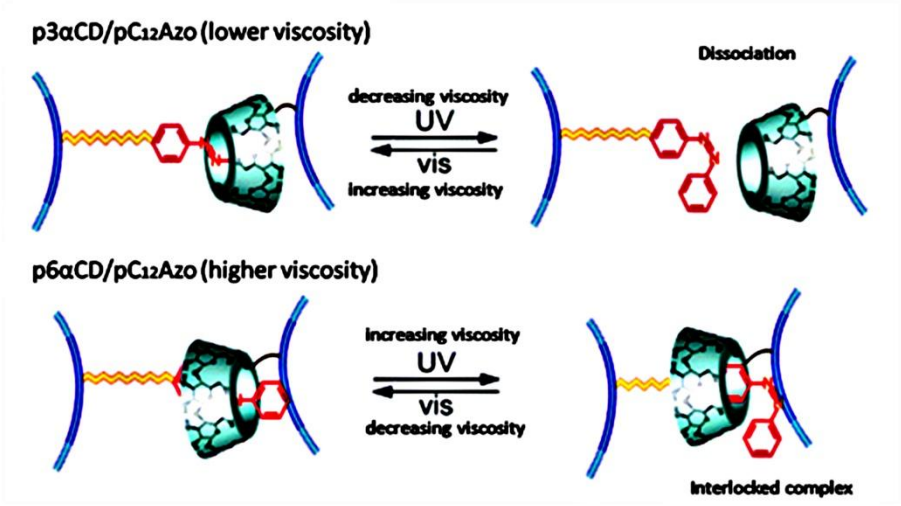

Figure 2.10: Schematic comparison between a P3αCD and a P6αCD photosensitive hydrogel systems. (ref. 190)

The factors that dictate the complexation of CD and a guest includes molecular size, molecular shape and structural flexibility. Tong et al.[192] investigated a variety of phenyl compounds and their ability to fit into the CD cavity. They found that C_8-double-bonded hydrocarbons with CD end-groups had a good fit and formed supramolecular polymers, whereas benzoyl CD did not. The guest molecule must be rigid enough to induce a good fit into the CD cavity. Double bonds of the C_8 hydrocarbons increased skeletal rigidity to form better defined and fitted structures. The flexible skeleton of the benzoyl CD was more susceptible to changes in molecular size or shape, making it less favourable for complexation.

Harada et al.[193, 194] studied multiple cinnamoyal CD compounds, 6-hydrocinnamoyl-β-CD, 6-hydrocinnamoyl-α-CD, 6-cinnamoyl-α-CD, and 6-cinnamoyl-β-CD. Using NMR, they concluded that in all four compounds, the phenyl ring formed ICs with the CD groups. For 6-hydrocinnamoyl-β-CD in D_2O, the molecule formed intramolecular complexes by including the phenyl ring into its own CD cavity. For 6-hydrocinnamoyl-α-CD, weak intermolecular complexes were formed in D_2O, but intramolecular complexes were formed in deuterated dimethyl sulfoxide (DMSO-d_6). For 6-cinnamoyl-α-CD, stronger intermolecular complexes formed in D_2O, and intramolecular structures formed in DMSO-d_6. Unfortunately, 6-cinnamoyl-β-CD was not very soluble in water, but was used to study the layered structure of the supramolecular polymer in solid state. Although not fully explained in the paper, it can be reasoned that the hydrocinnamoyl (HyCiO) groups were too flexible to form intermolecular complexes, but the cinnamoyl (CiO) groups with a double bond resulted in more rigidity and better induced fit into the CD cavities.

Inoue et al.[195, 196] expanded the study to 6-PEGacid-HyCiO-β-CD with a variety of PEG lengths. A 1-adamantane carboxylic acid (AdCA) molecule was used as a competitive guest for the CD cavity.

With no AdCA, the 6-PEGacid-HyCiO-β-CD molecule exhibited self-complexation, where the CD encapsulated with the phenyl group of the HyCiO. At half the molar equivalent of AdCA to polymer, both self-complexed molecules and AdCA complexed structures existed. At one molar equivalent of AdCA, only AdCA complexed structures were present. It was concluded that the conformational exchange rate between the two structures decreased as the length of the PEO segment increased due to the increased difficulty of threading.

Inoue et al.[191] took the 6-PEG$_{600}$acid-HyCiO-β-CD, with a reasonable conformational exchange rate, from the previous study and added an azobenzene to the end. In the trans state, the temperature dependence was investigated. At 80 ^{o}C, the polymer chain was void of any inclusions and dispersed freely in solution. At 60 ^{o}C, the molecule formed a self-inclusion complex between the CD and the azobenzene moiety. At 30 ^{o}C, the molecule formed self-inclusion complexes, alternatively including the HyCiO and azobenzene groups. At 1 ^{o}C, the molecule formed only a self-including complex with the HyCiO moiety. It was found that polymers in the trans state exhibited concentration dependence, which was concluded to be evidence for intermolecular complexation at high concentrations. When the polymer was in the cis conformation, it only formed a self-inclusion complex with the azobenzene moiety. It was shown to possess no temperature or concentration dependence and reported to be reversible by radiating the sample with visible light. It should be noted that the polymer possesses a β-CD, which has a cavity larger than that of α-CD; hence, it is able to complex with the azobenzene moiety in cis state. A summary of polymer UV-responsive CD assemblies is documented in Table 2-3.

Table 2-3: Photo-Responsive Cyclodextrin Systems

CD Type	Encapsulant	Polymer	Results	Noted Applications	References
α-CD	ADA	P(AA/C_{12})	Blank polymer: Gel Add CD: Sol Add ADA: Gel UV irradiation: Sol Visible light irradiation: Gel	Photonics Optical Storage Photoswitchable Materials	189
α-CD	Azo	P6αCD P3αCD PC_{12}Azo	Depending on which rim of the CD the polymer is attached to, the viscosity of the solution differs Samples increase or decrease in viscosity with UV irradiation depending on CD type		190
α-CD	Azo	HMC-Azo	HMC-Azo: Sol-to-gel transition temperature 57 ^{o}C UV Irradiation: Sol-to-gel transition temperature 49 ^{o}C	Sensors Optical switches Smart windows	13
α-CD	Azo	Azo-cellulose polymer	Azo in trans form readily forms ICs with CD Azo in cis form did not form ICs with CD		187
β-CD	Azo CiO	6-PEG_{600}acid-HyCiO-β-CD-Azo	Irradiation of UV light, polymer concentration and temperature affected self complexation		191

2.8 Redox-responsive Inclusion Complexes

CDs have been found to form ICs with a variety of metallocenes of various structures, depending on the size of the CD cavity[204-206]. Examples of redox responsive CD guests include cobaltocenium[203, 207], bypridinium[208], aminobiphenyl[209], and ferrocene derivatives[210].

Ferrocene (FC) and FC derivatives are among the most popular CD guests in electrochemically driven molecular complexes[198, 201, 210]. CDs have been found to interact more favourably with FC in its reduced state. Oxidation of the molecules imparted a positive charge and caused decomplexation[211, 212]. Redox-responsive inclusion complexes between CDs have been studied for over 25 years[213-215], but redox-responsive/CD polymer systems have recently gained increasing attention and popularity.

Tomatsu et al.[197] who studied the P(AA/C_{12}) and β-CD systems discussed previously, expanded their work to include a redox-responsive guest, ferrocenecarboxylic acid (FCAH). Similar to the

azobenzene studies, blank P(AA/C_{12}) samples exhibited a high viscosity and gel behaviour due to hydrophobic interactions of the C_{12} chains. With the addition of β-CD, the system decreased in viscosity due to the encapsulation of C_{12} side chains. When reduced FCAH was added to the system, the system regained its gel behaviour as CD preferred to complex with the FCAH, leaving the C_{12} side chains free. However, once the FCAH molecules were oxidized with sodium hypochlorite, the system exhibited gel-to-sol transition behaviour as the FCAH molecules decreased in their affinity for β-CD, and the CD recomplexed with the C_{12} side chains. An illustration of the system is shown in Figure 2.11. Due to the use of chemical redox reagents, repetitive conversion could not be observed. This type of system could be useful as gel actuators that could be controlled by applied electric potential.

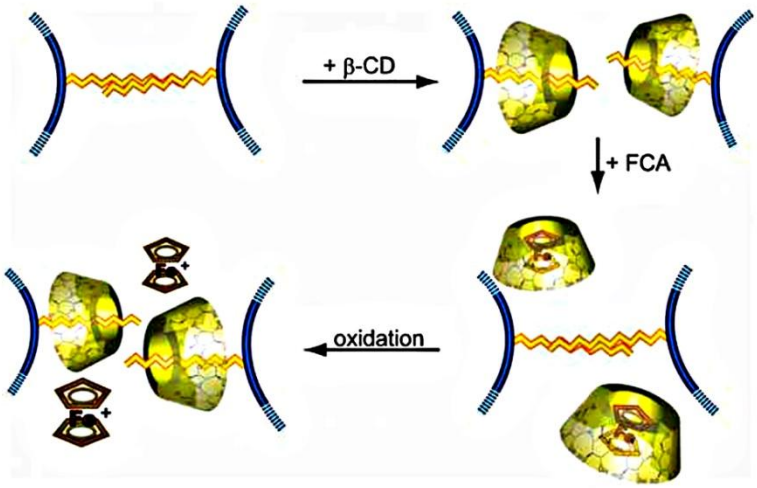

Figure 2.11: Illustration for P(AA/C_{12})/ β-CD redox-responsive hydrogel system. (ref. 197)

A poly(propylenimine) (PPI) dendrimer with ferrocene end units formed large supramolecular structures with β-CD. These structures dissociated upon oxidation of the ferrocene units[202] . It was observed that cobaltocenium groups do not form ICs with CD; however, upon the reduction of one

electron, the cobaltocenium became neutral. Accordingly, PPI dendrimers with cobaltocenium end groups did not form ICs with β-CD and, upon reduction, large supermolecular structures were produced[203] . These redox-active self-assembling dendrimers were used in micro-contact printing. Self-assembled monolayers on gold[221] and β-CDs on glass substrates have been developed. Ad-functionalized[222] and N-allykferrocene carboamide (FCN)-functionalized[198-200] PPI dendrimer guest molecules were used to interact with the host surface. In the reduced state, the dendrimers bound to the gold and SiO_2 surfaces (Figure 2.12). With local oxidation of the FCN-dendrimers by microelectrode-generated $[IrCl6]^{+2}$ ions (from the scanning electron microscope), the FCN-dendrimers were effectively removed from the host surface (Figure 2.13). The oxidation of FCN to FCN^+ led to a loss of affinity between the FCN group and the β-CD cavity[201] . Table 2-4 summarizes the polymer redox-responsive CD systems discussed in this section.

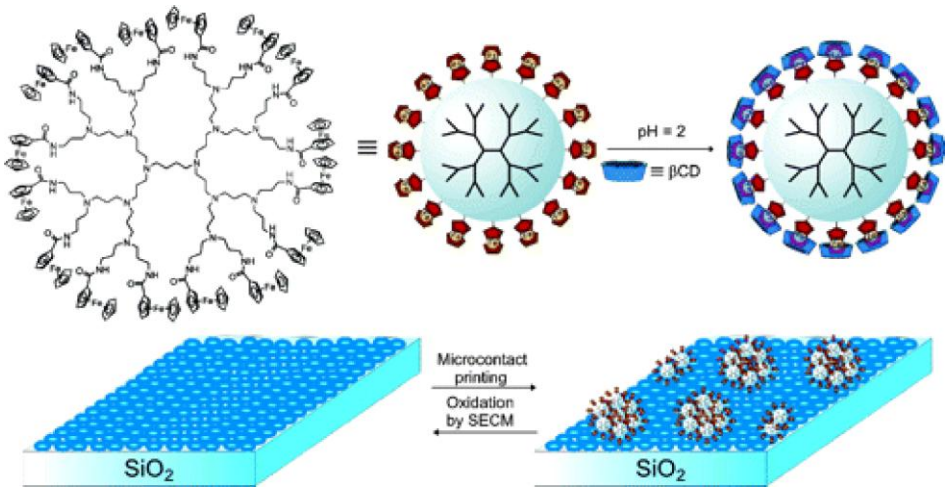

Figure 2.12: Complexation of β-CD to redox-sensitive dendrimers, and their immobilization onto a molecular printboard. (ref. 201)

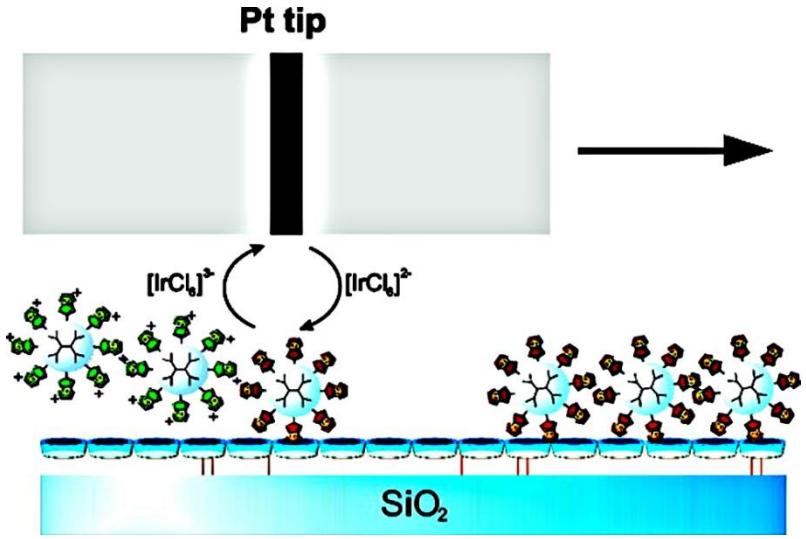

Figure 2.13: Mechanism of SEM-Induced desorption of the complexed dendrimers from the SiO_2 molecular printboard. (ref. 201)

Table 2-4: Redox-Responsive Cyclodextrin Systems

CD Type	Encapsulant	Polymer	Results	Noted Applications	References
β-CD	FCAH	p(AA/C_{12})	Blank polymer: Gel Add β-CD: Sol Add reduced FCAH: gel Oxidize FCAH: Sol	Gel actuators controlled by electric potential	197
β-CD	FC	PPI-FC dendrimers	Reduced: Forms large supramolecular structures Oxidized: Structures dissociate		198-202
β-CD	cobaltocenium	PPI-cobaltocenium dendrimers	Oxidized: No supramolecular structures Reduced: Forms large supramolecular structures		203

2.9 Multi-stimuli-responsive Inclusion Complexes

2.9.1 pH- and Temperature-Responsive Inclusion Complexes

Multi-stimuli-responsive polymers with multiple functionalities allow for more complex interactions and morphologies[223, 224]. pH- and thermal- sensitive supramolecular hydrogels composed of CD-PL showed specific host-guest interactions, as well as rapid and reversible responses to

changes in temperature and pH[104, 217, 218]. A cationic β-CD-PL polymer with 3-trimethylsilylpropionic acid (TPA) guest molecules was shown to exhibit reversible gel-sol behaviour with heating and cooling near the UCST. Ionizable α-amino groups of PL and the COOH groups of TPA could be used to control molecular aggregation. A system of α-CD with PL-Dex-2 showed gel-sol transitions upon heating and cooling. By lowering the pH, the system exhibited a gel-to-sol transition due to the protonation of the guest polymer resulting in the dissociation of the complex[216].

Hamcerencu et al.[140] copolymerized xanthan maleate and β-CD acrylate with NIPAM hydrogels to form interpenetrating polymer networks. The swelling of the hydrogel was found to be pH-dependent and it increased with increasing pH. At low pH values, the carboxylic acid groups of xanthan existed in the non-ionic form. Hydrogen bonding formed between the polymer chains, and the hydrogel deswelled. At a pH of 9.6, the carboxylic acid groups ionized, the hydrogen bonding of the xanthan chains decreased, and the electrostatic repulsion between the ionized groups caused the hydrogels to swell. The phase transition temperature (LCST) was found to be controlled by altering the feed composition ratios, and, as a drug carrier for water insoluble drugs, the collapse of the hydrogel above the LCST was noted as the mechanism for progesterone release.

Liu et al.[219] synthesized a linear PNIPAM chain with a β-CD pendant group. At a pH of 1.4, the guest, MO, produced ammonium and azonium tautomers formed by protonation of the azo groups. The hydrophobic interactions between MO and the β-CD cavity were weakened, and low complexation was observed. At a pH value of 4, the PNIPAM-β-CD polymer protonated, and the ionic interaction between protonated amino groups of the polymer and sulphate groups of MO resulted in more stable ICs. The system also exhibited phase separation properties above the LCST of the polymer.

Coacervation is the phase separation phenomenon in which a colloidal system forms droplets comprised of the concentrated polymer phase. Thermo-responsive coacervation had been found to be present in biomacromolecules, such as elastin[225, 224], and synthetic polymers, such as poly(N,N-dimethylacrylamide-co-N-phenyl-acrylamide) and poly(N-vinylamide-co-vinylacetate)[229, 230] . The behaviour of coacervate drops was induced for a poly(NIPAM-co-2-hydroxyisopropyl acrylamide) (P(NIPAM-co-HIPAM) and β-CD system. The particle size and cloud points could be altered by altering the HIPAM content of the copolymer. The particle size was also found to be independent of pH, but sensitive to salt addition. However, at pH 12, more MO molecules were encapsulated in β-CD. These coacervate droplets could be used in the purification of bioactive molecules[220] . A summary of polymer pH- and temperature-responsive CD assemblies is documented in Table 2-5.

Table 2-5: pH- and Temperature-Responsive Cyclodextrin Systems

CD Type	Encapsulant	Polymer	Results	Noted Applications	References
α-CD	Progesterone	Xanthan/ NIPAM /α-CD	Low pH: COOH of Xanthan in non-ionic form, More H-bonding High pH: Xanthan ionized, decrease in H-bonding, electrostatic repulsion, hydrogel swelling LCST controlled by feed composition ratios Above LCST: Hydrogel collapse releases drug	Drug Delivery	140
α-CD	PL-Dex-2	PL-Dex-2	Gel-to-sol transition in hydrogel structure when decreasing pH Gel-to-sol transitions upon heating and cooling		216
β-CD	TPA	β-CD-PL	Ionization of PL α-amino groups and TPA COOH groups controls molecular aggregation Reversible gel-sol behaviour with heat and cooling around UCST	Model for enzyme substrate interaction in biological systems Drug Delivery Separation operations in biotechnology Processing of agriculture productions sensors and actuators	104, 217, 218
β-CD	MO	NIPAM-β-CD/ EDA-β-CD	Very low pH: Protonation of MO, decrease in complexation Low pH: Interaction between protonated amino and sulfate groups LCST properties due to PNIPAM	Controlled Drug Delivery Carriers	219
β-CD	MO	P(NIPAM -co- HIPAM)	Coacervate droplet formation High pH: More MO in droplets	Separation and purification of solutes	220

2.9.2 pH- and Redox-responsive Inclusion Complexes

The inclusion equilibria of FC and FCAH with polymer films of β-CD were investigated by Kutner and Doblhofer[226]. In its reduced form, FC was found to be encapsulated by β-CD; however, in its oxidated form, the FC^+ was released from the polymer film. Due to the carboxylic acid groups, FCAH was found to be pH dependent. At low pH, the FCAH compound is encapsulated by the β-CD polymer, and, in the oxidized state, decomplexation occurs. At high pH, the ionized and reduced FCA(0)- compound complexes with β-CD and decomplexes with β-CD in its oxidized state (FCA(I)). However, since the carboxylic acid group is ionized, the free FCA(I) ions interact with the charged iron atom to form aggregating precipitates. Applications of these findings include selective drug release, design of electrochromic display devices, high performance capillary liquid chromatography columns, and novel electrode substrates. Table 2-6 summarizes the polymer pH- and redox-responsive CD systems.

Table 2-6: pH- and Redox- Responsive Cyclodextrin Systems

CD Type	Encapsulant	Polymer	Results	Noted Applications	References
β-CD	FC FCAH	Cross-linked β-CD polymer film	Reduced: Encapsulation by β-CD Oxidized: Decomplexation FCAH: Oxidization and at High pH: precipitates	Selective drug release Electrochromic display devices HPLC columns Electrode substrates	226

2.9.3 Temperature- and Photo-responsive Inclusion Complexes

The introduction of azobenzene onto temperature sensitive polymers, such as PNIPAM or poly(N,N-dimethyl acrylamide), allows the LCST of the polymer to be controlled by photo-irradiation[231]. Kungwatchakun and Irie[232] synthesized a copolymer of PNIPAM and N-(4-phenyl(azo)-phenyl-acrylamide) and they showed that, over a narrow range of composition and temperature, photo-stimuli may be used to control the solubility of the polymer in water. Luo et al.[227]

combined thermo-sensitive PNIPAM with photosensitive azobenzene end groups as illustrated in Figure 2.14. The surface of gold nanoparticles was capped with α-CD. In the trans state, the PNIPAM-Azo polymers were encapsulated by α-CD, forming a PNIPAM coating around the gold nanoparticle. Below the LCST of PNIPAM, the solution was clear, and above the LCST, the PNIPAM chains collapsed resulting in a turbid solution. With UV irradiation, the azobenzene converted to the cis-state and detached from the gold particles. These temperatures and photo-transitions were found to be reversible and repeatable. These thermo- and photo-sensitive nanoparticles are important for applications in photoactive materials and switching devices that can be controlled with light.

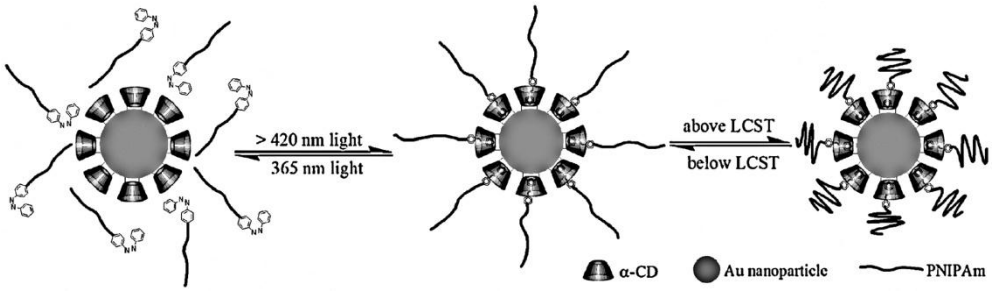

Figure 2.14: Illustration of a temperature- and UV-controlled self-assembly system composed of Azo-PNIPAM and Au nanoparticles. (ref. 227)

Luo et al.[228] also studied temperature- and photo-responsive ICs between α-CD and thermosensitive azobenzene polymers. The three polymers PNIPAM, N,N-diethylacrylamide (DEAM) and N,N-dimethylacrylamide (DMAM) were functionalized with azobenzene end groups. The LCST of the three polymers decreased with increasing azobenzene content because high azobenzene contents increased the hydrophobicity of the polymers and made them less soluble. The LCST of the polymers greatly increased with the addition of α-CD as the CD encapsulated the azobenzene groups and increased the system's hydrophilicity. Upon UV irradiation, the azobenzene

groups were expelled from the α-CD cavity due to steric hindrance, resulting in a reduction in the LCST due to an increase in hydrophobicity. This polymer would be useful in light controlled drug delivery.

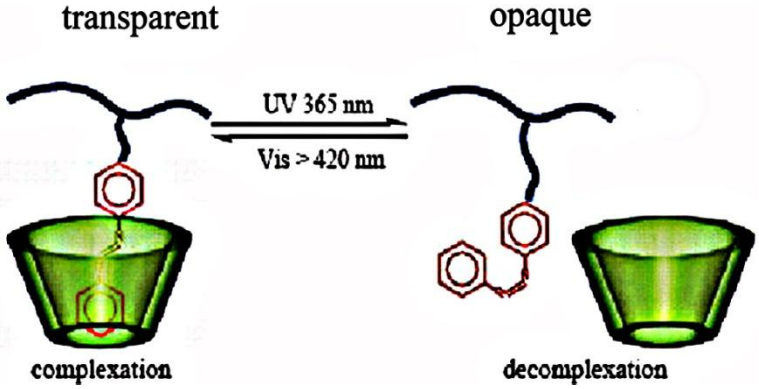

Figure 2.15: Reversible transition of PDMAA-co-PAPA/CD system upon UV and Vis light irradiation. (ref. 231)

Luo et al.[231] also extended their studies to include a poly(N,N-dimethylacrylamide)-co-poly(N-4-phenylazophenyl acrylamide) (PDMA-co-PAPA)/α-CD system (Figure 2.15) that was found to display a photoinduced phase separation phenomenon. Phase separation relies on a balance between hydrogen bond formation with water and hydrophobic intermolecular forces. The introduction of azobenzene caused the polymer to be less soluble and precipitate at a lower temperature. The LCST of the polymer tended to decrease with increasing azobenzene content. After UV irradiation, the azobenzene converted to the cis state, and the solubility increased, resulting in a small increase in the LCST. The addition of CD allowed for higher polymer solubility because of inclusion complexation with the trans azobenzene, and a large increase in LCST was demonstrated. After UV irradiation, the cis azobenzene decomplexed from the CD due increased, and caused a reduction in the LCST. In the trans state, the system was transparent due to complexation of the polymer with CD. After UV

irradiation, decomplexation produced an opaque solution. It was found that the association of polymer with polymer-CD molecules was tighter than association with α-, β-, HP-β-CD, The binding was also shown to favour polymers with higher hydrophobicity and longer hydrocarbon chains. A summary of temperature- and photo-responsive CD-polymer systems are documented in Table 2-7.

Table 2-7: Temperature- and Photo- Responsive Cyclodextrin Systems

CD Type	Encapsulant	Polymer	Results	Noted Applications	References
α-CD	Azo	PNIPAM-Azo	Below LCST: Polymers form coating around CD capped gold particles Above LCST: PNIPAM chains collapse, turbid solution UV irradiation: Conversion from trans to cis, polymer detachment from gold particles	Photoactive materials Switching devices	227
α-CD	Azo	PNIPAM-Azo DEAM-Azo DMAM-Azo	Increasing Azo content: LCST decreases Add α-CD: LCST increases UV irradiation: Azo leave α-CD cavity, LCST decreases	Light controlled drug delivery	228

2.9.4 Temperature- and Redox-responsive Inclusion Complexes

There are few studies that combine redox-responsive inclusion complexations with pH- or temperature-sensitive systems. Zuo et al.[233] synthesized a PNIPAM polymer with a FCN end group. By adding β-CD to the system, the β-CD complexed with the reduced ferrocene side groups and disrupted the hydrophobic interactions between side groups. This caused an increase in LCST and a decrease in viscosity. In the oxidized form, the addition of β-CD produced no change in specific viscosity or LCST as there was no interaction between the ferrocene groups and CD. This temperature- and redox-sensitive system was noted for applications in sensors and controlled release systems. Table 2-8 summarizes the polymer temperature- and redox-responsive CD systems.

Table 2-8: Temperature- and Redox-Responsive Cyclodextrin Systems

CD Type	Encapsulant	Polymer	Results	Noted Applications	References
β-CD	FCN	PNIPAM-FCN	Add β-CD: Increase in LCST Oxidation: No change in LCST	Sensors Controlled release systems	233

2.10 Conclusions

CD assisted supramolecular self-assemblies have attracted a great deal of interest due to their ability to form well-defined architectures, and because they may be controlled by external stimuli. In this literature review, a variety of dynamic self-assembly strategies are discussed. From the literature reviewed in the area of CD self-assemblies, it is evident that the most popular strategies involved are pH and temperature. By changing pH, one may change the interactions between the polymer, the medium, and CD. A change in temperature will cause temperature-sensitive segments to collapse and form micelles or intermolecular aggregates. This thesis investigates two polymers, PEO-b-PNIPAM and PPO-b-PMAA, which are pH and/or temperature responsive, and their solution behaviours with CD have yet to be studied. The topic of stimuli responsive inclusion complex systems is an active area of research, and the determination of the morphological changes of these double-hydrophilic block copolymers with CD resulting from pH or temperature alterations will result in the development of novel systems with possible commercial applications.

Chapter 3

Experimental Techniques and Equipment

3.1 Introduction

This chapter discusses the key experimental techniques used in the synthesis and characterization of PEO-b-PNIPAM/α-CD and PPO-b-PMAA/β-CD systems. Atom transfer radical polymerization (ATRP) is a controlled radical polymerization technique that was used to synthesize the PNIPAM block of the PEO-b-PNIPAM polymer. Surface tensiometry was used to determine self-assembly properties, such as the critical micellar concentration (CMC), of each of the systems at various temperatures. ITC experiments determined the thermodynamic parameters of CD binding and neutralization process of the polymethacrylic acid. LLS was used to determine the conformational behaviours of various polymers, and it monitored the behavior of these systems as a function of temperature and pH. DSC was used to measure the LCST of PEO-b-PNIPAM and of PEO-b-PNIPAM/α-CD systems. A comprehensive understanding of the two types of polymer/CD systems may be achieved by combining the data obtained from these various characterization methods.

3.2 Atom Transfer Radical Polymerization (ATRP)

PNIPAM polymers have been synthesized using a variety of methods. Traditionally, free radical polymerization techniques have been used, but they were unable to control the syntheses[1]. Living anionic polymerization techniques are able to produce PNIPAM polymers with well-defined molecular weights and polydispersities. Recently, interest has shifted to living radical polymerization methods, such as nitroxide mediated (NMP), radical addition fragmentation transfer (RAFT)[2], and ATRP[3-5] to synthesize polymers with well-defined molecular architectures. Using living radical

polymerization, end functionalized PNIPAM polymers have been synthesized using appropriate initiating and terminating agents.

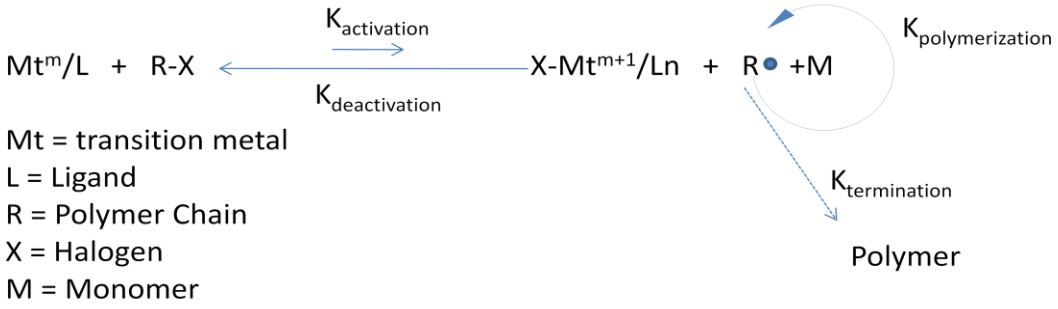

Figure 3.1: Schematic representation of the ATRP process.

Radical polymerizations are very practical as they may be used to synthesize a wide range of polymers in mild experimental conditions, and they may be performed in bulk, suspensions and emulsions. However, radical polymerizations suffer from their lack of control due to the fast and irreversible termination by coupling and disproportionation, which leads to high polydispersity. Controlled radical polymerizations have been proven to produce well-defined polymers with narrow molecular weight distributions and complex architectures[6]. ATRP is a catalytic process where a halogen transfer reaction activates and deactivates the polymer chains. The transition metal catalyst (M_t^n/ligand) reacts with an alkyl halide initiator and transfers the halogen (X) to the catalyst. This generates a radical that is active and available for the propagation reaction with the monomer (M). This radical chain is rapidly deactivated by reacting with the oxidized transition metal halide complex ($X\text{-}M_t^{n+1}$/ligand) and reforms its original oligomeric alkyl halide and catalyst. The chains grow in short controlled steps, and the process continues until the reaction is stopped, commonly by exposure to oxygen. A schematic of the ATRP Process may be found in Figure 3.1. The controlled behaviour is

due to two factors: (i) the equilibrium is strongly shifted to the dormant species which limits the termination between active species and (ii) the deactivation of active species is fast compared to the polymerization rate which provides the same growth rate for all chains to yield narrow molecular weight distributions. The polydispersity index (PDI) is usually under 1.5, but some ATRP reactions may commonly reach PDIs as low as 1.05. The degree of polymerization for ATRP is defined by

$$\boldsymbol{DP_n = \frac{\Delta[M]}{[I]_o}} \quad \textbf{(3.1)}$$

where DP_n is the degree of polymerization, $[M]$ is the monomer concentration, and $[I]_o$ is the initial initiator concentration. Copper catalysts have proven to be the most reactive with respect to other common transition metal catalysts, such as those involving I, Ni, and Ru. The ligand Me_6TREN has been used in numerous ATRP reactions and Cu(I)/Me_6TREN was deemed by Queffelec et al.[7] as the overall most effective catalyst/ligand pair for ATRP.

3.3 Surface Tensiometry

Surface tension data is obtained using the DataPhysics tensiometer (DataPhysics Instruments; Filderstadt, Germany) which uses software-controlled measurements to determine the interfacial tension of liquids and to determine the critical micelle concentration (CMC). The equipment uses a high precision weighing system to measure the Wilhelmy wetting forces as the polymer systems are dosed into the sample vessel. A thin plate, which is oriented perpendicular to the interface, comes in contact with a fluid surface, and the surface tension causes the formation of a meniscus around the plate's perimeter. The Wilhelmy equation describes the increase in weight with the surface tension (γ) as given by Equation 3.2.

$$F_w = L_w \gamma_{LV} \cos\theta \tag{3.2}$$

where F_w is the Wilhelmy wetting force, L_w is the wetted perimeter of the plate, γ_{LV} is the interfacial tension, and θ is the contact angle.

Amphiphilic polymer systems exhibit surface–active properties in aqueous solutions. In addition to their ability to self-assemble in aqueous solutions, these molecules can also adsorb strongly at the air-water interface to reduce the surface energy. As surfactants with limited solubility are added to the solution, the surface concentration (Γ) increases while the surface tension (γ) decreases. At the CMC, surfactant molecules aggregate in solution to form structures such as micelles. Beyond the CMC, adding more surfactant molecules results in the formation of additional structures, but both Γ and γ remain almost constant.

By plotting the surface tension against the concentration (γ vs. ln C), the CMC can be determined by locating the intercept of the two linear regions of the plot. The Gibb's equation (Equation 3.3) relates the slope of the linear region of the γ vs. ln C plot to the surface concentration (Γ).

$$\Gamma = \frac{-1}{RT}\left(\frac{\Delta\gamma}{\Delta \ln C}\right) \tag{3.3}$$

where Γ is the surface concentration, R is the gas constant, T is the temperature, γ is the surface tension, and C is the concentration of the surfactant. Using Avogadro's number, Γ may be converted to the head group area (a_0).

3.4 Isothermal Titration Calorimetry (ITC)

Heat is generated when substances non-covalently bind together, and the measurement of this heat allows parameters, such as binding constant (K), enthalpy (ΔH), entropy (ΔS), and heat capacity (C_p) to be obtained. Isothermal Titration Calorimetry (ITC) is a technique that provides a complete thermodynamic profile of the molecular interactions by measuring the enthalpy change in a binding experiment.

ITC has been widely used to characterize the binding thermodynamics of a variety of binding experiments including bimolecular interactions and supramolecular systems[8, 9]. For example, polymeric systems such as the study of polymer-surfactant interactions using the ITC have been widely studied[10-13]. Yui et al.[14] demonstrated the use of the ITC to elucidate the ICs between linear polymers and their corresponding CD based tube. Arnaud and Bouteiller[15] proved that the ITC was "perfectly suited" for their characterization of the self-association of supramolecular polymers. As discussed previously, Zheng et al.[16] used the ITC to study the inclusion complexation between CDs and azopolymers.

Calorimetric measurements were carried out using a Microcal Isothermal Titration Calorimeter (ITC; Microcal, LLC; Massachusetts, USA). This instrument measures enthalpy changes based on a power compensation technique. A 1.4 mL reference cell and a 1.4 mL sample cell, both composed of Hastelloy® Alloy C-276, are held within an adiabatic shield. Titrations are carried out in stepwise injections from a 250 µL injection syringe. The syringe contains a tailor-made tip that doubles as a stirrer for the cell, with a maximum stirring efficiency of 400 rpm. The injection schedule is controlled automatically through a software that allows the user to set parameters such as number of injections, volume of injections, and time between injections. As each injection is made, the

temperature difference between the reference and sample cells are measured, and the feedback power used to maintain the temperature equilibrium is integrated to determine the enthalpy change due macromolecule/titrant interactions. When the macromolecule in the cell is saturated with ligand, the heat signal diminishes to only the background dilution heat. The calorimetric information is sent to a computer program (Origin for ITC; OriginLab; Massachusetts, USA) for analysis.

The data is analyzed using a sequential binding site model. The binding constants are defined as

$$\boldsymbol{K_1 = \frac{[MX]}{[M][X]} \quad K_2 = \frac{[MX_2]}{[MX][X]} \quad K_3 = \frac{[MX_3]}{[MX_2][X]}} \tag{3.4}$$

where [M] is the concentration of free polymer and [X] is the concentration of free titrant. The fraction of total polymer having i bound ligands, F_i, is

$$\boldsymbol{F_0 = \frac{1}{P} \quad F_1 = \frac{K_1[X]}{P} \quad F_2 = \frac{K_1K_2[X]^2}{P} \quad F_i = \frac{K_1K_2 \ldots K_i[X]^i}{P}} \tag{3.5}$$

where

$$\boldsymbol{P = 1 + K_1[X] + K_1K_2[X]^2 + K_1K_2 \ldots K_i[X]^i\,,} \tag{3.6}$$

and the concentration of titrant in the bulk, X_t, is

$$\boldsymbol{X_t = [X] + M_t \sum_{i=1}^{n} iF_i} \tag{3.7}$$

Using the equations above, [X] may be solved using the Bisection numerical method. The heat content after the i^{th} injection, Q, is

$$Q = M_t V_0 (F_1 \Delta H_1 + F_2 [\Delta H_1 + \Delta H_2] + \ \ldots \\ + F_i [\Delta H_1 + \Delta H_2 + \Delta H_3 + \ \ldots + \Delta H_i] \tag{3.8}$$

The displaced volume is corrected and the heat effect of the i^{th} injection is

$$\Delta Q(i) = Q(i) + \frac{dV_i}{V_o}\left[\frac{Q(i) + Q(i-1)}{2}\right] - Q(i-1) \tag{3.9}$$

The Marquardt minimization routine is used to obtain the values of the fitting parameters.

3.5 Differential Scanning Calorimetry (DSC)

Differential scanning microcalorimetry (DSC) is a technique that measures the heat change that occurs during controlled increases and decreases in temperature. For temperature sensitive polymer systems, the DSC can provide information regarding enthalpy (ΔH), change in heat capacity (C_p) and the transition midpoint temperature (T_m) of phase transitions.

DSC has been widely used to measure phase transition temperatures for various temperature-sensitive polymer systems[17-20]. De Tang et al.[21] synthesized Y-shaped block copolymers composed of PEO and PNIPAM by ATRP, and they used the DSC to measure the phase transition temperatures of various polymer lengths. Shan et al.[22] used the DSC to compare the phase transition temperatures of gold particles grafted with PNIPAM brushes.

Calorimetric measurements are carried out using a Microcal Differential Scanning Microcalorimeter (DSC; Microcal, LLC; Massachusetts, USA). A 0.4 mL reference cell and a 0.5 mL sample cell, both composed of Tantaloy 61™, are held within an adiabatic shield. The experiment schedule is controlled automatically through software that allows the user to set parameters such as the number of scans, temperature range, and scan rate. The heat changes between the reference and

sample cells are measured as the temperature changes, and the feedback power used to maintain the temperature equilibrium is integrated to determine the enthalpy change due the system's phase transition. The calorimetric information is sent to a computer program (Origin for DSC; OriginLab; Massachusetts, USA) for analysis. The baseline is first subtracted and the ΔH of the transition may be found by integrating the calorimetric data.

$$\boldsymbol{\Delta H = \int_{T_1}^{T_2} C_p \, dT} \tag{3.10}$$

The ΔS of the transition may be determined by found by using the equation below.

$$\boldsymbol{\Delta S = \int_{T_1}^{T_2} \frac{C_p}{T} \, dT} \tag{3.11}$$

Finally, the Gibbs Free Energy at a given temperature may be determined using the Equation 3.12.

$$\boldsymbol{\Delta G = \Delta H - T\Delta S} \tag{3.12}$$

3.6 Laser Light Scattering

The microstructure of a sample is examined by a Brookhaven Laser Light Scattering system (Brookhaven Instruments Limited; Worcestershire, UK) with a BI200SMv2 Goniometer turntable, BI-APD photomultiplier tube detector, TurboCorr Correlator, and MiniL-30 636 nm laser. A variety of pinhole sizes may be chosen: 1, 2, or 3 mm for Static Light Scattering, or 100, 200 and 400 μm for Dynamic Light Scattering. The sample cell holder consists of a glass vat with an index matching liquid, Decalin (cis-trans decahydronapthalene). A minimum of 1.5 mL of sample is required to fill a

sample cell that is 55 mm tall and has an outside diameter of 12 mm. The sample is secured in the cell with Teflon caps. The BI-FC temperature controller is used to conduct experiments at multiple temperatures. The dη/dc measurements are performed using a BI-DNDCW differential refractometer.

According to the semi-classical light scattering theory, as light falls on molecules, the light's electric field causes oscillating polarization of the electrons in the molecules. The molecules then become secondary light sources, and they generate scattered light. The size, shape, and molecular interactions of the molecules affect the properties of the scattered light, including frequency shifts, angular distribution, polarization, and intensity. Combining this information with electrodynamic and time dependent statistical mechanics theories allows for the determination of the molecule's structure and dynamics.

The Brookhaven Laser Light Scattering system has the ability to perform two types of measurements. It uses the classical light scattering theory to measure the average time integrated intensity of light scattering, and it uses the Quasi Elastic Light Scattering (QELS) theory to measure the intensity fluctuations of the scattered light.

Two types of scattering are measured by the light scattering instrument. Rayleigh scattering can be measured for macromolecules that are smaller than the wavelength of incident light. These molecules (usually with radius less than 30nm) may be treated as point scatterers. The scattered light in the plane perpendicular to the polarization of the incident light is not dependent on the scattering angle. Since this scattered light is the same at every angle, the measure of Rayleigh scattering does not require angular dependence consideration. In contrast, the measure of Mie scattering requires angular dependence consideration. Mie scattering is exhibited by larger macromolecules as different parts of the macromolecule scatter light differently. This difference leads to constructive or destructive

interference. The Rayleigh-Gans-Debye theory strives to describe the net results. The theory assumes that each macromolecule is made of numerous elements that scatter light independently. Adjacent elements produce interference in certain directions, and by measuring the scattered light over a variety of angles, information regarding the molecules' morphology may be inferred.

3.6.1 Static Light Scattering

Static Light Scattering (SLS) measures the time-averaged intensity of scattered light as a function of angle and concentration. For dilute polymer solutions, SLS can be used to measure the weight average molecular weight (M_w), the root-mean-square radius (R_g), and the second virial coefficient (A_2), and it may also be used to determine structural information though the calculation of the R_g/R_h ratio.

The Rayleigh equation is most commonly used to determine the weight average molecular weight, M_w.

$$\frac{KC}{R_\theta} = \left(\frac{1}{M_w} + 2A_2C\right)\frac{1}{P_\theta} \tag{3.13}$$

where C is the sample concentration, A_2 is the second virial coefficient, M_w is the molecular weight of the sample, K is the optical constant, P_θ is the angular dependence of the sample scattering intensity, and R_θ is the Rayleigh ratio (ratio of scattered light to incident light of the sample).

The optical constant K may be calculated using the equation below,

$$K = \frac{2\pi^2}{\lambda_o^4 N_A}\left(n_o\frac{dn}{dc}\right)^2 \tag{3.14}$$

where N_A is Avogadro's number, n_o is the solvent refractive index, λ_o is the laser wavelength, and $\frac{dn}{dc}$ is the differential refractive index increment.

The $\frac{dn}{dc}$ is the difference in refractive index between a solution and that of the corresponding pure solvent as a function of solute concentration. The $\frac{dn}{dc}$ is the slope of the graph of refractive index of solute in solution divided by concentration.

The P_θ term in the Rayleigh equation accounts for the angular dependence of the sample scattering intensity. The angular dependence arises from Mie scattering; the angular dependence is due to the constructive and destructive interference of scattered light from different positions on a particle. If particles are smaller than the wavelength of incident light, only Rayleigh scattering is present, and P_θ is equal to one. The angular dependence of a sample's scattering intensity may be calculated using Equation 3.15.

$$\boldsymbol{P_\theta = 1 + \frac{16\pi^2 n_o^2 R_g^2}{3\lambda_o^2} sin^2\left(\frac{\theta}{2}\right)} \qquad \textbf{(3.15)}$$

where R_g is the radius of gyration, n_o is the solvent refractive index, λ_o is the laser wavelength, and θ is the scattering angle.

The standard approach for molecular weight calculation requires comparing the scattering intensity of the analyte to a standard liquid with known Rayleigh ratio to determine the excess scattering. Toluene is commonly used as the standard in SLS. The Rayleigh ratios of toluene are known over a range of wavelengths and temperatures. In addition, toluene is easily obtainable. The sample Rayleigh ratio may be calculated using the equation below.

$$R_\theta = \frac{I_A n_o^2}{I_T n_T^2} R_T \tag{3.16}$$

where I_A is the intensity of analyte (sample intensity – solvent intensity), n_o is the solvent refractive index, I_T is the intensity of standard (toluene), n_T is the standard's (toluene) refractive index, and R_T is the Rayleigh ratio of standard (toluene).

Zimm plots are constructed by measuring the intensity of light scattered from particles in solution over a variety of angles and concentrations. The data are extrapolated to zero angle and zero concentration. Combining the Equations 3.15 and 3.16 yields the Zimm plot equation

$$\frac{KC}{R_\theta} = \frac{1}{M_W}\left(1 + \frac{1}{3} q^2 R_g^2\right) + 2A_2 C \tag{3.17}$$

q, the scattering vector for vertically polarized light, is denoted by

$$q = \frac{4\pi n_o \sin\left(\frac{\theta}{2}\right)}{\lambda} \tag{3.18}$$

where n is the refractive index of solvent, θ is the scattering angle, and λ_o is the wavelength of the incident laser light in a vacuum.

In the plot $\frac{KC}{R_\theta}$ vs. $q^2 + kc$ over a series of concentrations and angles, the two slopes ($\frac{R_g^2}{3M_w}$ and $2A_2$) and intercept ($\frac{1}{M_w}$) give M_w, R_g, and A_2.

The radius of gyration (R_g) of a particle is the root mean square distance of a particle's extremities from its center of gravity or axis. R_g is calculated differently depending on particle shape. These equations are shown in Table 3-1 below.

Table 3-1: Equations for R_g Calculation

Shape	Equation
For spheres of Radius R	$R_g^2 = (3/5)R^2$
For Thin Rods of length L	$R_g^2 = L^2/12$
Random coil of mean-square end-to-end distance <r>^{2}	$R_g^2 = < r >^2/6$

The second virial coefficient (A_2) measures the solution's non-ideality:

$$A_2 = \left(\frac{1}{2} - \chi\right) N_A \frac{V}{n_{site}} \left(\frac{N}{M}\right)^2 \quad \textbf{(3.19)}$$

A solvent's ideality and its corresponding A_2 and χ values may be found in Table 3-2 below.

Table 3-2: Relationship between Solvent Ideality and the Second Virial Coefficient

Solvent Ideality	A_2	χ
Good	> 0	< 0.5
Flory (Θ)	= 0	= 0.5
Poor	< 0	> 0.5

For smaller particles, partial Zimm plots may be used to determine the R_g of the system. Partial plots only consider angular variation and, therefore, can only be used to determine the apparent weight-average molar mass (M_w^{app}). Concentration variation is required for the determination of the actual weight average molecular weight. The Zimm equation may be simplified to

$$\frac{1}{I_{ex}(q)} = C\left(1 + R_g^2 \frac{q^2}{3}\right) \tag{3.20}$$

where I_{ex} is the excess scattering.

The excess scattering of a sample is calculated by subtracting the intensity of the liquid without the polymer from the intensity of the solution.

$$I_{ex} = I_s - I_l \tag{3.21}$$

where I_s is the intensity of the solution of dissolved polymer and I_l is the intensity of the liquid without polymer.

Using the partial Zimm equation, the R_g may be determined by the slope and intercept of a $\frac{1}{I_{ex}(q)}$ vs. q^2 plot[23].

3.6.2 Dynamic Light Scattering

Dynamic Light Scattering (DLS) measures the fluctuation of intensity of scattered light with time. These fluctuations can be caused by translational diffusion, from the motion of particles as they move in and out of the scattering volume and from the rotations of non-spherical particles within the scattering volume. Therefore, correlation functions of the intensity fluctuations with time, and the

scattered properties may be used to describe the response of molecules to the transferred kinetic energy from the incident light.

DLS correlates the intensity fluctuation over a short time scale (μs) to determine the diffusion coefficient (D_T), hydrodynamic size (R_h), polydispersity and particle size distribution. DLS measurements yield the relaxation distribution function at different scattering angles. The modes of the relaxation distribution observed correspond to the sizes of particles present. For example, a monomodal distribution indicates that the system is monodispersed.

During a DLS experiment, the temporal intensity fluctuations (intensity vs. time) are measured by a photon counter to obtain I(t). Using Equation 3.22, the second order intensity autocorrelation function is obtained.

$$\boldsymbol{g_2(\tau) = \frac{\langle \frac{I(t)}{t+\tau} \rangle}{\langle I(t)^2 \rangle} = \lim_{T\to\infty} \frac{1}{T} \int_0^T \frac{I(t)/(t+\tau)dt}{I(t)^2}} \quad \textbf{(3.22)}$$

where $I(t)$ is the intensity of scattered light at time t and τ is the delay (the amount that a duplicate intensity trace is shifted from the original curve before the averaging is performed).

The $\frac{I(t)/(t+\tau)}{I(t)^2}$ is often plotted against the lag time (τ).

Using a non-linear least squares fitting algorithm, the autocorrelation function is then converted to the decay rate distribution.

$$\boldsymbol{g_1(\tau) = \left(1 - g_2(\tau)\right) = \int w(\Gamma) e^{(-\Gamma\tau)} d\Gamma} \quad \textbf{(3.23)}$$

Graph τA(τ) vs. log (τ) over a various angles.

The diffusion coefficient (D_T) is given by

$$\boldsymbol{D_T = \frac{\Gamma}{q^2}} \tag{3.24}$$

where Γ is the decay rate, and q is the magnitude of the scattering vector. A different coefficient is measured for each measurement angle.

Here q is the magnitude of the scattering vector and is given by

$$\boldsymbol{q = \frac{4\pi n_o \sin(\frac{\theta}{2})}{\lambda}} \tag{3.25}$$

where n_o is the solvent's index of refraction, λ = is the vacuum wavelength of incident light and θ is the scattering angle.

A linear relationship in the plot of Γ vs. q^2 confirms that the shift in distribution function with changing angle is caused by the translational diffusion of the particles[24].

The hydrodynamic radius (R_h) is the radius of a hypothetical hard sphere that has the same diffusion speed as the particles. Although these hard spheres do not exist in reality, the hydrodynamic radius is calculated from the diffusional properties and can be used to infer the apparent size of the solvated sample particle. The diffusion constant can be used to calculate R_h of a diffusing sphere via the Stokes- Einstein Equation.

$$\boldsymbol{R_h = \frac{k_B T}{6\pi\eta D_T}} \tag{3.26}$$

where R_h is the hydrodynamic diameter, k_B is the Boltzmann's constant, T is the absolute temperature, η is the viscosity, and D_T is the diffusion coefficient.

3.6.3 Conformational Ratios

The parameter ρ compares R_g and R_h, and this value is commonly used to indicate the morphology of microstructure of the aggregates[25].

$$\boldsymbol{\rho = \frac{R_g}{R_h}} \qquad \textbf{(3.27)}$$

Table 3-3 displays the corresponding conformation information[24].

Table 3-3: Conformational Information from R_g/R_h

$\frac{R_g}{R_h}$	Structure
< 0.6	Core-shell
~ 0.774	Hard Sphere
~ 1	Vesicle
~ 1.5	Gaussian Chain
> 2	Long Rod

3.6.4 Sample Preparation

In light scattering experiments, two major issues must be considered to achieve meaningful results. The first is stray light and the second is dust. To prevent stray light from affecting the detector, the LS

goniometer was carefully aligned, the laser was properly maintained, and the vat and sample cells were checked for scratches. Dust is considered to be any undesirably large scatterer that may contribute to the signal detected. These particles can lead to systematic errors and increase measurements of molecular weight, average size and size distribution. Dust scatterers are more problematic in polar solvents and when the signal is measured at lower angles.

To minimize dust scattering, samples must be prepared with extreme care. A three step process is used to remove dust from samples before measurements: solvent purification, cell cleaning and solution preparation. The water solvent used is first deionized to remove any ions that may induce stability or flocculation and, thus, affect the shape and scattering of the sample molecules. The water solvent is then purified by the Millipore Milli-Q Advantage System to reach a conductivity of 18.2 MΩ-cm and a total organic content less than 5 ppb. Trace amounts of organic material may alter the Rayleigh ratio of a sample and affect the intensity measurements. For cell cleaning, the cells are first rinsed with purified water. After, they are placed in the oven upside down to dry. The samples are then prepared using the purified solvent. The sample is passed through a 0.45μm Millipore mixed cellulose ester (HAWP) membrane filter that has been pre-flushed with purified water. The samples are centrifuged for 30-60 mins at a speed of 4500 rpm immediately before use. All apparatuses used in the preparation of light scattering samples are pre-cleaned with purified water. Samples are treated with extreme care. Once prepared, they should not be shaken as this may cause dissolution of air into the solvent. The samples are used within 2-3 days to discourage bacterial growth.

Chapter 4

Self-Assembly of PEO-block-PNIPAM/α-CD system

4.1 Introduction

Block copolymers composed of hydrophilic and hydrophobic blocks are able to spontaneously self-assemble into various ordered micellar structures[1-4]. The hydrophobic segments self-organize into spherical nanostructures comprising a hydrophobic core and hydrophilic shell that enhances the stability of the system in aqueous medium. These polymeric micelles have attracted the attention of the scientific community due to the potential use of these nanostructures for applications, such as controlled drug delivery[5-10] and catalysis[11]. The most common micellar morphologies include spherical-, cylindrical-, and vesicle-shaped micelles. The size and shape of these micelles are dependent on the curvature between the condensed phase and the extended phase. The curvature is determined by the volume fraction of each block and environmental factors, such as solvent polarity, ionic strength, temperature and pH[12].

Stimuli-sensitive copolymers with inclusion complex capabilities are extremely interesting as they have the ability to form hierarchical self-assembled structures with multiple control elements. PEO-b-PNIPAM is one of these polymers and can be developed to produce novel materials that allow for precise control of architecture. The PNIPAM component is temperature sensitive and collapses at around 32 °C. PEO-b-PNIPAM has been found to micellize above the LCST, forming a hydrophobic PNIPAM core and hydrophilic PEO corona[13]. PEO is a biocompatible polymer that is FDA approved for biomedical applications[14, 15] and Pluronics are commercially available as drug delivery vehicles[16-18]. PEO can increase the biocompatibility of synthetic materials due to its high solubility and minimal interfacial energy[19]. Since the PEO segment has the ability to complex with α-CD, this project seeks

to investigate the self-assembly behavior of stimuli-sensitive block copolymer inclusion complexes of PEO-b-PNIPAM and α-CD.

4.2 Synthesis of PEO-co-PNIPAM

4.2.1 Materials

Poly(ethylene glycol) methyl ether (98.5 % purity, MW = 4970, PDI = 1.04), N-isopropylacrylamide (NIPAM, 97 %), 2-bromoisobutyryl bromide (98 %), copper (I) bromide (CuBr, 99.999 %), and isopropyl alcohol (99.5 %) were purchased from Sigma Aldrich (Missouri, USA). Tris(2-aminoethyl)amine (TREN, 96 %) was purchased from ACROS Organics (Geel, Belgium). Triethylamine (99 %), formic acid (98 %), formaldehyde solution (37 %), hydrochloric acid (HCl, PUR), and hexane (99.95 %), were purchased from Fisher Scientific (New Hampshire, USA). Sodium hydroxide (NaOH), methanol (99.8 %), methylene chloride (99.5%), and tetrahydrofuran (THF, reagent grade) were purchased from Caledon Lab Chemicals (Ontario, CAN). Benzene (ACS grade) was purchased from EMD Chemicals (New Jersey, USA). HPLC grade toluene (99.9+ %) was purchased from Honeywell (New Jersey, USA). Argon (99.998 % oxygen free) was purchased from Praxair (Connecticut , USA). Poly(ethylene glycol) methyl ether and NIPAM were stored in the refrigerator. Water was purified through a Millipore Milli-Q Advantage System (Millipore Corporation; Massachusetts, USA).

4.2.2 Synthesis of PEG Macroinitiator

The synthesis of the PEG macroinitator was performed according to the scheme in Figure 4.1. 1.0 g poly(ethylene glycol) methyl ether (PEO-OH, MW=5000 Da) was dissolved in 85 mL of dried HPLC grade toluene in a 100 mL round bottom flask. Azeotropic distillation was performed on the solution

using a 5 mL stark trap. The solution was then cooled to 0 °C. After cooling 50 µL triethylamine was added under constant stirring, and then 50 µL 2-bromoisobutyryl bromide was then added via syringe over a period of 1 hour. The reaction mixture was stirred overnight at room temperature, and then filtered hot to remove triethylamine hydrobromide. After filtration, the solution was concentrated (by either rotary evaporation or vacuum oven) and precipitated in a 10-fold excess of cold hexane. The precipitate was then filtered off and dried under vacuum. The powder was redissolved in dried HPLC grade toluene, and this reaction process was repeated to ensure complete coupling of end groups. The polymer was then dissolved in water, adjusted to pH 8-9 using NaOH, and extracted three times with dichloromethane. The organic layers were collected and dried in the vacuum oven. The remaining solid was dissolved in THF and precipitated in 10-fold excess of cold hexane, and the resulting white powder was collected via vacuum filtration.

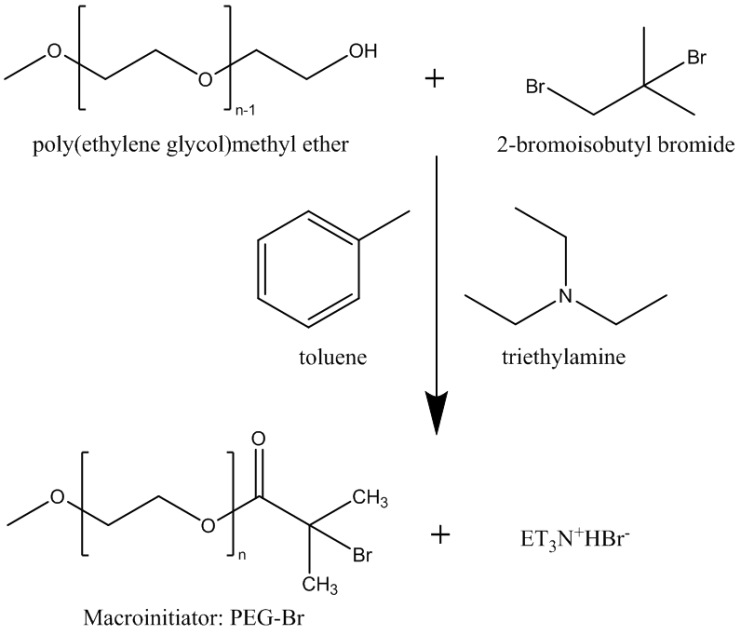

Figure 4.1: Synthesis scheme for PEO-Br macroinitiator.

4.2.3 Synthesis of Tris(2-(dimethylamino)ethyl)amine (Me_6TREN)

First, hydrochloric salt of TREN ($ClNH_3CH_2CH_2)_3$) was prepared by adding 30 mL of 3.0 M HCl in methanol dropwise to a solution of 4.0 mL TREN and 50 mL methanol. The mixture was stirred at room temperature for one hour. The resulting white precipitate was collected by vacuum filtration and carefully washed using 50 mL of methanol. Then, the Me_6TREN was synthesized by dissolving the salt in a mixture of 45 mL formaldehyde (37 % (w/w)), 45 mL formic acid (90 % (w/w)), and 10mL of water. The mixture was refluxed overnight at 95 °C. After cooling to room temperature, the volatile fractions were removed by rotary evaporation. The distinctly brown residue was treated with a saturated sodium hydroxide aqueous solution at pH > 10, producing an oily layer that was repeatedly extracted into methylene chloride three times. The organic phase was dried in a vacuum oven to produce a yellow oil.

4.2.4 Synthesis of PEO_{110}-*b*-$PNIPAM_{243}$ using ATRP

The synthesis of the PEO-b-PNIPAM was performed according to the scheme in Figure 4.2. NIPAM was purified by recrystallization in a benzene/n-hexane mixture and dried in a vacuum. 0.5 g of PEG-Br, 0.05 g CuBr, and 3.0 g NIPAM were added to a 20 mL solvent mixture of isopropyl alcohol and water (1:1 by volume) in a schlenk flask. The solution was degassed using the "freeze-pump-thaw" method until no gas bubbles evolved during the thawing stage. 0.1 g of Me_6TREN ligand was purged with argon and added to the reaction flask. Polymerization was performed at 0 °C for 24 hours. The synthesis medium was transferred into a Spectra/Por$^{(R)}$ molecular porous membrane tubing having a molecular weight cut off of 3500 Da. The solution was dialysized for two weeks at room temperature while replacing the Millipore water every day. The resulting solution was then transferred to a dialysis tubing having a molecular cut off of 12 000 - 14 000 Da. and dialysized

against Millipore water for an additional two weeks at 40 °C. The sample was centrifuged, and the polymer solution was frozen and the water sublimated at low pressure in the freeze-drying process (FreeZone 1L Benchtop Freeze Dry System; Labconoco Corporation; Missouri, USA) to yield a white powder.

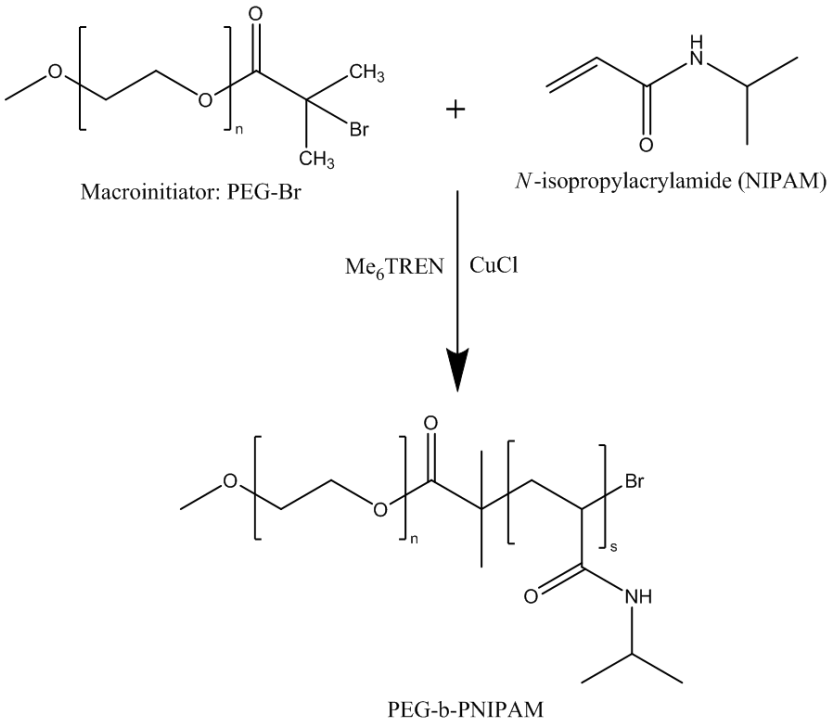

Figure 4.2: ATRP synthesis scheme for PEO-b-PNIPAM.

4.3 Measurements

4.3.1 Sample Preparation

The polymer solutions were prepared individually by dissolving PEO-b-PNIPAM in purified Millipore water, unless otherwise specified. For the study of PEO-b-PNIPAM/α-CD complexes, the appropriate amount of α-CD (98 %; Sigma Aldrich; Missouri, USA) was added to the PEO-b-

PNIPAM solutions. The resulting solution was stirred and agitated ultrasonically to promote dissolution. The samples were then stored overnight prior to use to allow time for the self-assembly process to reach an equilibrium. All samples were stored in the refrigerator until use.

4.3.2 Characterization

^{1}H NMR analyses on the polymer samples for synthesis characterization were conducted using a Bruker 300 MHz high resolution Ultra Shield™ spectrometer (Bruker BioSpin Corporation; Massachusetts, USA). Morphology characterization experiments were conducted with a Bruker 600 MHz high resolution Ultra Shield™ spectrometer (Bruker BioSpin Corporation; Massachusetts, USA).

Gel Permeation Chromatrography (GPC) system was used to determine the distribution and PDI of polymer samples. The GPC system consisted of a Millipore pump, a Wyatt MiniDawn light scattering detector and a Millipore Waters 410 differential refractometer (Waters Corporation; Massachusetts, USA). The data was analyzed using the Advanced Sysinfo Tool and Reporting Assistant for Windows software (Sysinfo Lab).

Surface tension data was obtained using a DataPhysics dynamic contact angle meter and tensiometer (DataPhysics Instruments; Filderstadt, Germany) equipped with a Wilhelmy plate, based on the increasing concentration method. For the first experiment, 0.1 wt% PEO-b-PNIPAM was titrated into 50 mL of water at 40 °C. For the second experiment, 0.1wt% PEO-b-PNIPAM in 0.009826 M α-CD was titrated into 50 mL of water at 25 °C. The surface tension data was plotted to gain information on the CMC and head group size of the systems.

Calorimetric titration measurements were carried out using a Microcal Isothermal Titration Calorimeter (ITC; Microcal, LLC; Massachusetts, USA) with a 1.4 mL sample cell in an adiabatic

shield. The stirring rate was set to 400 rpm and the time between injections was set to 250 seconds. The data were recorded automatically, and the Microcal Origin for ITC program (OriginLab, Massachusetts, USA) was used to integrate and generate differential enthalpy curves. For the ITC, a PEO-b-PNIPAM solution and α-CD solution was prepared at 0.1 wt% and 2 wt% respectively. The reference cell was filled with water. The α-CD was titrated into the polymer solution at both 25.0 ± 0.02 ^{0}C and 40.0 ± 0.02 ^{0}C.

Additional calorimetric experiments were conducted using a Differential Scanning Calorimeter (DSC; Microcal, LLC; Massachusetts, USA) with a 0.5 mL sample cell, which is held in an adiabatic shield. Data on the enthalpy change due to a system's phase transition evaluated using the ORGIN software (OriginLab, Massachusetts, USA). DSC samples were prepared by adding the appropriate amount of α-CD to 0.1wt% PEO-b-PNIPAM. DSC measurements were conducted from 10 to 90 ^{0}C in both upscan and down scan directions.

The microstructure of the sample was examined by a Brookhaven Laser Light Scattering system (Brookhaven Instruments Limited; Worcestershire, UK). The system has a BI200SMv2 goniometer, TurboCorr Coorelator and a MiniL-20 636 nm laser. The DLS time-correlation functions were analyzed using the GENDIST software package with the probability of reject set to 0.5. The autocorrelation functions were used to compute the particles' diffusion coefficients, which were then used to compute the R_h of the particles. Dn/dc measurements were conducted using a Brookhaven BI-DNDC differential refractometer (Brookhaven Instruments Limited; Worcestershire, UK).

4.4 Polymer Characterization

4.4.1 Nuclear Magnetic Resonance (NMR)

NMR experiments were performed on PEO-Br, Me_6TREN, and PEO-b-PNIPAM. The spectras are shown in Figure 4.3, Figure 4.4, and Figure 4.5, respectively. The ^{1}H NMR spectras revealed that the hydroxyl group of PEO-OH was fully esterified and the PEO-b-PNIPAM was synthesized successfully. The molecular weight of the polymer was calculated using the integration of the PEO peaks to the PNIPAM peaks (1.15 and 3.6 ppm, respectively). The molecular weight of the polymer was determined to be 32, 500 g/mol, which corresponded to approximately 90 % conversion of the NIPAM monomer.

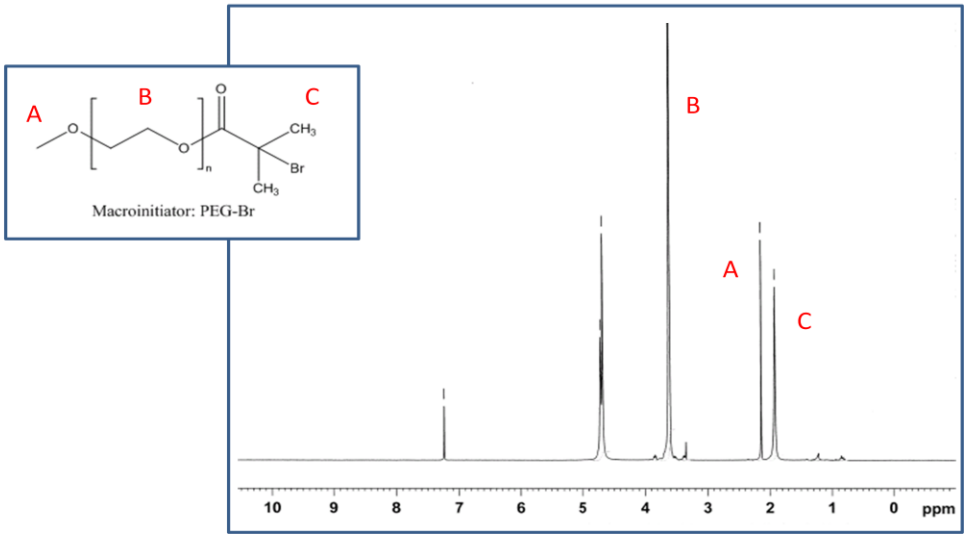

Figure 4.3: NMR spectra for PEO-Br in $CDCl_3$.

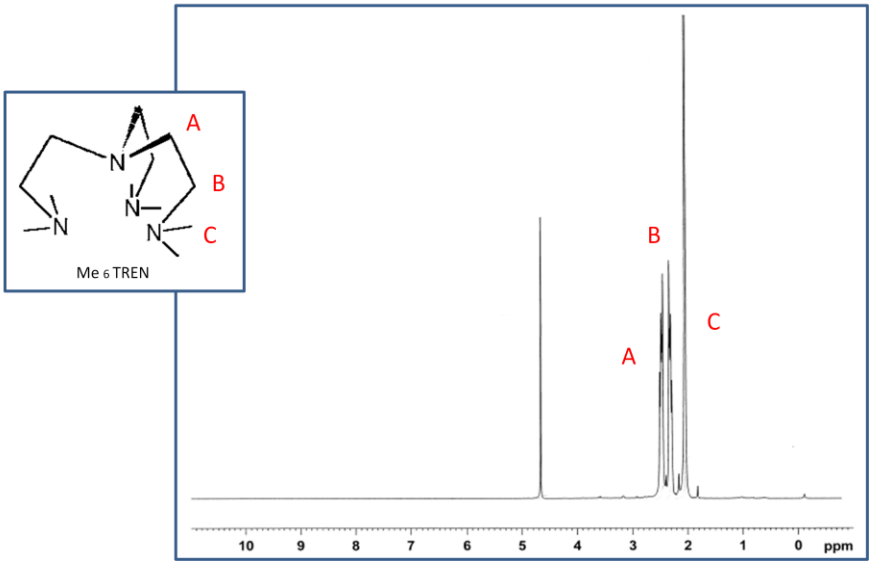

Figure 4.4: NMR spectra for Me_6TREN in D_2O.

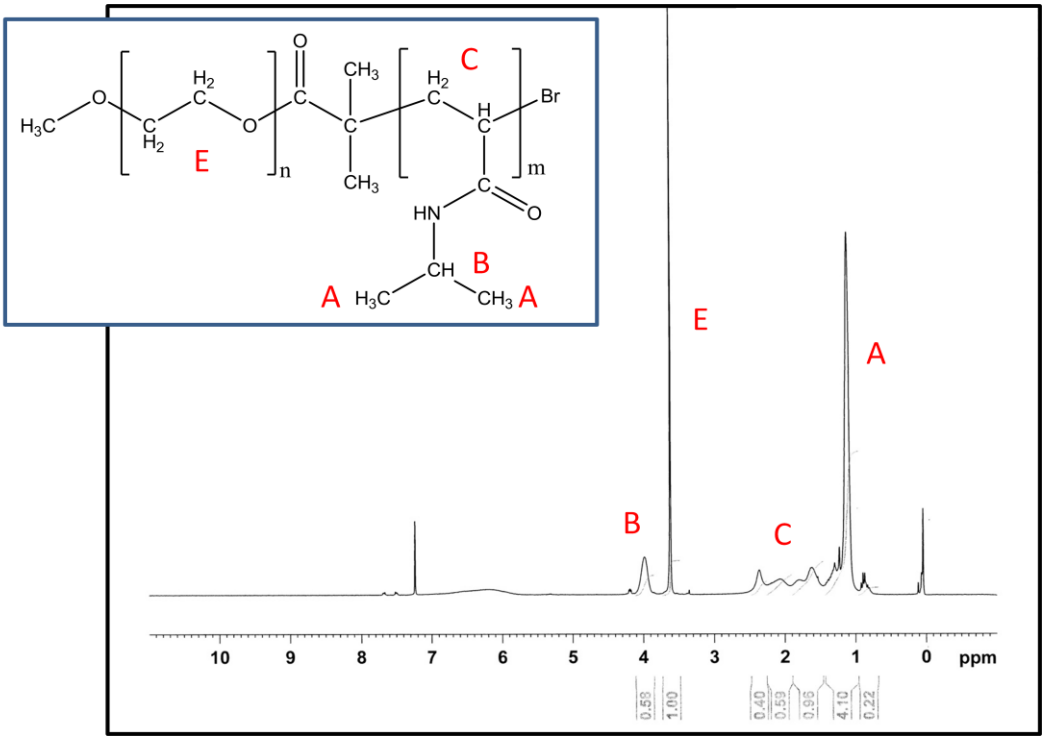

Figure 4.5: NMR spectra for PEO-b-PNIPAM in $CDCl_3$.

4.4.2 Gel Permeation Chromatography

Figure 4.6 shows the GPC traces of the PEO-OH starting material and the final PEO-b-PNIPAM product. The final polymer had a lower retention volume than that of the starting material, and this was evidence of polymerization since higher weight polymers elute faster through the column. Both graphs showed a unimodal distribution which confirmed that only one size of polymer existed in both samples. The GPC showed a PDI of 1.2 for the PEO-OH and 1.6 for PEO-b-PNIPAM. The PDI of PEO-OH is stated to be 1.04 by Sigma Aldrich.

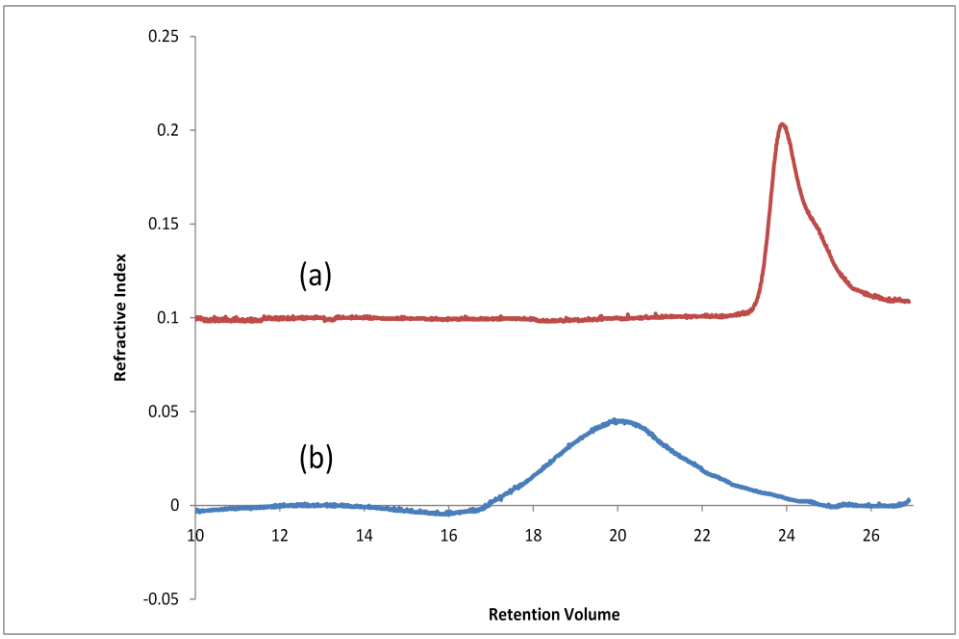

Figure 4.6: GPC trace for (a) PEO-OH and (b) PEO-b-PNIPAM.

4.5 Results and Discussion

4.5.1 Observations

PEO-b-PNIPAM solutions of 0.1 wt% were clear at room temperature which suggested that both segments were hydrophilic, and the polymer behaved as free chains. Increasing the temperature above the LCST caused the solution to become opaque; however, the particles did not agglomerate to form precipitates like PNIPAM homopolymers, which was an indication of micellization. The PNIPAM segments most likely formed the core and the PEO segments stabilized the particles by forming the surrounding corona.

The addition of α-CD to the PEO-b-PNIPAM solution did not change the visual characteristics of the solution below the LCST. Above the LCST, the solution became stable and opague (Figure 4.7).

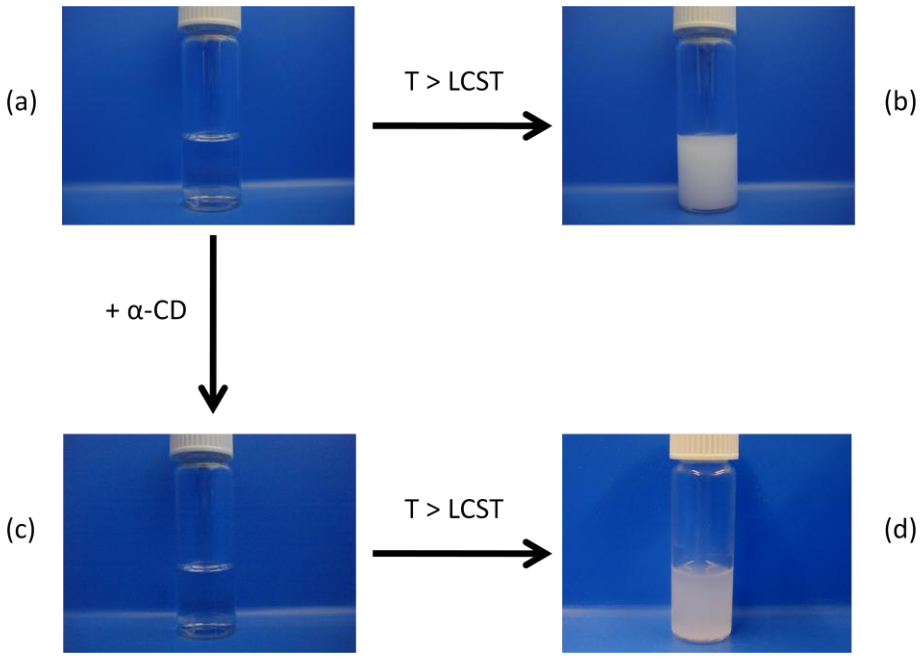

Figure 4.7: Photographs of PEO-b-PNIPAM solutions at various conditions: (a) 25 °C, (b) 40 °C, (c) 25 °C with α-CD, and (d) 40 °C with α-CD

4.5.2 Surface Tension

CMC is an important property used to characterize the self-assembly property of aqueous block copolymer solutions. The CMC is defined as the minimum concentration at which the copolymers self-assemble into micellar aggregates and is usually linked to a sharp change in solution properties, such as surface tension, turbidity and viscosity. The Wilhelmy pate method was used to measure the surface tension by titrating 0.1wt% polymer solutions into water. A plot of surface tension with polymer concentration allows the determination of the critical micellar concentration of the polymer solutions. Surface tension measurements of 0.1 wt% PEO-b-PNIPAM at 40 °C and of 0.1wt% PEO-b-PNIPAM in 0.00695 M α-CD at 25 °C are shown in Figure 4.8, and their CMC values are 0.00058 g/L and 0.0012 g/L, respectively. The CMC was obtained from the plot by extrapolating two lines from the linear regions of the last two segments and locating the intercept. Below the CMC, the surface tension decreased with increasing polymer or polymer/CD concentration due to the localization of molecules at the air-water interface. Above the CMC, the air-water interface was saturated, and the reduction in the surface tension with concentration decreased as micellar aggregates were formed. In both cases, free energy was minimized. From Figure 4.8, it can be observed that the CMC of PEO-b-PNIPAM was comparatively lower than that of PEO-b-PNIPAM/α-CD, which indicated that the hydrophobic PNIPAM segments were less soluble than the PEO/α-CD complexes. The surface excess concentration was used to calculate the head group area of the molecules. For PEO-b-PNIPAM and for PEO-b-PNIPAM/α-CD, the areas were 29.2 $Å^2$ and 14.7 $Å^2$. Smaller polymer aggregates partition to the air-water interface with a higher packing efficiency that individual polymer chains[20]. The diameter of α-CD is approximately 4.5 Å[21]. The area of a single α-CD corresponded closely with the surface area/molecule of PEO-b-PNIPAM/α-CD. This indicated that the α-CD included column structures stand perpendicular to the water surface.

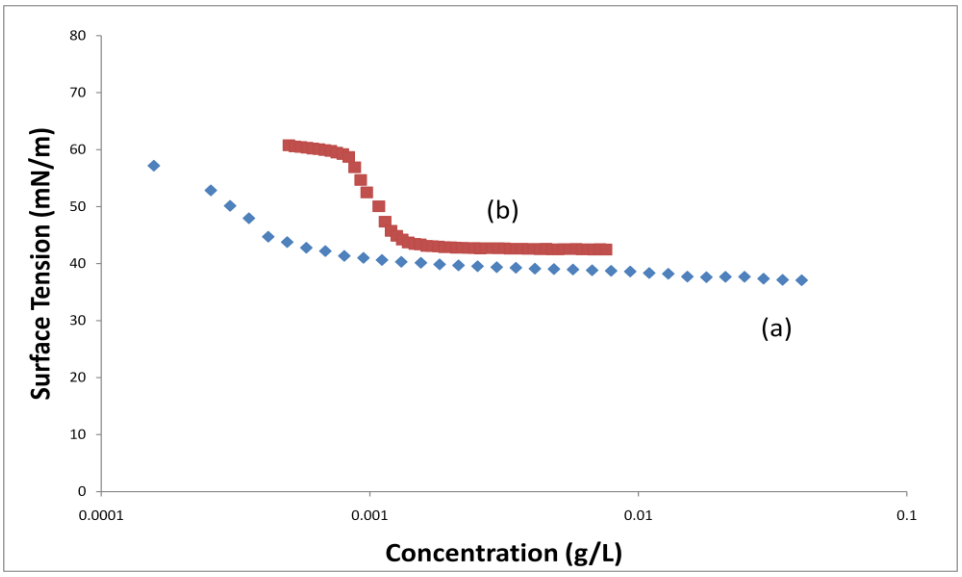

Figure 4.8: Surface tension data from the (a) titration of PEO-b-PNIPAM at 40 °C (b) titration of PEO-b-PNIPAM/α-CD at 25 °C.

4.5.3 Isothermal Titration Calorimetry

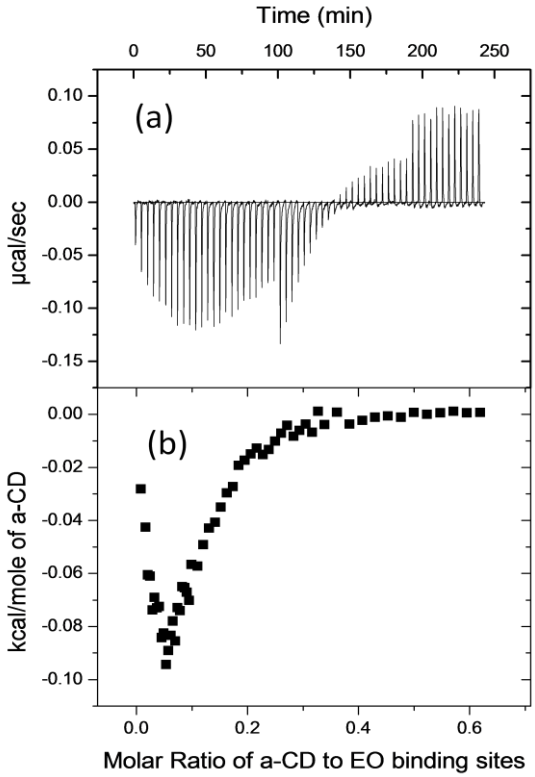

Figure 4.9: Calorimetric titration of 2 wt% α-CD into 0.1 wt% PEO-b-PNIPAM solution at 25 °C. (a) Thermogram showing the cell feedback power versus time. (b) Differential enthalpy versus molar ratio of α-CD to EO binding sites.

ITC was used to characterize the thermodynamics of binding and the self-assembly of polymer systems. Calorimetry measurements were conducted as α-CD was titrated into the PEO-b-PNIPAM solution at both 25.0 ± 0.02 ^{0}C and 40.0 ± 0.02 ^{0}C. In both cases, the raw data resulting from titrating α-CD into PEO-b-PNIPAM solutions were subtracted from the titration isotherm for α-CD into water and integrated to attain the ΔH binding curve. Figure 4.9 shows the titration of 2 wt% α-CD into 0.1 wt% PEO-b-PNIPAM at 25 ^{0}C. A clear binding curve can be seen with a binding ratio of

approximately 38 %. The threading of α-CD was impeded by the self-assembly of the system. The initial data points did not fit in a traditional ΔH CD binding curve. PEO is known to aggregate into three dimensional network structures[22]. As CD is titrated, the hydrogen bonds and hydrophobic interactions that created these network structures must first be broken before CD threading can occur. Further evidence of the existence of these structures were shown by LLS and discussed in Section 4.5.4. The initial data points were removed, and a three-site sequential binding model (Equations 3.4-3.9) was used to fit the calorimetric data of binding. The results are displayed below in Table 4-1.

Table 4-1: Calorimetric Data from Three-Site Sequential Binding Model for PEO-b-PNIPAM/α-CD.

	1	2	3
K (L/mol)	$9.04 \times 10^4 \pm 1.3 \times 10^4$	$1.04 \times 10^5 \pm 2.1 \times 10^4$	$1.11 \times 10^5 \pm 3.0 \times 10^4$
ΔH (cal/mol)	-158.5 ± 7.79	549.4 ± 41.0	-757.7 ± 95.6
ΔS (cal/mole/K)	22.1	24.8	20.5

The fitting of the three site model indicated three sequential events occurring as α-CD was added. It is believed that the first was the threading of α-CD to the PEO segment; the second was the formation of a simple micellar structure; and the third was the formation of a more complex aggregated structure.

Figure 4.10 shows the titration of 0.2 wt% α-CD into 0.1 wt% PEO-b-PNIPAM at 40 ^{0}C. In contrast to Figure 4.9, no binding curve resulted. At 40 ^{0}C, since no α-CD threading was shown by the ITC results, it was believed that the polymer system would exhibit properties similar to those of

the blank polymer without (α-CD); the PEO-b-PNIPAM formed micelles with PNIPAM cores. α-CD is known to have difficulty threading at elevated temperatures[23].

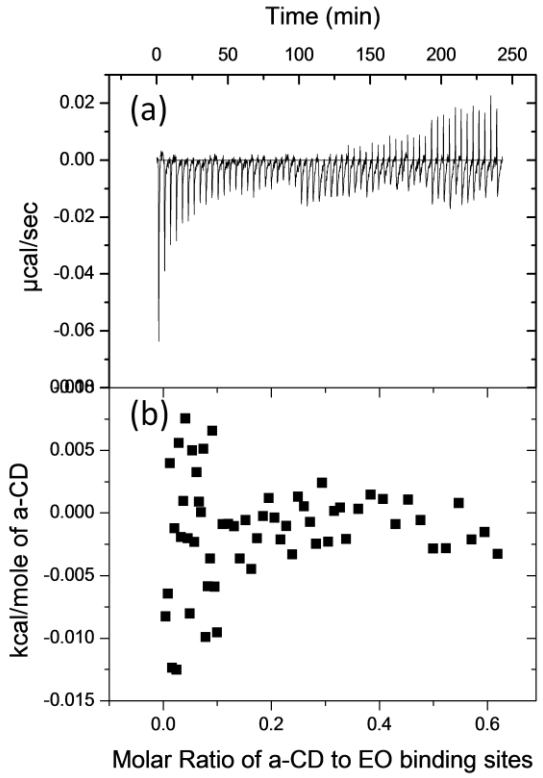

Figure 4.10: Calorimetric titration of 2 wt% α-CD into 0.1 wt% PEO-b-PNIPAM solution at 40 °C. (a) Thermogram showing the cell feedback power versus time. (b) Differential enthalpy versus molar ratio of α-CD to EO binding sites.

4.5.4 Light Scattering

The size and conformation of the self-assembled morphology of PEO-b-PNIPAM and PEO-b-PNIPAM/α-CD over a range of temperatures was studied using dynamic and static light scattering techniques. For DLS, the temporal intensity fluctuations for a sample were measured at 60°, 75°, 90°, 105°, 120°, 135°, and 150°. The data from the detector was transferred to the GENDIST (General

Distribution) software package to perform the inverse Laplace transform. GENDIST uses the REPES (Regularized Positive Exponential Sum) algorithm, which was developed by Jakes at the Institute for Macromolecular Chemistry in Prague[24]. REPES is a mode-free fitting model that calculates the transform using a second order regularizer, and the fitting is performed directly on the intensity of the autocorrelation function $g_2(t)$, rather than on the field autocorrelation function $g_1(t)$. The probability of rejection was set to 0.5. The outputs from GENDIST were then transferred to Origin for plotting and further data analysis. The distribution functions of relaxation times were normalized, and a representative plot of 0.1 wt% PEO-b-PNIPAM in 0.00695 M α-CD at 45 °C is displayed in Figure 4.11. Due to the translational diffusion of particles, the figure shows distinct peaks that are shifted to lower relaxation times with increasing scattering angles. A linear relationship in the plot of Γ vs. q^2 was used to confirm that the scattering is attributed to translation diffusion. Using Equations 3.24 and 3.25, a plot of Γ vs. q^2, like the one displayed in Figure 4.12, may be generated. The average diffusion coefficient or the particles was obtained from the slope of the Γ vs. q^2 plot. Using the Stokes-Einstein equation (Equation 3.26), the R_h was calculated. For the representative sample, the particle size was determined to be 129.7 nm.

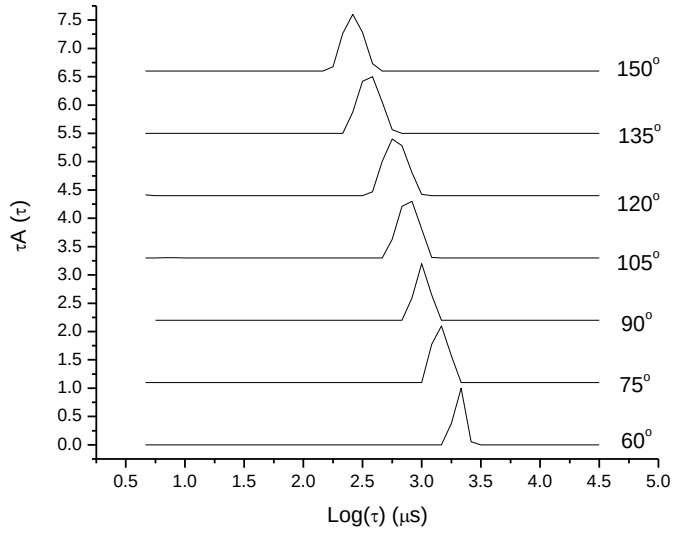

Figure 4.11: Characteristic distribution functions of relaxation times for 0.1 wt% PEO-b-PNIPAM in 0.00695 M α-CD at 45 °C.

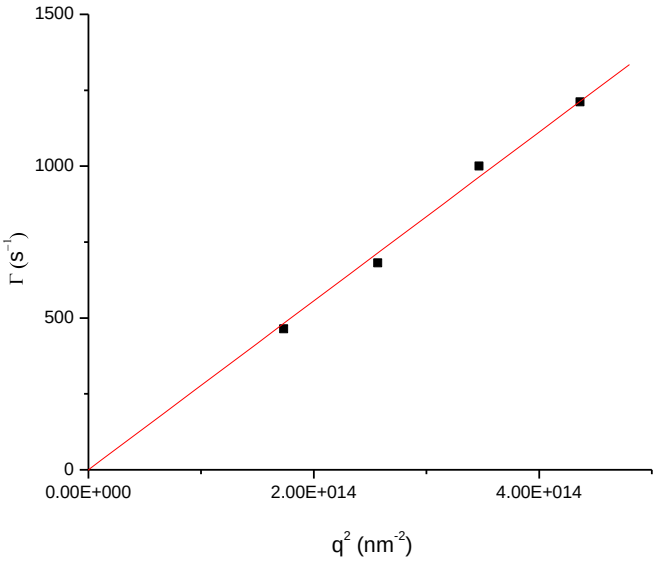

Figure 4.12: Plot of Γ vs. q^2 in the determination of particle coefficient for 0.1 wt% PPO-b-PMAA in 0.00695 M α-CD at 45 °C.

For SLS, the time-averaged intensities of scattered light for a sample was measured at angles ranging from 50° to 150° in 10° intervals. For single concentration samples, the partial Zimm equation (Equation 3.20) was used to determine the R_g values. Light scattering analyses for polymer systems at different temperatures were analyzed using the same method.

Dn/dc measurements were performed on the PEO-b-PNIPAM sample and the dn/dc was found to be $1.642 \times 10^{-1} \pm 2.6 \times 10^{-3}$ mL/g. Count rate measurements were performed for 0.1 wt% PEO-b-PNIPAM and 0.0025 wt% PEO-b-PNIPAM in 0.000174 M α-CD. Their results are displayed in Figure 4.13 and Figure 4.14. Below the LCST, PEO-b-PNIPAM chains were hydrophilic, and they existed as unimeric chains as indicated by the low count rate. Above the LCST, micelles were formed, and this corresponded to a large jump in count rate. Similarly, for the PEO-b-PNIPAM/α-CD sample, supramolecular structures formed at low temperature; but, at low concentrations, these structures did not scatter light intensely either. Above the LCST, a sudden increase in count rate occurred, which corresponded to aggregation in the system.

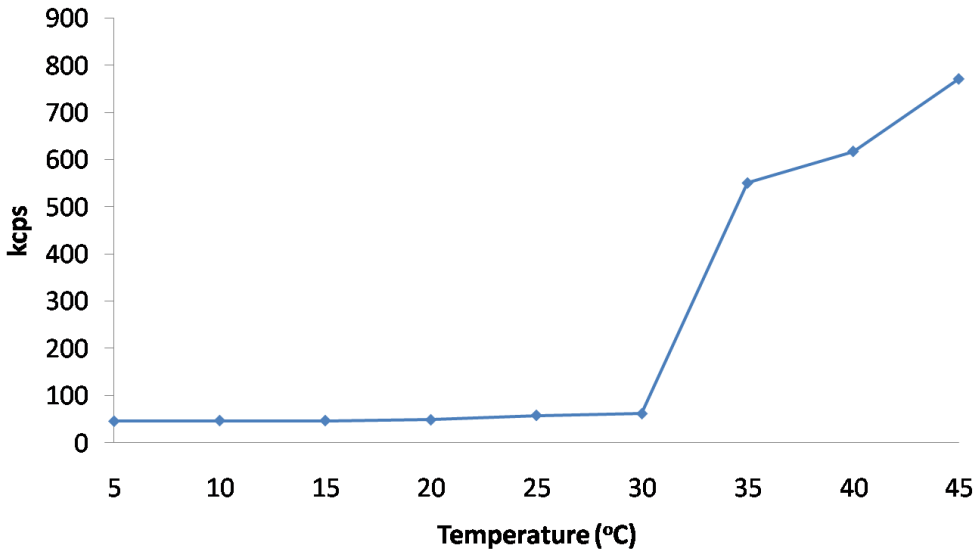

Figure 4.13: Plot of count rate versus temperature for 0.1 wt% PEO-b-PNIPAM.

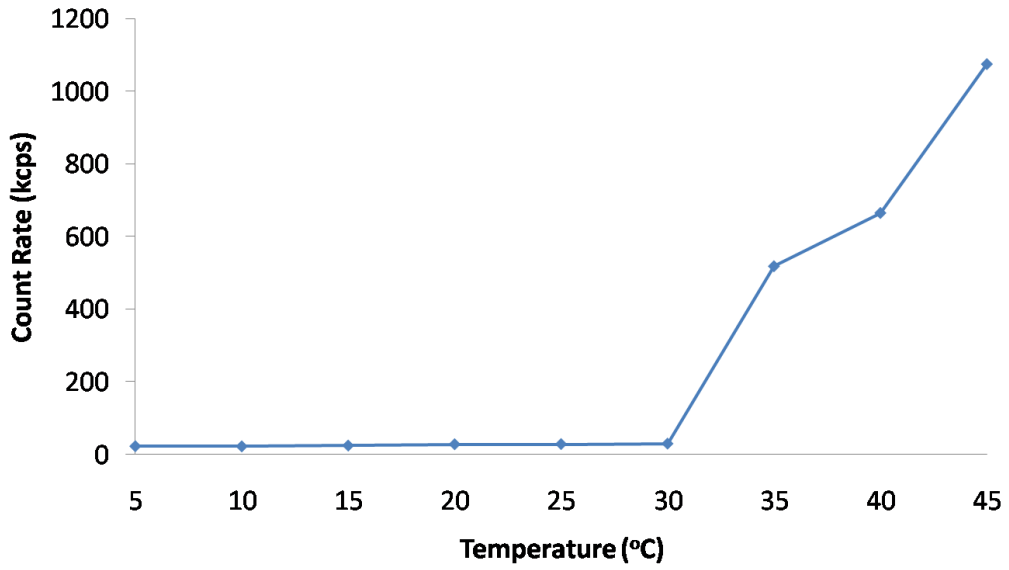

Figure 4.14: Plot of count rate versus temperature for 0.0025 wt% PEO-b-PNIPAM in 0.174 mM α-CD.

Due to large scattering of the PEO-b-PNIPAM/α-CD structures, the count rate experiment for PEO-b-PNIPAM/α-CD was performed at lower concentration, laser strength, and pin hole size. The 0.1 wt% PEO-b-PNIPAM started at 45.1 kcps and increased to 770.6 kcps, and the 0.0025 wt% PEO-b-PNIPAM/α-CD increased from 21.8 to 1074.5 kcps. This difference in count rate increase indicated that the change of the PEO-b-PNIPAM/α-CD over temperature was greater than that of PEO-b-PNIPAM only.

DLS and SLS measurements were conducted on PEO-b-PNIPAM and PEO-b-PNIPAM/α-CD samples. Below the LCST, the decay time distributions were seen to show two decay modes. PEO is known to be soluble in water at room temperature due to the formation of hydrogen bonds between the ether groups and water. However, PEO aggregation is commonly seen. There are two explanations for the aggregation of PEO into three dimensional structures. The first is the interaction

between the hydrophobic -(CH_2CH_3)- and end groups. The second are the hydrogen bonded water molecules acting as cross-linkers for the PEO clusters in solution. In the research of Dai and Tam[22], they found that samples of 0.1 wt% PEO (300 K) in water showed two angular dependent decay modes with R_h values of 26 nm and 275 nm with diffusion coefficients of 9.4×10^{-12} m^2/s and 8.9×10^{-13} m^2/s, respectively. It was determined that the fast decay mode with the small R_h values corresponded to unimeric PEO chains and the slow decay mode with the larger R_h values corresponded to the aggregation of PEO clusters. Figure 4.15 shows the time distribution for 0.1 wt% PEO-b-PNIPAM at 20 °C. Both decay modes were q^2 dependent, and, therefore, the two peaks were due to two types of particles in solution. The R_h values were determined to be 11.6 nm and 73.4 nm. The diffusion constants were determined to be 1.9×10^{-11} m^2/s and 2.9×10^{-12} m^2/s. Since the molecular weight of PEO-b-PNIPAM was much lower than that of the PEO from the Dai and Tam study, it is understandable that the R_h values determined were also lower. The 11.6 nm particles with the faster diffusion coefficient were attributed to unimeric PEO-b-PNIPAM chains, and the 73.4 nm particles with the slower diffusion coefficient were attributed to the aggregated PEO clusters. It was noted that filtration removes the aggregated particles; however, measurements must be taken immediately. This was not possible for this set of experiment due to the centrifugation in the sample preparation method, the temperature equilibration before each measurement, and the number of measurements with the sample. Above the LCST, only one decay mode was present.

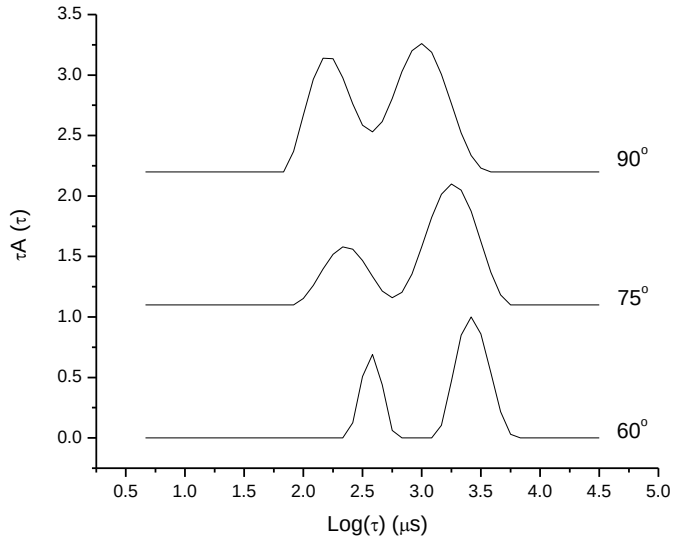

Figure 4.15: Decay distribution functions for 0.1 wt% PEO-b-PNIPAM at 20 °C.

The resulting R_h and R_g data is shown for PEO-b-PNIPAM and PEO-b-PNIPAM/α-CD samples in Figure 4.16 and Figure 4.17, respectively. For PEO-b-PNIPAM, the R_h values below the LCST were small, averaging 11.6 nm, which corresponded to free polymeric chains in solution. At the LCST, the R_h increased to over 145 nm, which clearly indicated a change in the morphology[22]. Data for R_g values were not attainable below the LCST, and this was confirmation of free chains in solution as free polymers do not display angular dependence. Figure 4.18 displays the R_g/R_h values calculated from the previous data. Above the LCST, the R_g/R_h values clearly corresponded to core-shell micelle structures, which agreed with previous reported studies[13].

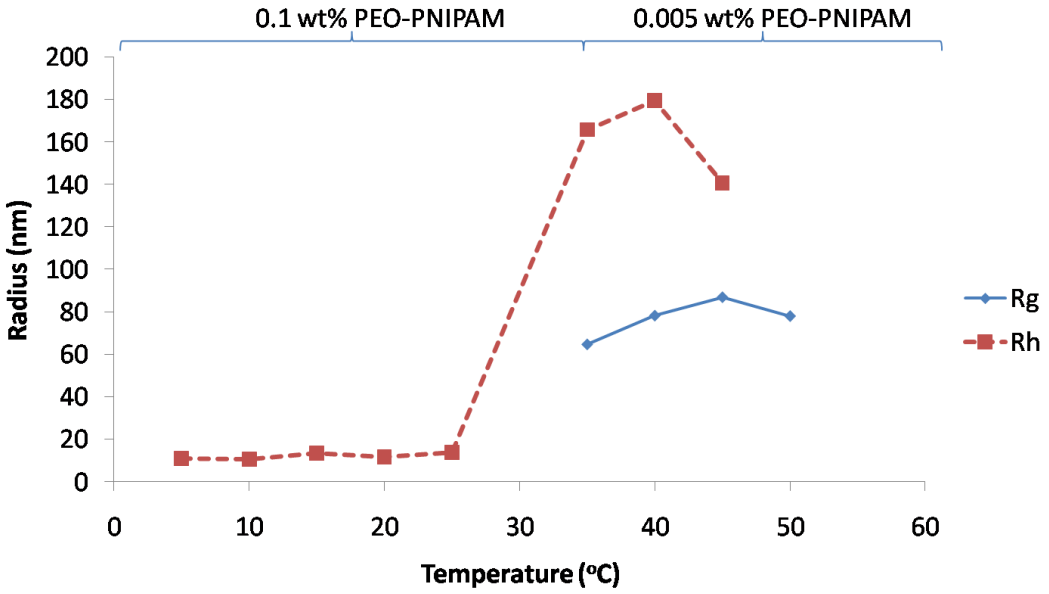

Figure 4.16: Effect of temperature on the R_g and R_h of PEO-b-PNIPAM.

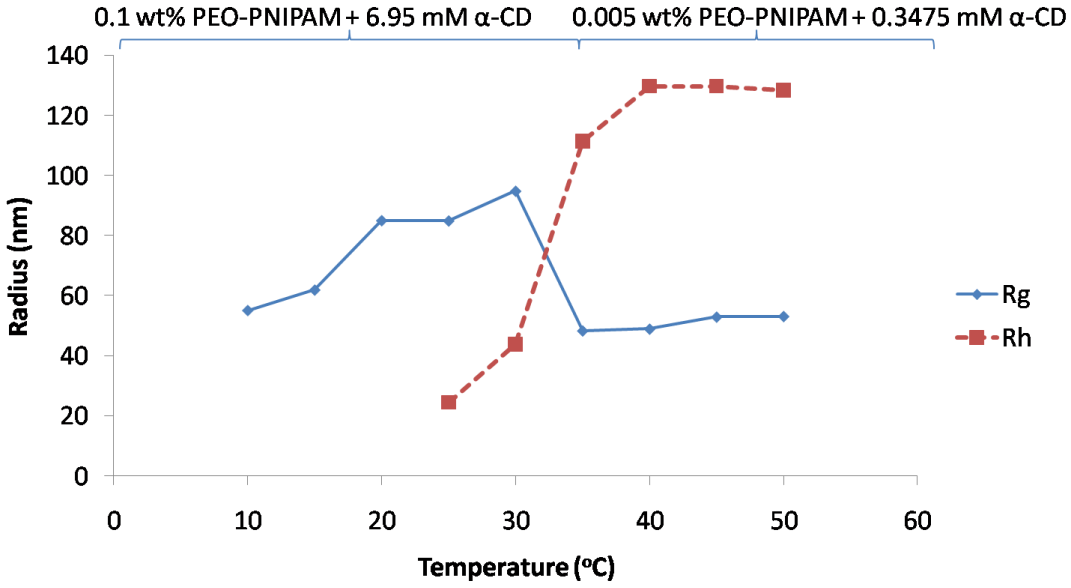

Figure 4.17: Effect of temperature on the R_g and R_h of PEO-b-PNIPAM/α-CD.

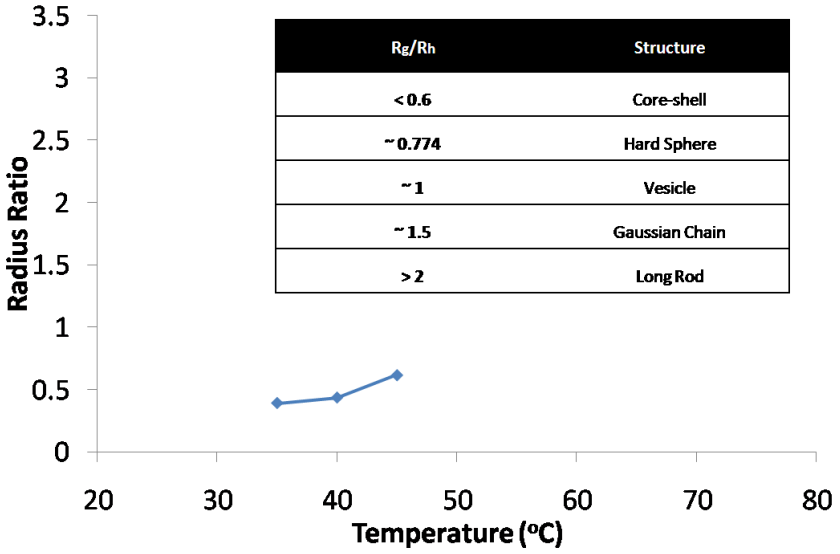

Figure 4.18: Effect of temperature on the conformational ratios for PEO-b-PNIPAM.

For PEO-b-PNIPAM/α-CD, the R_h values below the LCST were significantly larger than those of PEO-b-PNIPAM, and these values indicated that the polymer chains were not in their unimeric form. Above the LCST, R_h increased, showing a change in morphology. R_g values for PEO-b-PNIPAM/α-CD, below the LCST increased with increasing temperature. However, it should be noted that due to the condensation on the vat and the sample tube, data below 20 °C or 25 °C may be unreliable. Above the LCST, there was a sharp decrease in R_g values, which indicated possible morphological change. The R_g/R_h values are displayed in graphical form in Figure 4.20. Below the LCST, the data showed a rod-like configuration, and, above the LCST, the values corresponded to spherical micelles. The R_g/R_h values of these micelles were similar to those of blank PEO-b-PNIPAM. This indicates that the α-CD has dethreaded from the polymer, and micelles of PNIPAM core and PEO corona were formed. If the micelles were composed of PNIPAM core and PEO/α-CD corona, the R_g value of the system

would be larger than that of PEO-b-PNIPAM (due to increased weight in the corona) and the R_g/R_h values would increase. Figure 4.19 displays a schematic to illustrate this point.

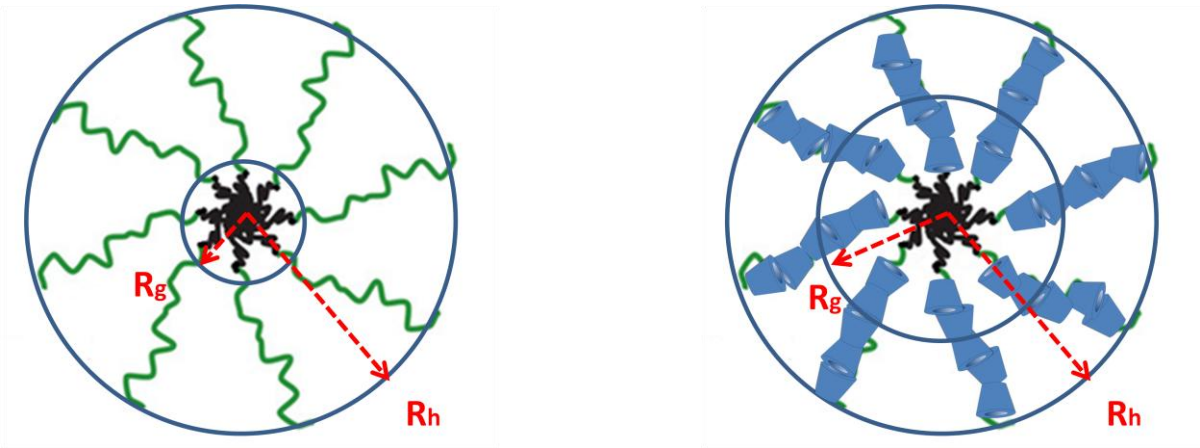

Figure 4.19: Schematic illustrating the different R_g radii resulting from two potential morphologies of the system.

DLS measurements of the samples were then performed using a vertical-horizontal polarizer. Weak correlations were found for the system at 25 °C, 90 ° angle, and at high concentration only. Insufficient data could be collected for proper analysis of the rod dimensions. However, the weak correlation indicated that the rod was flexible.

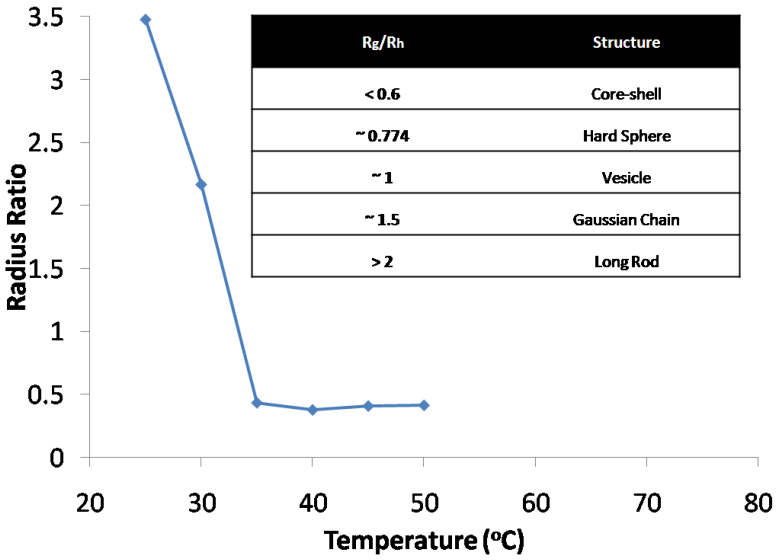

Figure 4.20: The effect of temperature on the conformational ratios for PEO-b-PNIPAM/α-CD

4.5.5 Temperature analyses with NMR

Figure 4.21 and Figure 4.22 display the ^{1}H NMR spectra of PEO-b-PNIPAM and PEO-b-PNIPAM/α-CD at 25 °C and 40 °C. For the block copolymer, at 25 °C, the signals at 1-2 ppm and 3.75 ppm corresponded to the PNIPAM segments. These peaks were clearly detected in the spectrum and were indicative that the PNIPAM block was solvated in the solvent (D_2O). At 40 °C, the PNIPAM peaks disappeared, and the PEO peaks were observed to only show changes attributed temperature increase. This information revealed that the polymer was in free chain form, at 25 °C, and formed core-shell micelle composing of a PNIPAM core at 40 °C. For the PEO-b-PNIPAM/α-CD sample at 25 °C the signals at 1-2 ppm and 3.75 ppm corresponded to the PNIPAM segment. These peaks were clearly detected in the spectrum and were indicative that the PNIPAM block was solvated in the solvent (D_2O). The CD peaks were seen at this temperature due to an excess of CD in solution.

At 40 °C, the PNIPAM peaks disappeared, and the PEO and CD peaks were observed to be stronger. This information reveals that the rod-shaped micellar structure with PEO/α-CD condensed phase at 25 °C reversed to a core-shell micelle of PNIPAM core at 40 °C[25].

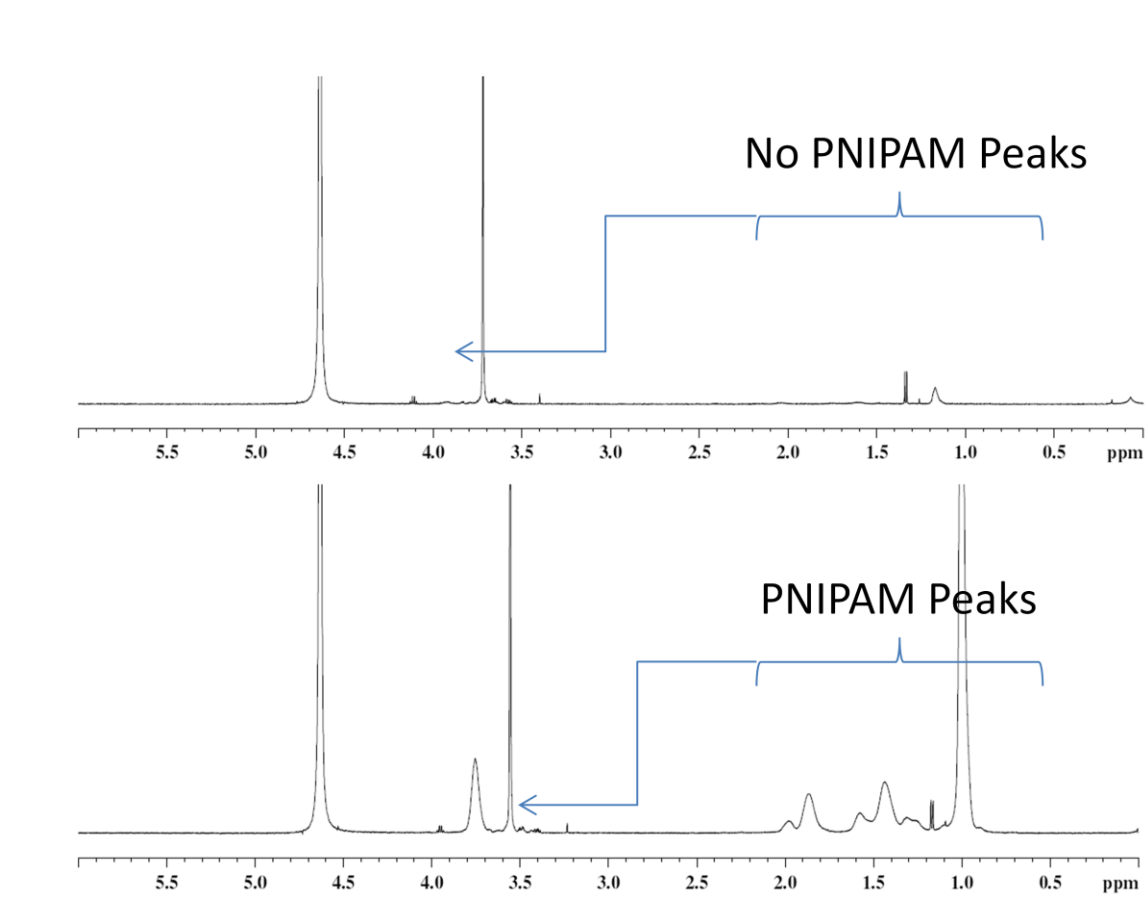

Figure 4.21: NMR spectra of PEO-b-PNIPAM at (a) 40 °C and (b) 25 °C in D_2O.

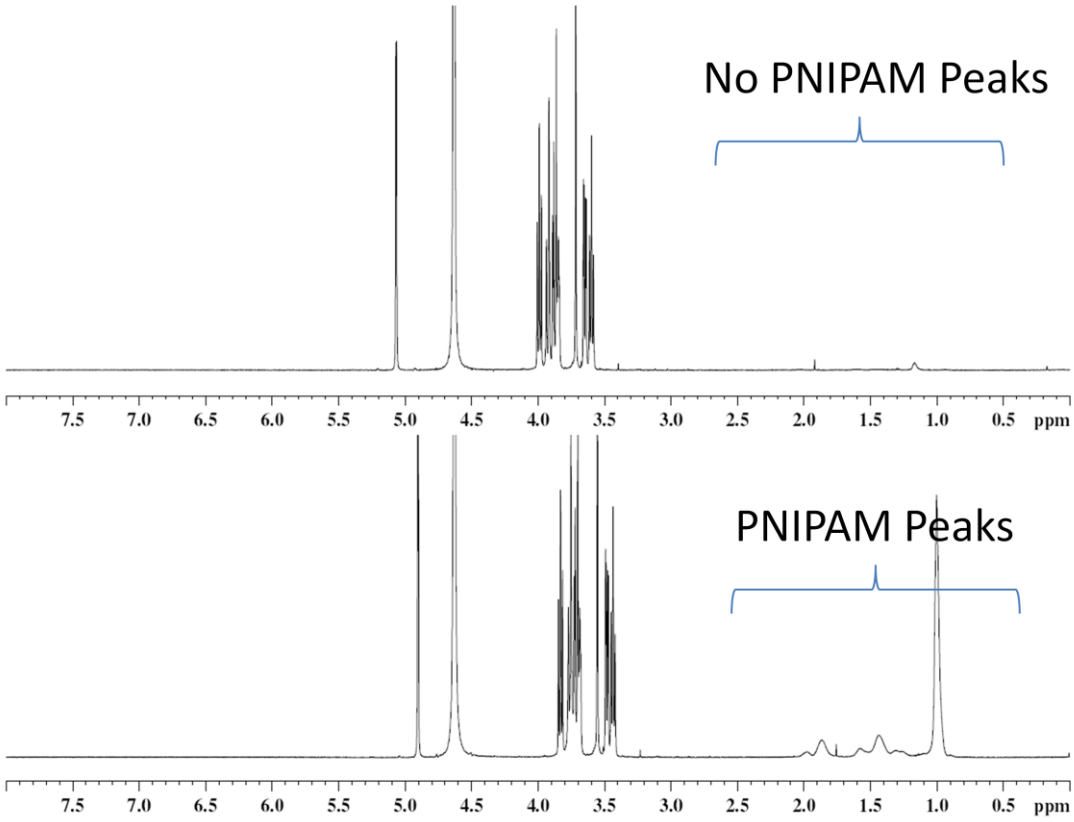

Figure 4.22: NMR spectra of PEO-b-PNIPAM/α-CD at (a) 40 °C and (b) 25 °C in D_2O.

4.5.6 Differential Scanning Calorimetry

DSC is a technique used to measure the heat change that occurs during controlled increases and decreases in temperature. For PEO-b-PNIPAM, DSC can provide information regarding enthalpy (ΔH), change in heat capacity (C_p), and the LCST of the phase transition. The C_p data attained was normalized, and the baseline was subtracted. Equations 3.10, 3.11, and 3.12 were used to determine ΔH, ΔS, and ΔG values of the transition. A summary of results is displayed in Table 4-2, where T_m is the transition temperature, and T* and T** are the temperatures at which the phase transition begins

and ends (i.e. the temperature at which the C_p data deviates and merges from the baseline – Figure 4.23).

Table 4-2: Calorimetric Data for Phase Transitions of PEO-b-PNIPAM/α-CD.

Mole Ratio of α-CD to PEO-b-PNIPAM	Mole Ratio of α-CD to EO units	T_m (°C)	ΔH (cal/mol)	ΔS (cal/mol/°C)	ΔG at T* (cal/mol)	ΔG at T** (cal/mol)
0	0	34.47	4.413×10^5	1.245×10^4	1.373×10^5	-8.818×10^4
119.75	0.53	35.51	4.177×10^5	1.180×10^4	1.313×10^5	-1.183×10^5
145.60	0.64	34.79	3.968×10^5	1.126×10^4	1.298×10^5	-9.116×10^4
669.38	2.96	34.58	3.451×10^5	9.648×10^3	9.406×10^4	-9.551×10^4
1339.20	5.93	34.62	3.179×10^5	8.753×10^3	3.243×10^4	-1.175×10^5
4806.45	21.26	35.07	2.796×10^5	7.712×10^3	2.074×10^4	-8.448×10^4

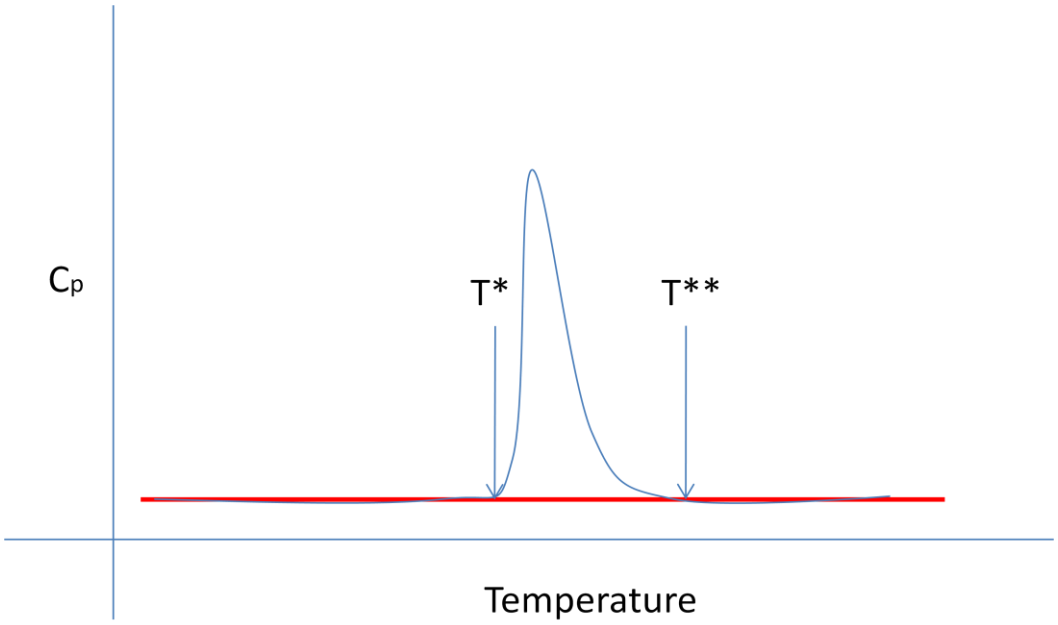

Figure 4.23: Schematic representation of a phase transition curve which marks the hypothetical locations of T* and T.**

The LCST of PEO-b-PNIPAM was higher than that of PNIPAM homopolymer. The hydrophilicity of the PEO segment made it more difficult for the polymer to phase transition. With increasing mole ratio of α-CD to polymer, the transition temperature increased, and the transition enthalpy decreased. The phase transition became increasingly more difficult as CD was added. This was thought to be due to both the threading of the CD onto the EO segment and the hydrogen bonding of the CD to the polymer.

4.6 Summary

PEO-b-PNIPAM and PEO-b-PNIPAM/α-CD systems were studied using the surface tension, ITC, LS, and DSC techniques. For PEO-b-PNIPAM at 40 °C and PEO-b-PNIPAM/α-CD at 25 °C, the CMC values were 0.00058 g/L and 0.0012 g/L, respectively, and the surface group sizes were 29.2 $Å^2$

and 14.7 $Å^2$, respectively. At 25 °C, CD was shown to bind with PEO-b-PNIPAM, but not at 40 °C. This indicated that the hydrophobicity of PNIPAM at 40 °C deters CD binding. Below the LCST, the PEO-b-PNIPAM samples showed no angular dependence and small R_h values, and these results were indicative of solvated free chains. PEO-b-PNIPAM samples above the LCST showed larger R_g values and smaller R_g/R_h values than that of PEO-b-PNIPAM/α-CD. This data was evidence that the polymer chains formed a micellar structure with solvated chains. For PEO-b-PNIPAM/α-CD, samples below the LCST displayed angular dependence and larger R_g/R_h values values than those of PEO-b-PNIPAM. Along with the polarized DLS observations, the data corresponded to flexible rod morphology. Above the LCST, it was believed that the CD de-threaded from PEO segment, and core-shell micelles with a PNIPAM core and PEO corona reformed. Above the LCST, the PNIPAM ^1H NMR peaks disappeared, which indicated structure formation that contained a PNIPAM core and PEO/α-CD desolvated chains. A summary of morphology may be found in Figure 4.24. By comparing the thermodynamic parameters of the phase transitions for samples at multiple CD concentrations, it was observed that the addition of CD hindered the ability of the system to phase transition.

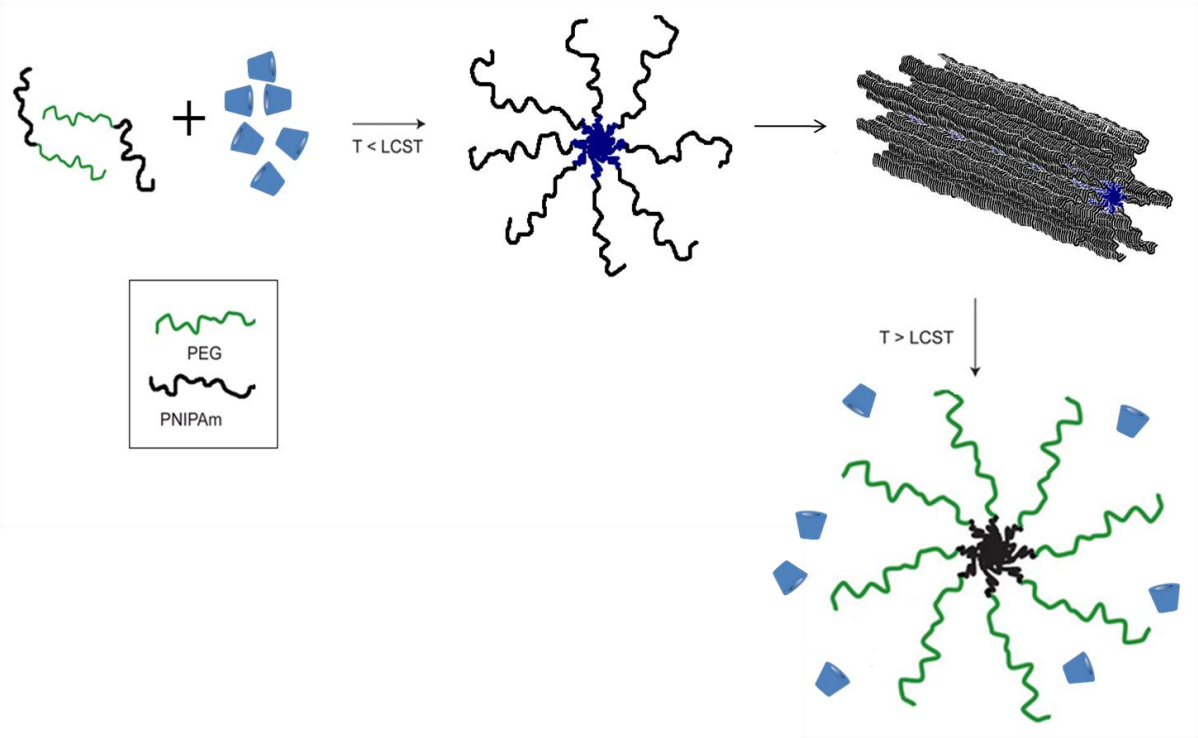

Figure 4.24: Schematic representation of the morphology of PEO-b-PNIPAM/α-CD.

Chapter 5

Self-Assembly of PPO-block-PMAA/β-CD system

5.1 Introduction

The self-assembly of ordered micellar structures[1, 2] is spontaneous for block copolymers composed of incompatible hydrophilic and hydrophobic blocks. Stimuli-sensitive copolymers that behave as free chains in solution in one external condition, but micellize in a different condition are useful in a variety of applications[3]. Adding the ability to form inclusion complexes with CD increases the level of complexity by allowing the system to contain multiple control elements.

Poly(methacrylic acid) (PMAA) is a pH-responsive polymer that is hydrophobic at low pH and hydrophilic at high pH. PEO-b-PMAA is known to form micelles at low pH. He et al.[4] studied the binding and release of cationic drugs on a four-armed, star-shaped PEO-PMAA block copolymer system using the ITC. The negatively charged carboxylic groups at high pH bound with cationic drugs due to electrostatic interaction, but released the drug at low pH. The PPO component is temperature sensitive, and at a molecular weight of 1000 g/mol, the polymer has a broad LCST transition of around 40 °C[5]. PPO is a component of Pluronics, which are commercial polymers that are widely used in drug delivery vehicles[6]. In addition, the PPO segment has the ability to complex with β-CD[7]. This project seeks to investigate the pH phase transition, temperature phase transition, and the complexation of PPO-b-PMAA with β-CD.

5.2 Measurements

5.2.1 Sample Preparation

PPO-b-PMAA polymer was synthesized using the ATRP technique[8]. The polymer solutions were made individually by dissolving PPO-b-PMAA in purified Millipore purified water, unless otherwise specified. The solutions were adjusted to the final pH by the addition of NaOH (1 N; ACROS; Geel, Belgium) or HCl (1 N; ACROS; Geel, Belgium). All prepared polymer sample solutions were stored in the refrigerator. For the study of PPO- PMAA/CD complexes, appropriate amounts of β-CD (99 %; ACROS; Geel, Belgium) and α-CD (98 %, Sigma Aldrich; Geel, Belgium) were added to the PPO-b-PMAA solutions. The resulting solution was stirred and agitated ultrasonically to promote dissolution, and they were stored overnight prior to use to allow time for the self-assembly process to reach an equilibrium. Samples with β-CD were stored at room temperature for no more than one day prior to use.

5.2.2 Characterization

^{1}H NMR analyses of the polymer samples for synthesis characterization were conducted with a Bruker 600 MHz high resolution Ultra Shield™ spectrometer (Bruker BioSpin Corporation; Massachusetts, USA). Morphology characterization experiments were conducted with a Bruker 600 MHz high resolution Ultra Shield™ spectrometer (Bruker BioSpin Corporation; Massachusetts, USA).

Surface tension data was obtained using a DataPhysics dynamic contact angle meter and tensiometer (DataPhysics Instruments; Filderstadt, Germany) equipped with a Wilhelmy plate, based on the increasing concentration method. For the first experiment, 0.1 wt% PPO-MAA was titrated into 50 mL of water at 25 °C. For the second experiment, 0.1 wt% PPO-b-PMAA was titrated into 50

mL of water at 60 °C. The surface tension data was plotted to gain information on the CMC and head group size of the systems.

Calorimetric titration measurements were carried out using a Microcal Isothermal Titration Calorimeter (ITC; Microcal, LLC; Massachusetts, USA) with a 1.4 mL sample cell in an adiabatic shield. The stirring rate was set to 400 rpm, and the time between injections was set to 250 seconds. The data was recorded automatically, and the Microcal Origin for ITC program (OriginLab; Massachusetts, USA) was used to integrate and generate differential enthalpy curves. For the ITC, PPO-b-PMAA solutions, β-CD and α-CD solutions, and HCl/NaOH solution were prepared at 0.1 wt%, 1.85 wt%, 3.625 wt%, 0.01 M, and 0.01M respectively. For CD binding experiments, a PPO-b-PMAA solution and β-CD solution were prepared at 0.1 and 0.185 wt% respectively. The reference cell was filled with water. Temperature dependence experiments were run at 25.0 ± 0.02 ^{0}C and 60.0 ± 0.02 ^{0}C.

The microstructure of the sample was examined by a Brookhaven Laser Light Scattering system (Brookhaven Instruments Limited; Worcestershire, UK). The system has a BI200SMv2 goniometer, TurboCorr Coorelator and a MiniL-20 636 nm laser. The DLS time-correlation functions were analyzed using the GENDIST software package with the probability of reject set to 0.5. The autocorrelation functions were used to compute the particles' diffusion coefficients, which were then used to compute the R_h of the particles. Dn/dc measurement was conducted using a Brookhaven BI-DNDC differential refractometer (Brookhaven Instruments Limited; Worcestershire, UK).

5.3 Results and Discussion

5.3.1 Nuclear Magnetic Resonance (NMR)

NMR experiments were performed on PPO-b-PMAA. The spectra is shown in Figure 5.1. The molecular weight of the polymer was calculated using the integration of the PPO peaks (MW of 1000 Da – 1.0 ppm) to the PMAA peaks (0.85 ppm). The molecular weight of the polymer was determined to be 2220 g/mol.

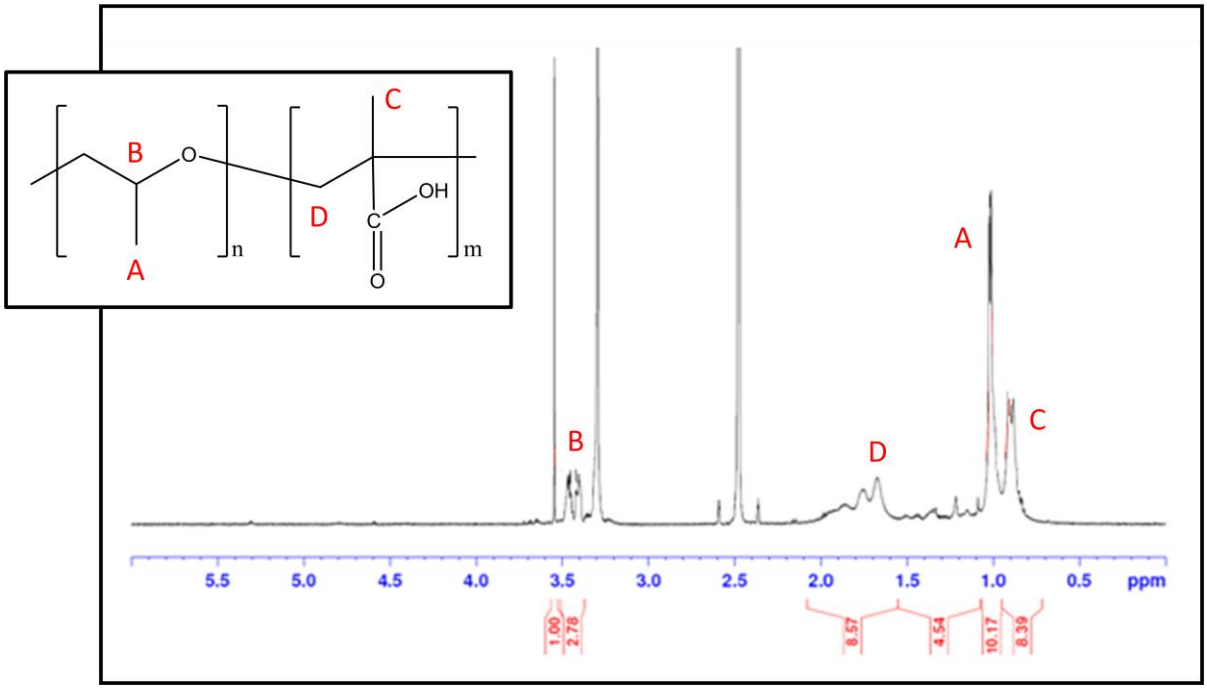

Figure 5.1: NMR spectra for PPO-b-PMAA in DMSO-d_6.

5.3.2 Observations

PPO-b-PMAA was difficult to dissolve in neutral water. Neutral PPO-b-PMAA suspensions were opaque at room temperature. At neutral pH, the PMAA segments were expected to protonate and, therefore, making the segments hydrophobic. In addition, the carboxylic acid groups of the PMAA

segment were expected to hydrogen bonded with the oxygen groups of the PPO segments. This was believed to cause inter- and intra-molecular aggregation of the polymer. At pH 10, PPO-b-PMAA solutions (0.1 wt%) were clear at room temperature as both segments are known to be hydrophilic in basic conditions[9, 10] (Figure 5.2).

The addition of β-CD into a pH 10 PPO-b-PMAA solution produced a clear solution. At pH 4, the addition of β-CD to the opaque PPO-b-PMAA solution became clear over time. This observation indicated that β-CD helped PPO-b-PMAA dissolve in solutions of low pH. There were no visual changes of the systems with the increase of temperature over the LCST.

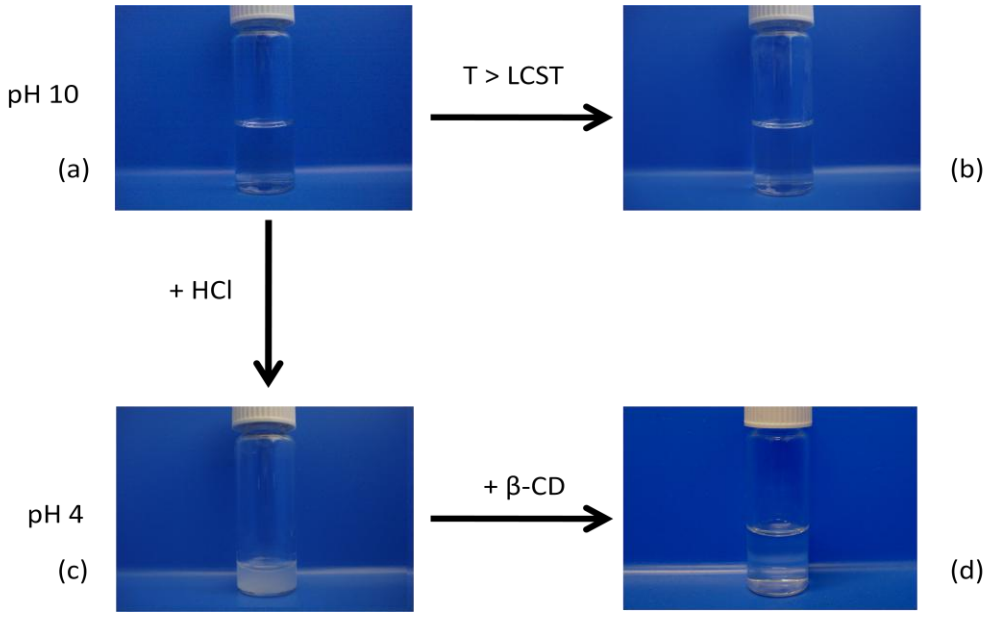

Figure 5.2: Photographs of PPO-b-PMAA solutions at various conditions: (a) pH 10 at 25 °C , (b) pH 10 at 60 °C, (c) pH 4 at 25 °C, and (d) pH 4 and β-CD at 25 °C.

5.3.3 Surface Tension

CMC is an important property used to characterize the self-assembly property of aqueous block copolymer solutions. The CMC is defined as the minimum concentration at which the copolymers

self-assemble into micellar aggregates, and this is usually linked to a sharp change in solution properties, such as surface tension, turbidity, and viscosity. The Wilhelmy pate method was used to measure the surface tension by titrating 0.1wt% pH 10 polymer solutions into aqueous solution at pH 10. A plot of surface tension with polymer concentration allows the determination of the critical micellar concentration of the polymer solutions. Surface tension measurements of 0.1 wt% PPO-b-PMAA at 25 °C and of 0.1wt% PPO-b-PMAA at 60 °C are shown in Figure 5.3. The surface tension experiment for 0.1wt% PPO-b-PMAA at 60 °C showed a CMC value of 0.00922 g/L. The CMC is obtained from the plot by extrapolating two lines from the linear regions of the last two segments and locating the intercept. Below the CMC, the surface tension decreased with increasing polymer or polymer/CD concentration due to the localization of molecules at the air-water interface. Above the CMC, the air-water interface was saturated, and the reduction in the surface tension with concentration decreased as micellar aggregates were formed. In both cases, free energy was minimized. For the experiment at 25 °C, no CMC was found. However, there was a slight decrease in surface tension with increasing of polymer concentration. This decrease may have been due to surface effects of PPO[11]. PPO can hydrogen bond with water molecules and may have led to a decrease in surface tension as strong water networks were interrupted. The surface excess concentration was used to calculate the head group area of the molecules. For PPO-b-PMAA at 60 °C the area was 18.9 $Å^2$.

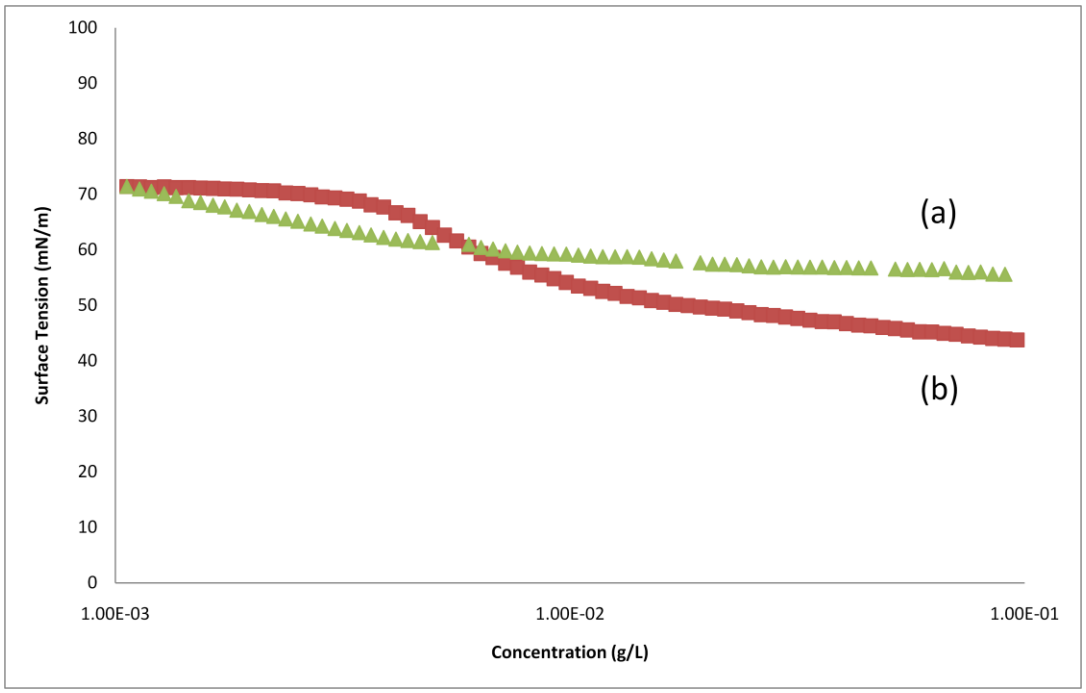

Figure 5.3: Surface tension data from the (a) titration of PPO-b-PMAA at 25 °C (b) titration of PPO-b-PMAA at 60 °C.

5.3.4 Isothermal Titration Calorimetry

ITC was used to characterize the thermodynamics of binding, neutralization, and the self-assembly of polymer systems. To study the pH-sensitivity of the PPO-b-PMAA system, calorimetry measurements were conducted as HCl and NaOH were titrated into the PPO-b-PMAA solutions at 25.0 ± 0.02 ^{0}C and 60.0 ± 0.02 ^{0}C. In both cases, the raw data resulting from the titration of acid/base into polymer titrations were subtracted from the titration isotherm of acid/base into aqueous solution and integrated to determine the ΔH curve. Figure 5.4 shows the titration of 0.01 M HCl into 0.1 wt% PPO-b-PMAA a pH 10, at 25 ^{0}C. By superimposing the titration isotherm of 0.01 M HCl into pH 10 aqueous solution, it was hypothesized that acid-aqueous solution neutralization occurred from 0.0 to 0.7 molar ratio. Beyond 0.7 molar ratio, the data was highly endothermic due to hydrogen bonds

formation from protonation of PMAA, and the particles aggregated. Figure 5.5 shows the titration of 0.01 M NaOH into 0.1 wt% PPO-b-PMAA at pH 3 at 25 ^{0}C. By superimposing the titration isotherm of 0.01 M NaOH into pH 3 aqueous solution, it was hypothesized that the base-aqueous solution neutralization occurred from 0.0 to 0.55 molar ratio. Beyond 0.55 molar ratio, the data was highly exothermic and was most likely due to the neutralization of PMAA groups, the breaking of hydrogen bonds between PPO and PMAA, and the dissociation of the aggregates. Figure 5.6 shows the titration of 0.01 M HCl into 0.1 wt% PPO-b-PMAA at pH 10, and at 60^{0}C. Again, by superimposing the titration isotherm of 0.01 M HCl into pH 10 aqueous solution, it was hypothesized that acid-aqueous solution neutralization occurred from 0.0 to 0.7 molar ratio. Beyond 0.7 molar ratio, as acid was titrated, the PMAA groups were neutralized (as seen in the exothermic portion of the graph), which should increase the hydrophobicity of the PMAA segments. As the PMAA segments increase in hydrophobicity, they were believed to collapse and cause intermolecular aggregation (as seen in the endothermic portion of the graph).

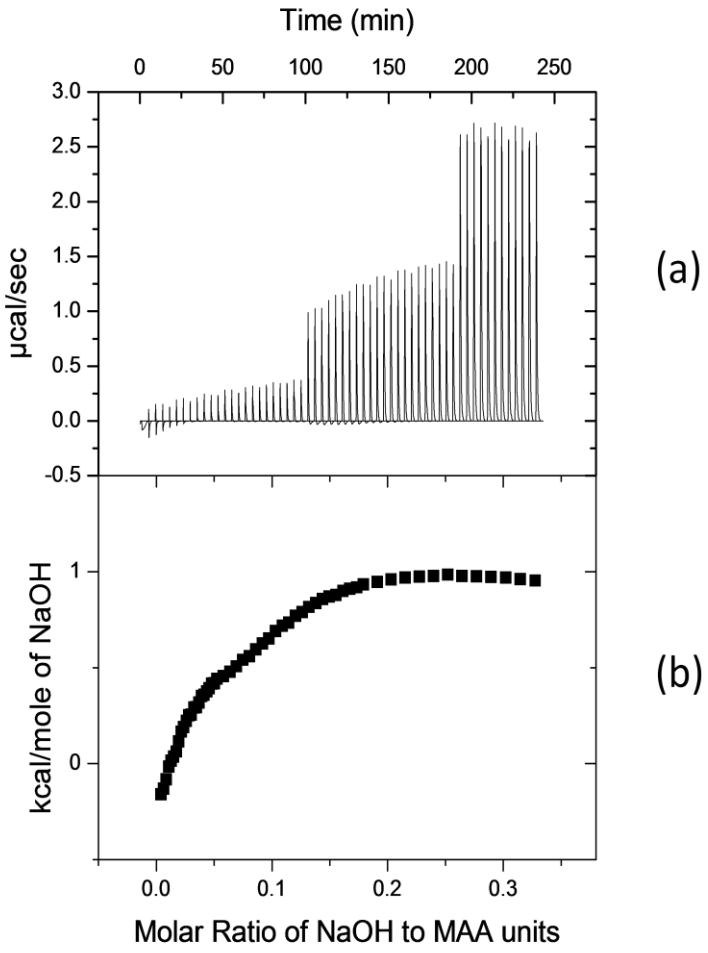

Figure 5.4: Calorimetric titration of 0.01 M HCl into a pH 10 0.1 wt% PPO-b-PMAA solution at 25 °C. (a) Thermogram showing the cell feedback power versus time. (b) Differential enthalpy versus molar ratio of HCl to MAA units.

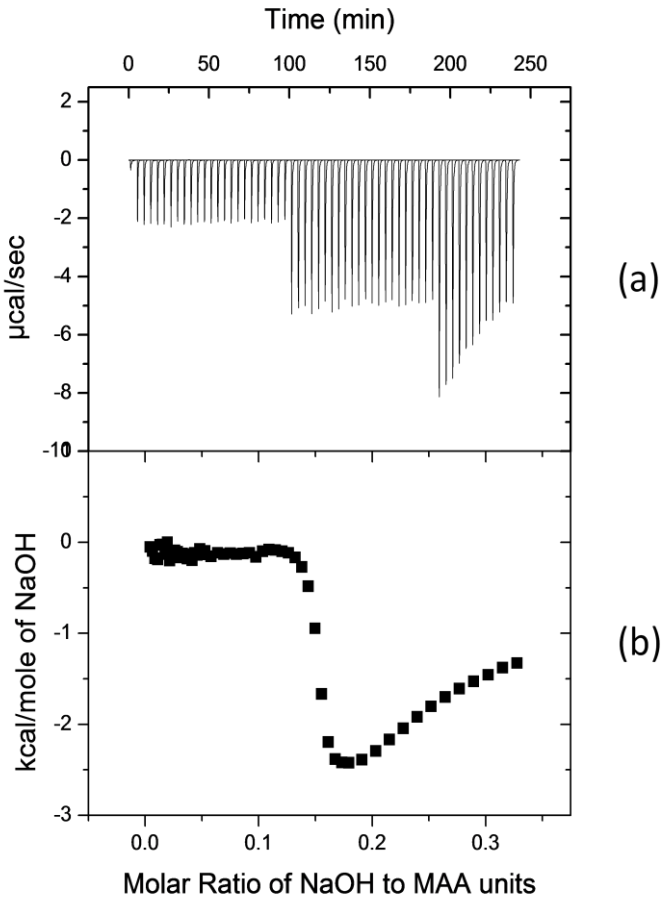

Figure 5.5: Calorimetric titration of 0.01 M NaOH into a pH 3 0.1 wt% PPO-b-PMAA solution at 25 °C. (a) Thermogram showing the cell feedback power versus time. (b) Differential enthalpy versus molar ratio of NaOH to MAA units.

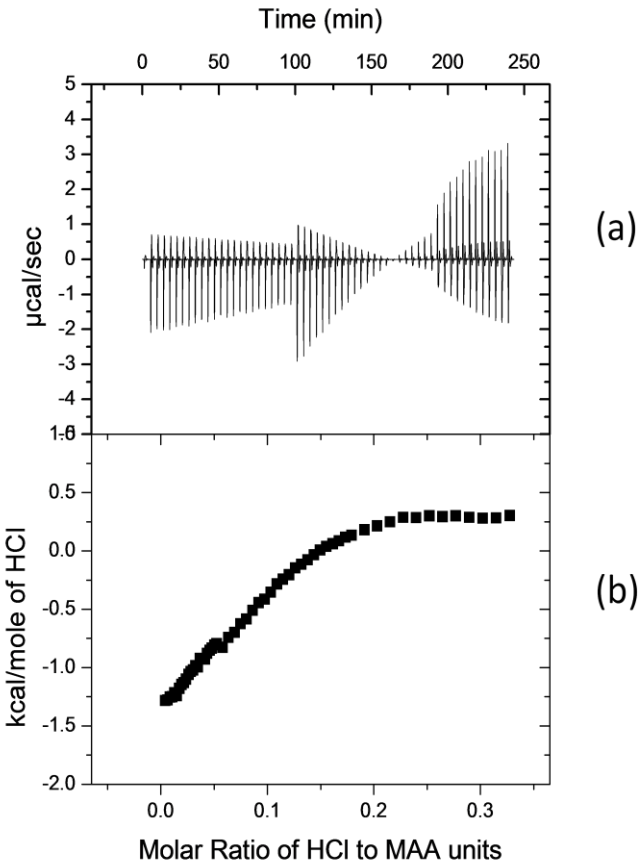

Figure 5.6: Calorimetric titration of 0.01 M HCl into a pH 10 0.1 wt% PPO-b-PMAA solution at 60 °C. (a) Thermogram showing the cell feedback power versus time. (b) Differential enthalpy versus molar ratio of HCl to MAA units.

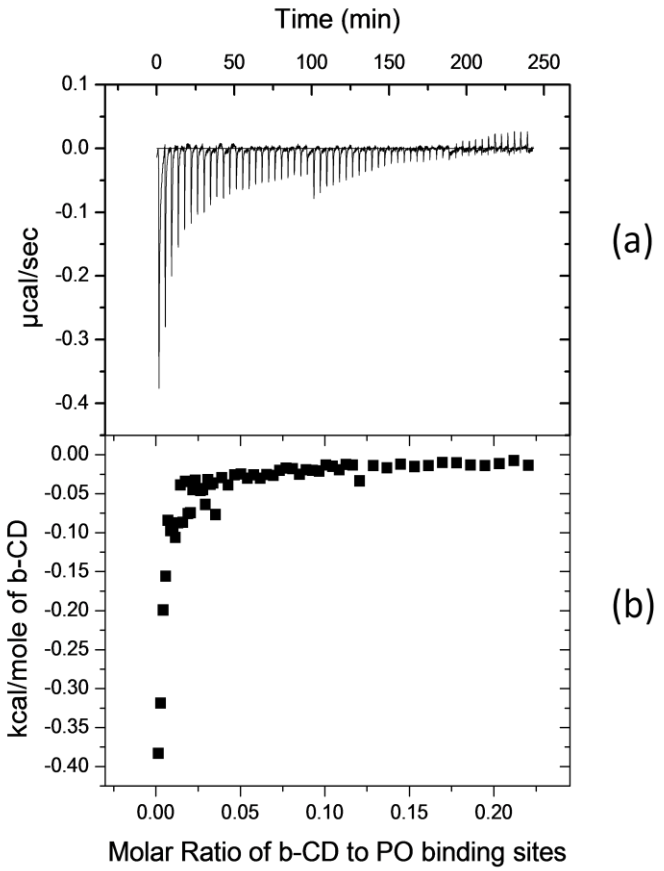

Figure 5.7: Calorimetric titration of pH 10 1.85 wt% β-CD solution into a pH 10 0.1 wt% PPO-b-PMAA solution at 25 °C. (a) Thermogram showing the cell feedback power versus time. (b) Differential enthalpy versus molar ratio of β -CD to PO units.

To study the thermodynamics of binding of β-CD to PPO-b-PMAA, calorimetric measurements were conducted as β-CD was titrated into the PPO-b-PMAA solution at 25.0 ± 0.02 ^{0}C. All solutions were adjusted to a pH of 10. The raw data resulting from the β-CD into polymer titrations was subtracted from the titration isotherm of β-CD into water. Figure 5.7 shows the titration of 1.85 wt% β-CD into 0.1 wt% PPO-b-PMAA at 25 ^{0}C. A clear binding curve can be seen with a binding ratio of

approximately 18 %. The onset of self-assembly was believed to impede the threading of CD. A two-site sequential binding model (Equations 3.4-3.9) was used to fit the calorimetric data of binding and the results are displayed below in Table 5-1.

Table 5-1: Calorimetric Data from Two-Site Sequential Binding Model for PPO-b-PMAA/β-CD.

	1	2
K (L/mol)	$248 \pm 1.7 \times 10^2$	$1.36 \times 10^5 \pm 6.5 \times 10^4$
ΔH (cal/mol)	-821.5 ± 170	867.0 ± 167
ΔS (cal/mole/K)	8.20	26.4

The fitting of the two site model indicated two sequential events occurring as β-CD was titrated. The first was believed to be the threading of β-CD to the PPO segment and, the second, was the formation of a micellar structure.

Titration of 3.625 wt% α-CD into 0.1 wt% PPO-b-PMAA at 25 ^{0}C is shown in Figure 5.8. α-CD is not known to thread onto PPO due to the size of the cavity. Therefore, it can be seen that the majority of the data lies at 0.0 kcal/mole of α-CD. The initial endothermic reaction at the beginning of the experiment was believed to be due to hydrogen bonding of α-CD to the oxygen of PPO and PMAA groups, there was an The pH effects on the binding of β-CD to PPO-b-PMAA were also studied by titrating 1.85 wt% of β-CD into 0.1 wt% PPO-b-PMAA, where all the solutions were adjusted to a pH of 4. The titration curve, after subtracting the dilution data, was shown in Figure 5.9. From physical observation, was noted that PPO-b-PMAA does not dissolve in water at pH 4. However, with the addition of β-CD the solution became clear. This indicated that the β-CD associates onto the PPO

segment and caused micellization and dissolution of the system. It was hypothesized that the first segment (0.00 to 0.02 molar ratio) was due to the association of β-CD into the polymer chain and the interruption and breaking of the hydrogen bonds within the polymer. The second segment (0.02 to 0.03 molar ratio) was due to breaking up of larger polymer particles into smaller ones. The third segment (0.03 to 0.04 molar ratio) was continued association of β-CD into the polymer chain and the interruption and breaking of the hydrogen bonds within the polymer. In the last segment (beyond 0.04 molar ratio), the exothermic binding and dissociation processes dominated. In comparison to the β-CD titration experiment at pH 10, the multiple simultaneous exothermic reactions produced a much greater negative **Δ**H values at pH of 4.

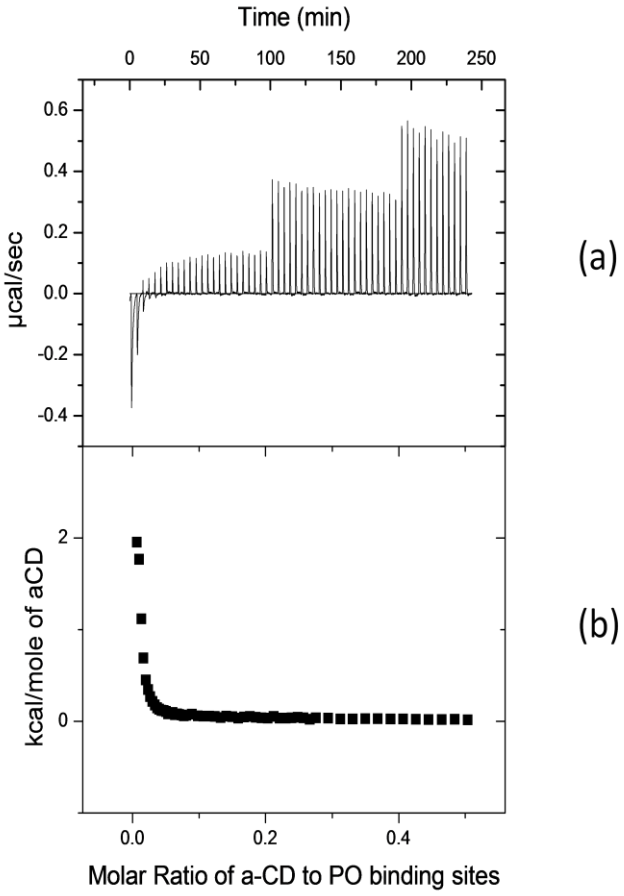

Figure 5.8: Calorimetric titration of pH 10 3.625 wt% α-CD solution into a pH 10 0.1 wt% PPO-b-PMAA solution at 25 °C. (a) Thermogram showing the cell feedback power versus time. (b) Differential enthalpy versus molar ratio of α-CD to PO units.

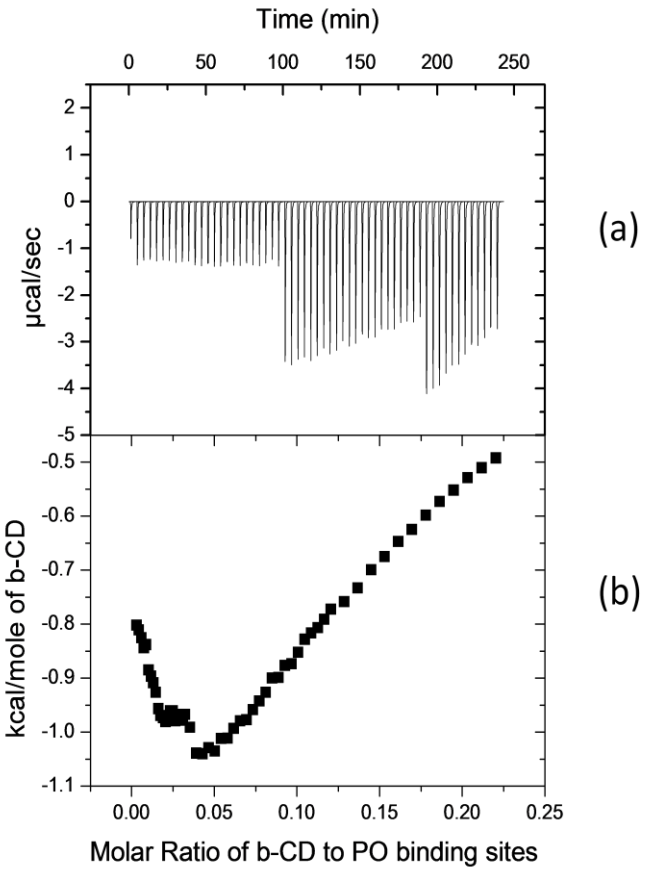

Figure 5.9: Calorimetric titration of pH 4 1.85 wt% β-CD solution into a pH 4 0.1 wt% PPO-b-PMAA solution at 25 °C. (a) Thermogram showing the cell feedback power versus time. (b) Differential enthalpy versus molar ratio of β-CD to PO units.

The temperature effects on the binding of β-CD to the PPO-b-PMAA system were studied by titrating 1.85 wt% of β-CD into 0.1 wt% PPO-b-PMAA at 60.0 ± 0.02 ^{0}C, where all the solutions were adjusted to a pH of 10. The results are shown in Figure 5.10. Due to the thermal-sensitivity of the PPO, β-CD was not expected to thread onto PPO at 60 ^{0}C. This explained the random scattering of data points.

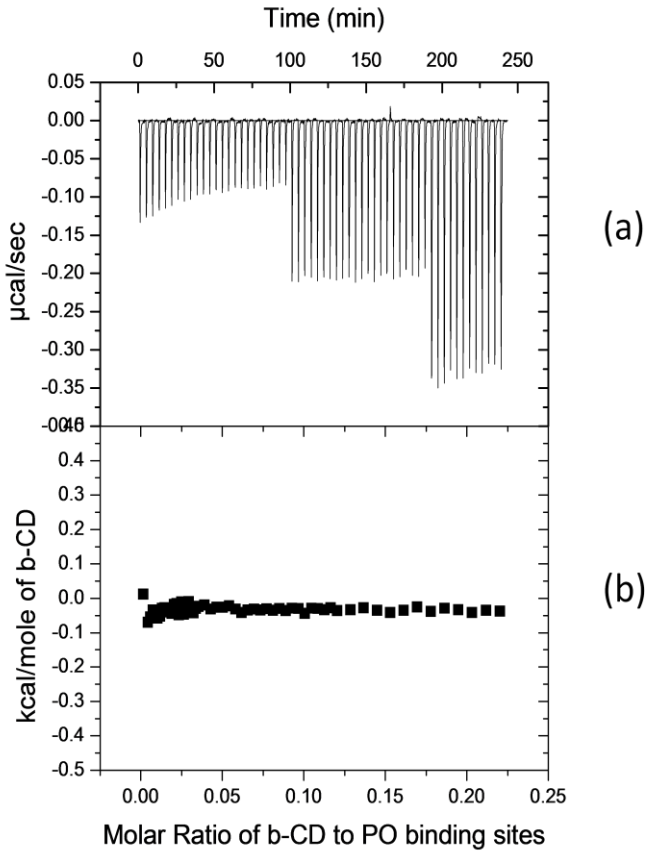

Figure 5.10: Calorimetric titration of pH 10 1.85 wt% β-CD solution into a pH 10 0.1 wt% PPO-b-PMAA solution at 60 °C. (a) Thermogram showing the cell feedback power versus time. (b) Differential enthalpy versus molar ratio of β-CD to PO units.

5.3.5 Light Scattering

The size and conformation of the self-assembled morphology of PPO-b-PMAA and PPO-b-PMAA/β-CD over a range of temperatures was studied using the Dynamic and Static Light Scattering techniques. For DLS, the temporal intensity fluctuations for a sample were measured at 60°, 75°, 90°, 105°, 120°, 135°, and 150°. The data from the detector was transferred to the GENDIST (General Distribution) software package to perform the inverse Laplace transform. GENDIST uses the REPES

(Regularized Positive Exponential Sum) algorithm, which was developed by Jakes at the Institute for Macromolecular Chemistry in Prague[12]. REPES is a mode-free fitting model that calculates the transform using a second order regularizer, and the fitting was performed directly on the intensity of the autocorrelation function $g_2(t)$, rather than the field autocorrelation function $g_1(t)$. The probability of rejection was set to 0.5. The outputs from GENDIST were then transferred to Origin for plotting and further data analysis. The distribution function of relaxation times were normalized, and a representative plot of 0.1 wt% PPO-b-PMAA in 15.48 mM β-CD at 40 °C is displayed in Figure 5.11. Due to the translational diffusion of particles, the figure shows distinct peaks that are shifted to lower relaxation times with increasing scattering angle. A linear relationship in the plot of Γ vs. q^2 was used to confirm that the scattering is attributed to translation diffusion. Using Equations 3.24 and 3.25, a plot of Γ vs. q^2, like the one displayed in Figure 5.12, may be generated. The average diffusion coefficient or the particles was obtained from the slope of the Γ vs. q^2 plot. Using the Stokes-Einstein equation (Equation 3.26), R_h may be calculated. For the representative sample, the particle size was determined to be 127.0 nm.

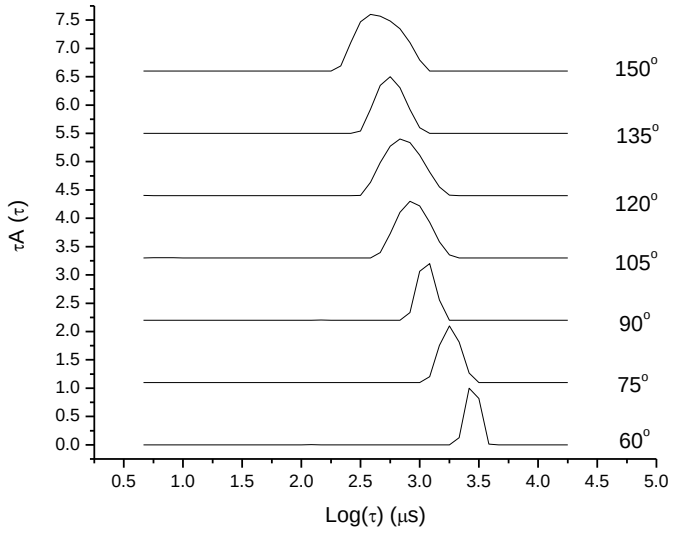

Figure 5.11: Characteristic distribution functions of relaxation times for pH 10 0.1 wt% PPO-b-PMAA in 15.48 mM β-CD at 40 °C.

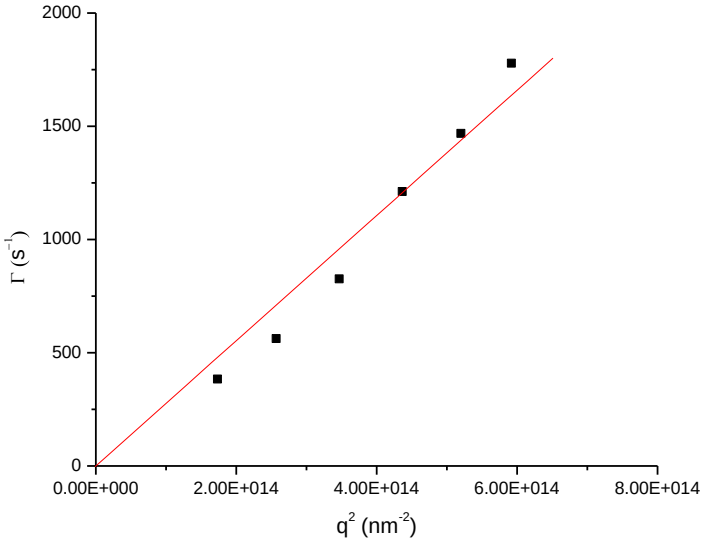

Figure 5.12: Plot of Γ vs. q^2 in the determination of particle coefficient for pH 10 0.1 wt% PEO-b-PNIPAM in 15.48 mM β-CD at 40 °C.

For SLS, the time-averaged intensities of scattered light for a sample was measured at angles ranging from 50° to 150° in 10° intervals. For single concentration samples, the partial Zimm equation (Equation 3.20) was used to determine the R_g values. Light scattering analyses for polymer systems at different temperatures were analyzed using the same methods.

Dn/dc measurements were performed on the PPO-b-PMAA sample, and the dn/dc was found to be $2.397 \times 10^{-1} \pm 1.6 \times 10^{-2}$ mL/g . Count rate measurements were performed for 0.1 wt% PPO-b-PMAA and 0.1 wt% PPO-b-PMAA in 15.48mM β-CD at pH 10, and the results were shown in Figure 5.13 and Figure 5.14. Below the LCST, PPO-b-PMAA did not form large structures and, therefore, had a lower count rate. Above the LCST, the increase in the count rate signified the formation of larger supramolecular structures. In contrast, the PPO-b-PMAA/β-CD did not show any change with increasing temperature, which suggested that an increase in temperature may have no affect on the supramolecular structure of the system. It can also be noted that below the LCST, PPO-b-PMAA/β-CD particles scattered light more intensely that those of PPO-b-PMAA. However, above the LCST, the PPO-b-PMAA particles scattered light more intensely that those of PPO-b-PMAA/β-CD.

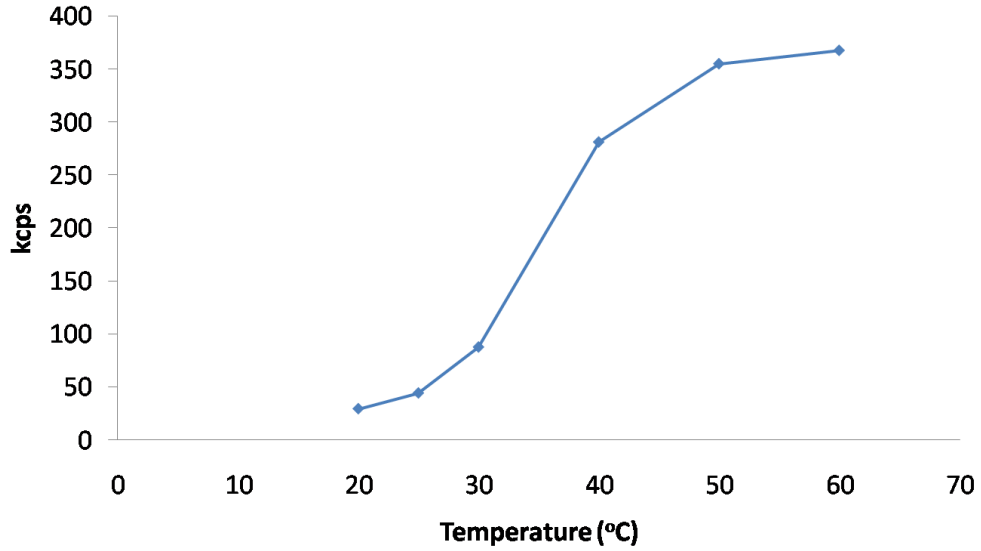

Figure 5.13: Plot of count rate versus temperature for pH 10 0.1 wt% PPO-b-PMAA.

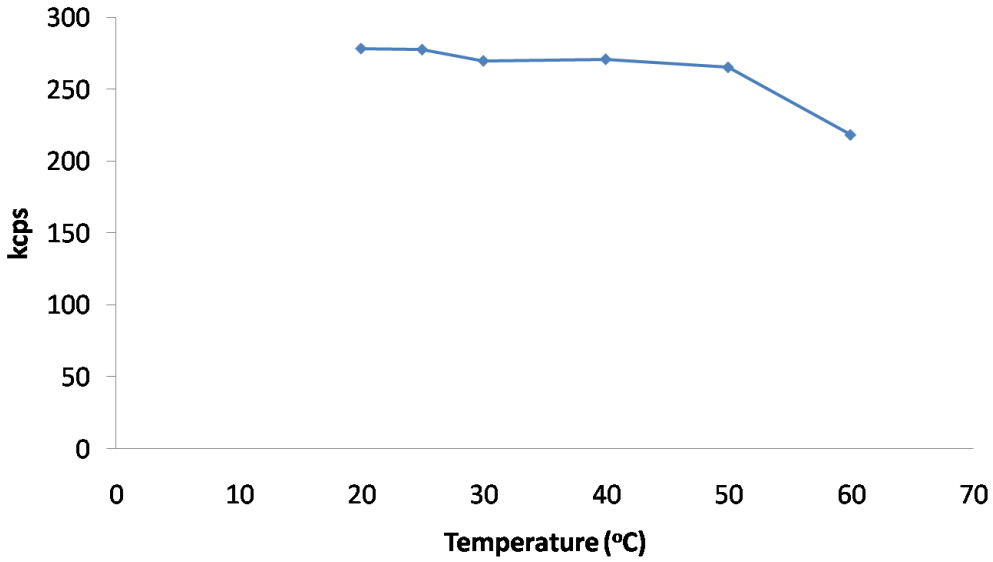

Figure 5.14: Plot of count rate versus temperature for pH 10 0.1 wt% PPO-b-PMAA in 15.48 mM β-CD .

DLS and SLS measurements were conducted on PPO-b-PMAA and PPO-b-PMAA/β-CD samples. Due to time dependent aggregation of the polymer the PPO-b-PMAA experiments were performed with modifications to the sample preparation procedure. The polymer samples were filtered before data collection at every temperature and the centrifugation step was omitted. For these experiments, below the LCST, the DLS results showed bimodal distributions, with R_h values of approximately 2.5 nm and 55 nm respectively. The small peaks corresponded to free chains in solution, while the larger peak corresponded to aggregation of several polymeric chains. Figure 5.15 shows the distribution functions over a range of temperatures. In addition, the size of the smaller peak decreased with increasing temperature. At temperatures above 45 °C, the small peak was almost nonexistent. Below the LCST, the large peak was shown the be very broad, which was indicative of unorganized aggregation, and above the LCST, the peak was shown to sharpen, which is indicative of uniform structure formation. Figure 5.16 depicts the ratio of the small peak size to the large peak size as a function of temperature. This ratio's decreasing trend revealed that as the temperature increases, the hydrophobicity of the unassociated polymeric chains was enhanced resulting in the formation of larger structures. Above the LCST, negligible free chains exist in solution.

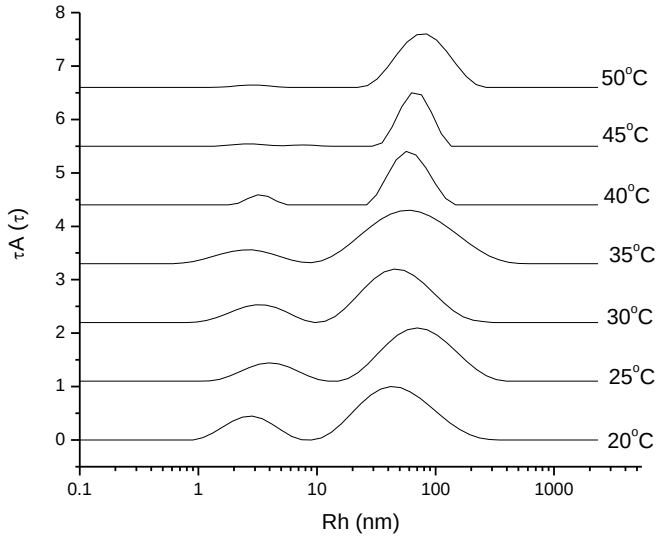

Figure 5.15: Effect of temperature on the decay distributions of pH 10 0.1 wt% PPO-b-PMAA at various temperatures.

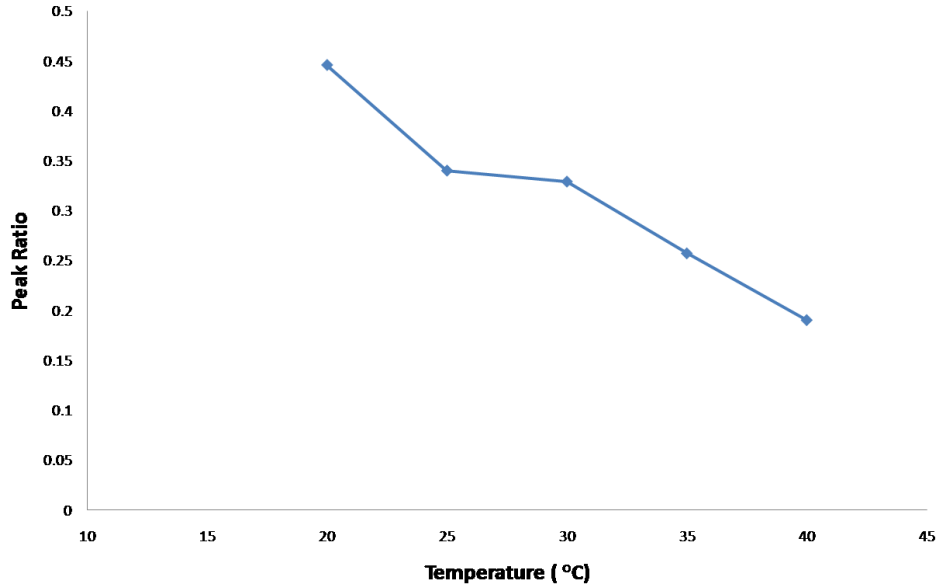

Figure 5.16: The effect of temperature on the ratio of peaks in the decay distributions of pH 10 0.1 wt% PPO-b-PMAA at 20 °C.

For PPO-b-PMAA/β-CD samples, the DLS experiments were performed using the original sample preparation procedure and the DLS spectra showed unimodal distributions with large R_h and R_g values. Above the LCST, there was little change to the R_g and R_h values, showing no change in the morphology. This result indicated that the PPO-b-PMAA/β-CD formed supramolecular structures that did not vary with temperature. The resulting R_h and R_g data is shown for PPO-b-PMAA/β-CD sample in Figure 5.17. The R_g/R_h values of PPO-b-PMAA/β-CD were displayed in graphical form Figure 5.18 and showed formation of vesicles above and below the LCST.

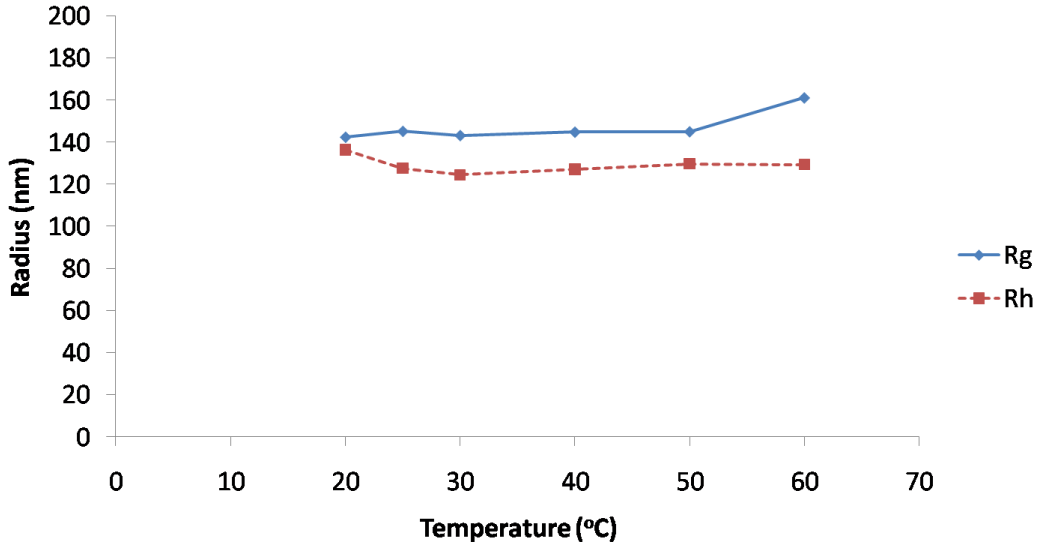

Figure 5.17: Effect of temperature on the (a) R_g and (b) R_h of pH 10 0.1 wt% PPO-b-PMAA in 15.48 mM β-CD.

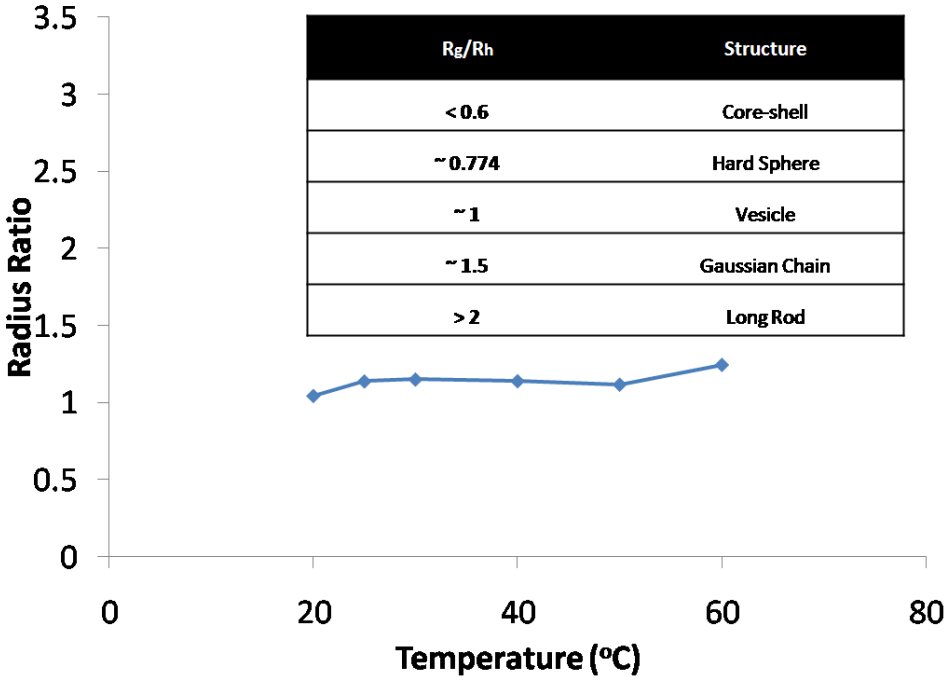

Figure 5.18: The effect of temperature on the conformational ratios for PPO-b-PMAA/β-CD.

5.3.6 Temperature Analysis with NMR

Figure 5.19 displays the ^{1}H NMR spectra of PPO-b-PMAA/β-CD at 25 °C and 60 °C respectively. The NMRs were conducted in D_2O and adjusted to high pH using NaOH. The NMR spectra showed no change. The NMR experiments were repeated in DMSO, and the NMR spectra also showed not apparent change with temperature. For PPO-b-PMAA/β-CD, no change in the NMR was expected as the PPO groups were believed to be encapsulated by β-CD. β-CD peaks continued to be seen in the NMR at high temperature due to excess β-CD.

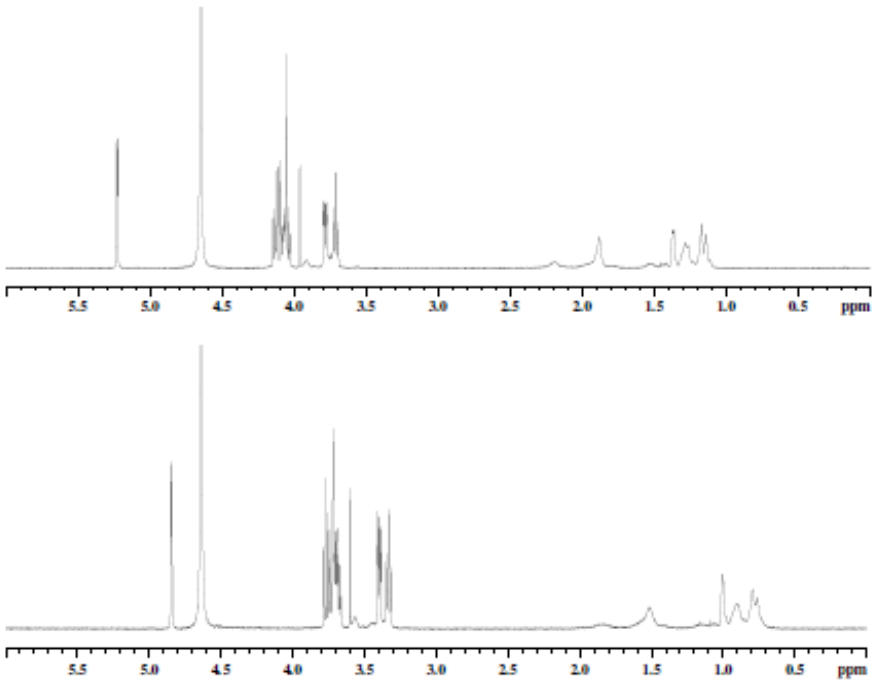

Figure 5.19: NMR spectra of PPO-b-PMAA/β-CD at (a) 60 °C and (b) 25 °C in D_2O that is adjusted by NaOH.

5.4 Summary

PPO-b-PMAA and PPO-b-PMAA/β-CD systems were studied using the surface tension, ITC, and LS. The morphology of this system was complex, and a variety of factors (e.g. pH, temperature, time and CD complexation) competed in the control the system's microstructures. Surface tension experiments showed that PPO-b-PMAA at 60 °C has a CMC of 0.00922 g/L and a headgroup size of 18.9 Å. The titration of pH 10 PPO-b-PMAA solution into pH 10 aqueous solution showed no CMC, but the decreasing surface tension data was evidence that the polymer had surface active properties that disrupted the water's hydrogen bonding interactions. At low pH values, PPO-b-PMAA was observed to be highly aggregated and was found to not dissolve in water. The PPO and PMAA

segments exhibited hydrogen bonding to form large intermolecular aggregated structures. At 25 °C, PPO-b-PMAA at pH 10 existed in both in monomeric and structure formation. It was shown that the contribution from the monomeric chains decreased with increasing temperature. The addition of β-CD induced the formation of vesicles that were not affected by temperature increase.

Chapter 6

Conclusions and Recommendations for Future Study

CD assisted supramolecular stimuli-sensitive self-assemblies allow for careful control of a system's morphological architecture using multiple control elements. Due to their numerous potential applications, the area of polymer self-assemblies has captured the interest of the academic and scientific world.

In this thesis, PEO-b-PNIPAM and PPO-b-PMAA polymer systems were investigated to determine the morphological changes exhibited as a result of cyclodextrin complexation, temperature phase transition, and pH alteration. Using techniques, such as surface tensiometry, ITC, LLS, and DSC, the micellization characteristics of the PEO-b-PNIPAM/α-CD and PPO-b-PMAA/β-CD systems were elucidated. These studies provide a basis for future studies in the area of stimuli-sensitive, double-hydrophilic polymer inclusion complexes.

6.1 The PEO-block-PNIPAM/α-CD system

The experimental evidence collected as a part of this thesis was found to support the following morphological characteristics of the PEO-b-PNIPAM system. At room temperature, double-hydrophilic PEO-b-PNIPAM behaved similarly to free chains in solution. Above the LCST of the polymer, the thermosensitive PNIPAM block condensed, and the copolymer self-assembled into micelles with a PNIPAM core and a hydrophilic PEO corona. PEO has the ability to complex with α-CD, and the threading of α-CD onto the polymer was found to induce micellization of the system to form rod-shaped nanostructures. At a temperature above the LCST of the system, the PNIPAM block collapsed, the α-CD dethreaded, and the system forms the traditional core-shell micelle.

6.2 The PPO-block-PMAA/β-CD system

The experimental evidence collected as a part of this thesis was found to support the following morphological characteristics of the PPO-b-PMAA system. At low pH, MAA groups hydrogen bonded with the PO groups to become intermolecularly aggregated. The addition of β-CD was shown to aid in polymer dissolution. At high pH, the PPO-b-PMAA was found to be highly soluble and β-CD was shown to thread onto the PPO segment to from vesicle nanostructures. Increasing the temperature of the system above the LCST of PPO showed no change to the system's morphology.

Both studies showed that supramolecular structures may be induced with the complexation of CD. The systems studied contain an additional level of complexity by incorporating a pH and/or temperature stimuli-sensitive component. The PEO-b-PNIPAM/α-CD system releases the cyclodextrin molecules with increased temperature. This system, with the biocompatible PEO shell, may prove useful in drug delivery applications because it has the ability to release CD conjugated drug molecules at body temperature. In contrast, the PPO-b-PMAA/β-CD provides the opposite characteristics. The system is temperature stable and retains its vesicle formation even with increased temperature. The system's micellization and collapse may be controlled through pH changes. The ability to control the architecture of a polymer system through external stimuli allows the systems to be potentially incorporated into sophisticated applications.

6.3 Recommendations for Future Study

Future studies should include comparisons of different block lengths and induced micellization and dissolution by introducing additional stimuli-sensitive components. Changing the block lengths of the polymer segments can alter the polymer's hydrophilic-hydrophobic balance. For example, longer blocks of PNIPAM decrease the LCST of PEO-b-PNIPAM due to increased hydrophobicity of the

PNIPAM block. In addition, changing the block lengths can alter the way in which the system assembles due to changes in packing structure.

Significant opportunities exist in combining a variety of control strategies to tailor the morphology of nanostructures to suit a specific application. Notable areas of interest include combining temperature, pH, light, and redox sensitivities to create systems with multi-state transitions. A stimuli-responsive component, such as azobenezenes or ferrocenes, which have a higher affinity to the cyclodextrin cavity than the polymer has, may be introduced into the system. This additional component may compete for the CD cavity, and external stimuli, such as light or oxidizers, can alter the molecule's hydrophobicity. This change may result in supramolecular re-arrangement of the polymer complexes and may allow for the system's morphology to be controlled by additional external stimuli to create a multi-stimuli responsive system.

Stimuli-responsive inclusion complexes have found applications in area such as thickeners, membranes, and separations. The PEO-b-PNIPAM/α-CD and PPO-b-PMAA/β-CD systems can certainly have interesting applications in these areas. However, the area of greatest commercialization potential is drug delivery. By using CDs with conjugated drug molecules, the stimuli-induced changes in morphology can be used in the delivery and release of active compounds in controlled drug delivery applications.

It is anticipated that the topic of multi-stimuli responsive inclusion complex systems will continue to be an active area of research that will result in the development of novel systems with possible commercial applications.

Appendix A

PEO-b-PNIPAM – Raw Data

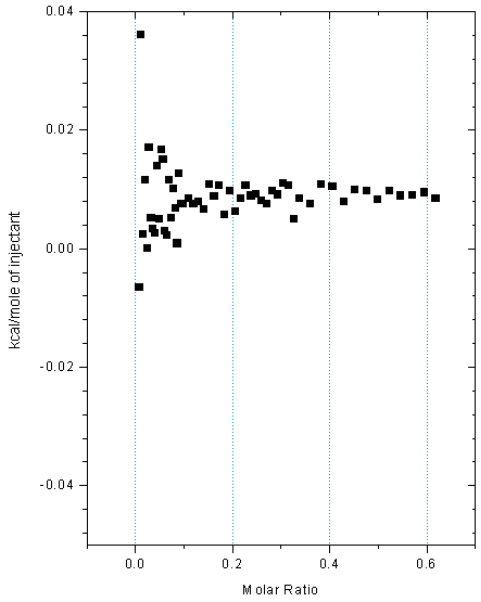

Figure A. 1: ITC results - 2 wt% α-CD into Water at 25 °C.

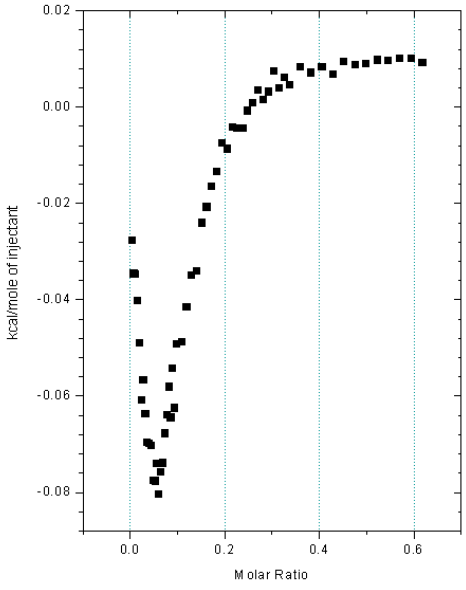

Figure A. 2: ITC results - 2 wt% α-CD into 0.1 wt% PEO-b-PNIPAM at 40 °C.

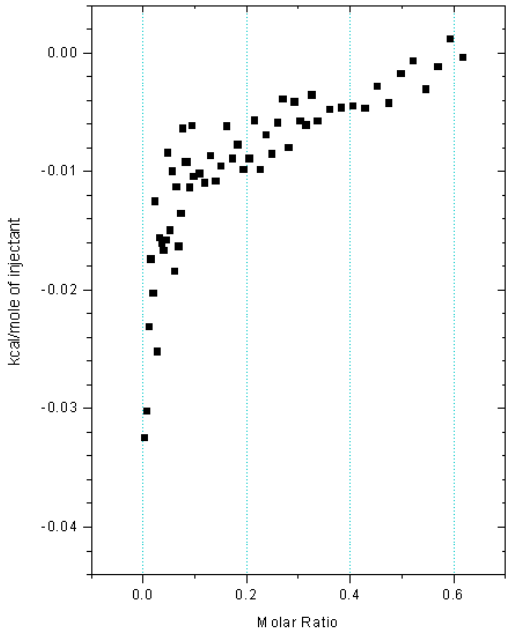

Figure A. 3: ITC results - 2 wt% α-CD into Water 40 °C.

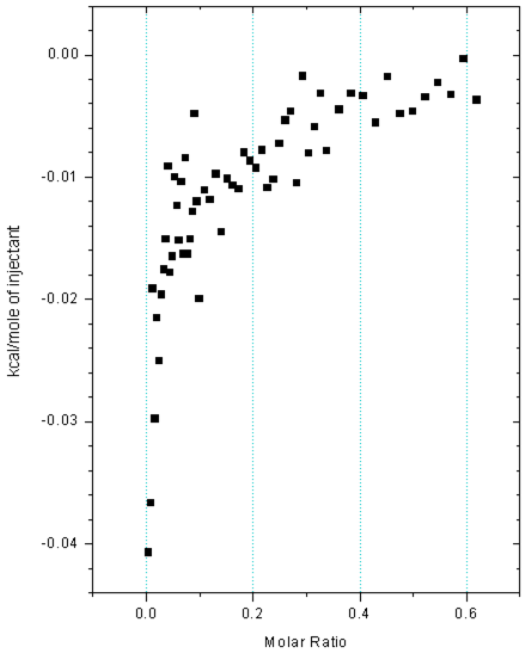

Figure A. 4: ITC results - 2 wt% α-CD into PEO-b-PNIPAM 40 °C.

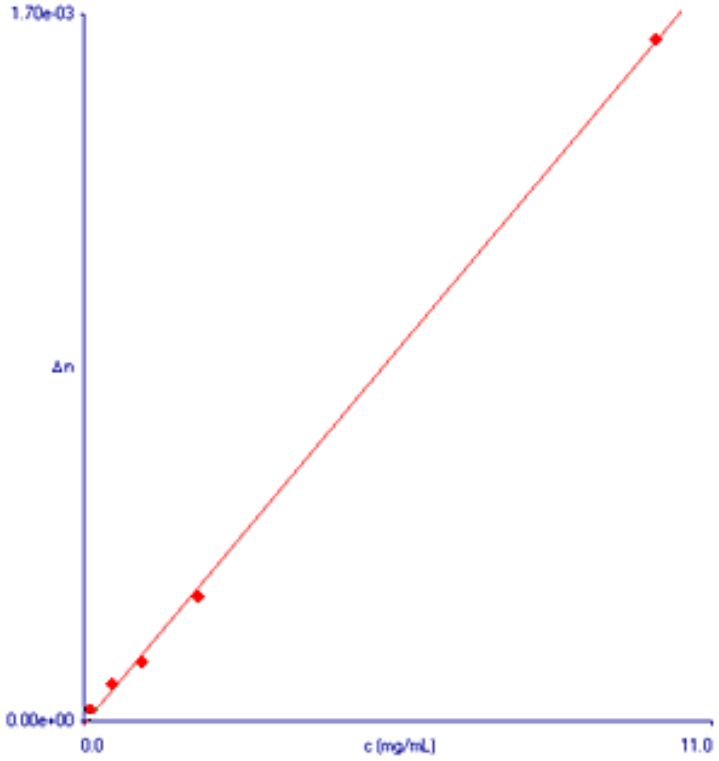

Figure A. 5: Plot of Δn vs. c in the dn/dc measurement of PEO-b-PNIPAM.

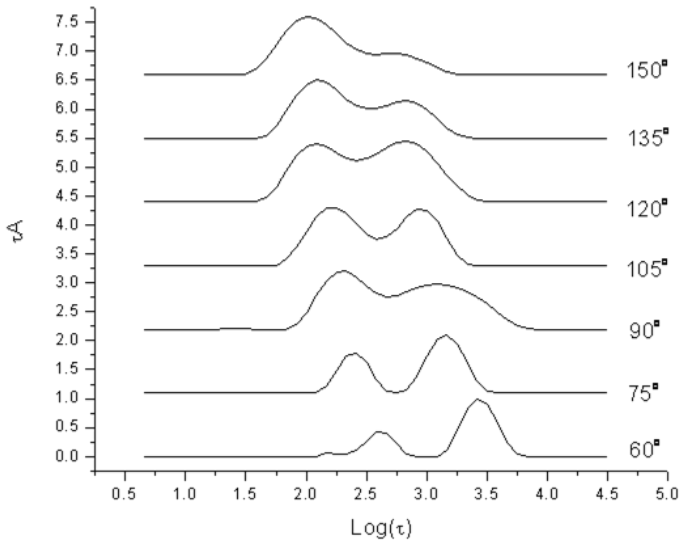

Figure A. 6: Relaxation time distribution functions for 0.1 wt% PEO-b-PNIPAM at 15 °C.

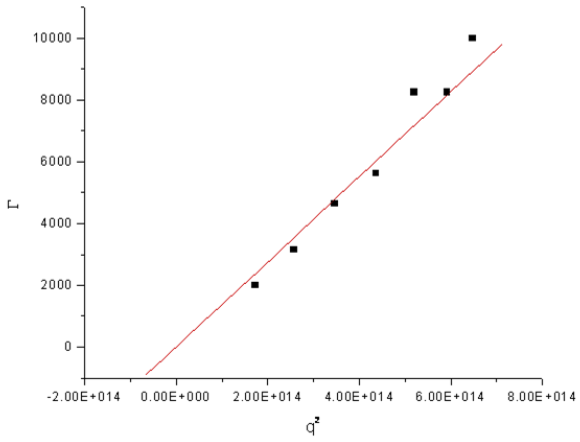

Figure A. 7: Plot of Γ vs. q^2 for 0.1 wt% PEO-b-PNIPAM at 15 °C.

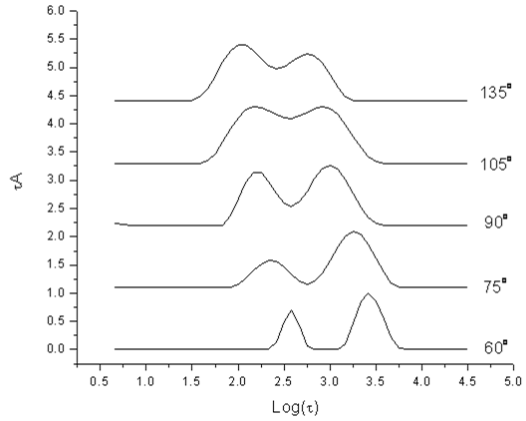

Figure A. 8: Relaxation time distribution functions for 0.1 wt% PEO-b-PNIPAM at 20°C.

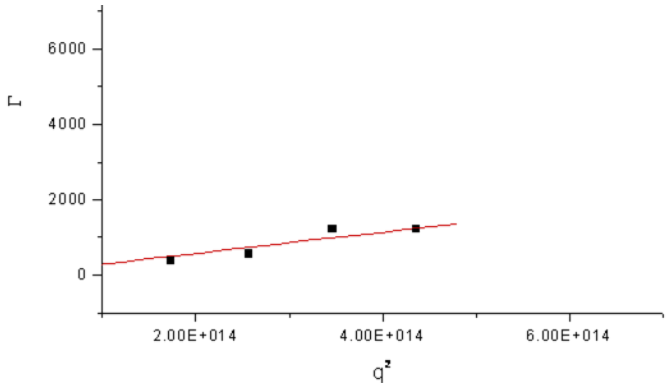

Figure A. 9: Plot of Γ vs. q^2 for 0.1 wt% PEO-b-PNIPAM at 20 °C.

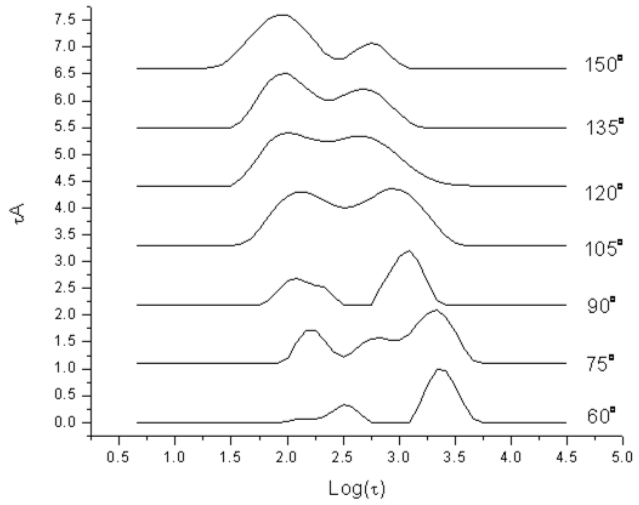

Figure A. 10: Relaxation time distribution functions for 0.1 wt% PEO-b-PNIPAM at 25 °C.

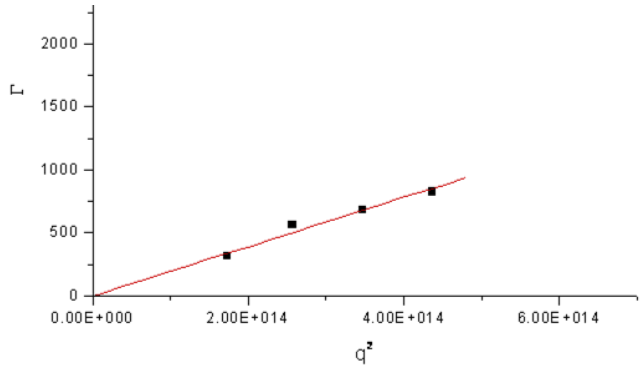

Figure A. 11: Plot of Γ vs. q^2 for 0.1 wt% PEO-b-PNIPAM at 25 °C.

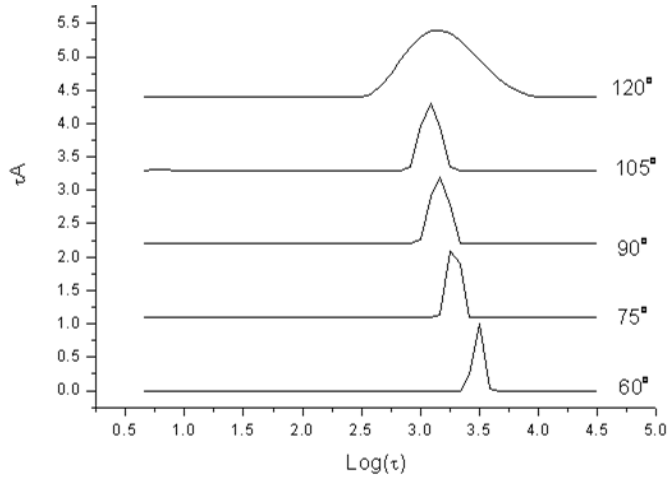

Figure A. 12: Relaxation time distribution functions for 0.005 wt% PEO-b-PNIPAM at 35 °C.

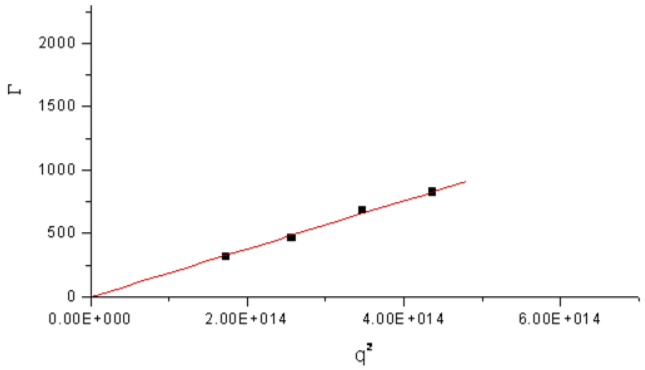

Figure A. 13: Plot of Γ vs. q^2 for 0.005 wt% PEO-b-PNIPAM at 35 °C.

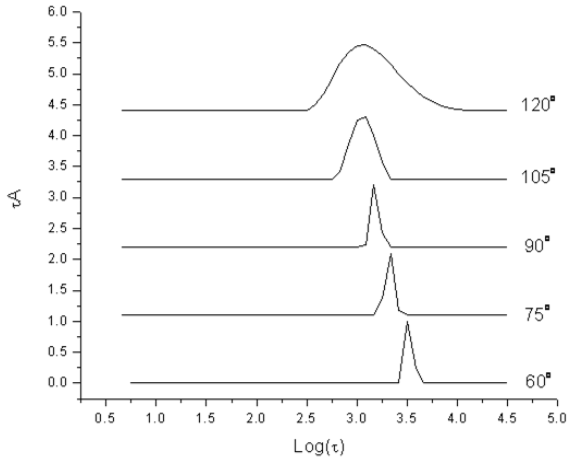

Figure A. 14: Relaxation time distribution functions for 0.005 wt% PEO-b-PNIPAM at 40 °C.

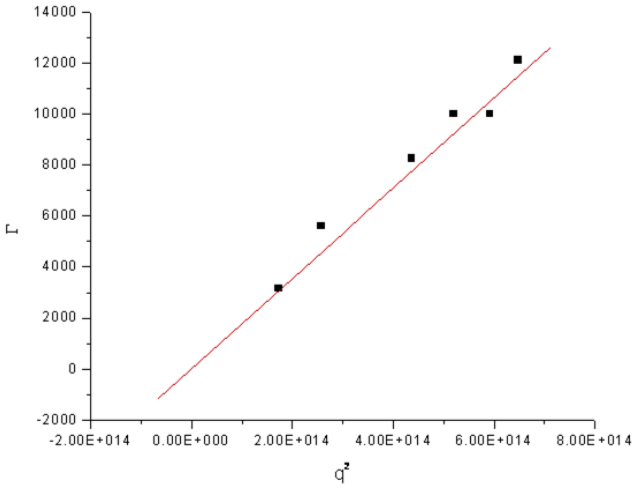

Figure A. 15: Plot of Γ vs. q^2 for 0.005 wt% PEO-b-PNIPAM at 40 °C.

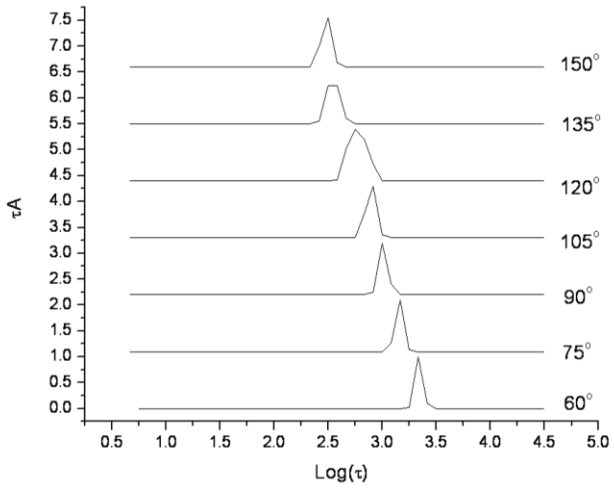

Figure A. 16: Relaxation time distribution functions for 0.005 wt% PEO-b-PNIPAM at 45 °C.

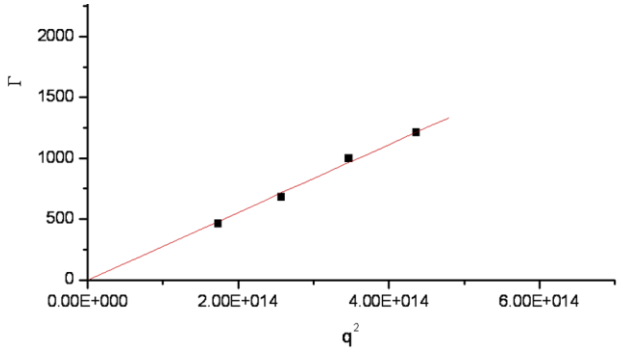

Figure A. 17: Plot of Γ vs. q^2 for 0.005 wt% PEO-b-PNIPAM at 45 °C.

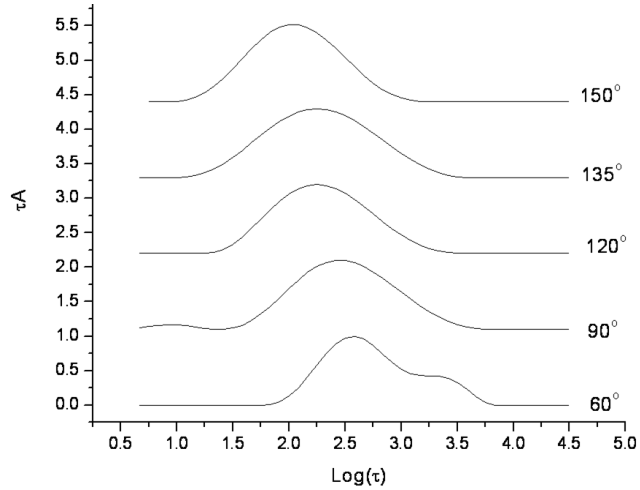

Figure A. 18: Relaxation time distribution functions - 0.1 wt% PEO-b-PNIPAM in 6.95 mM α-CD at 25 °C.

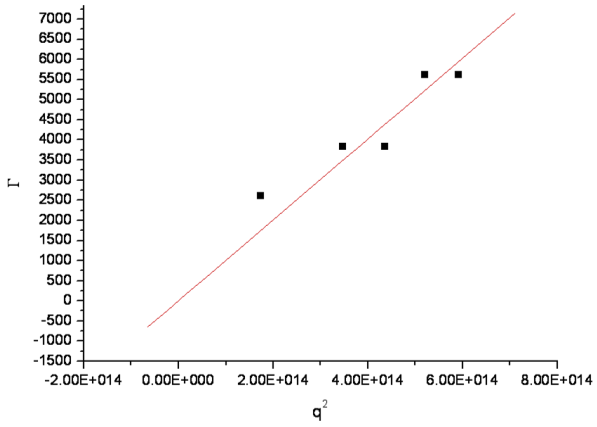

Figure A. 19: Plot of Γ vs. q^2 for 0.1 wt% PEO-b-PNIPAM in 6.95 mM α-CD at 25 °C.

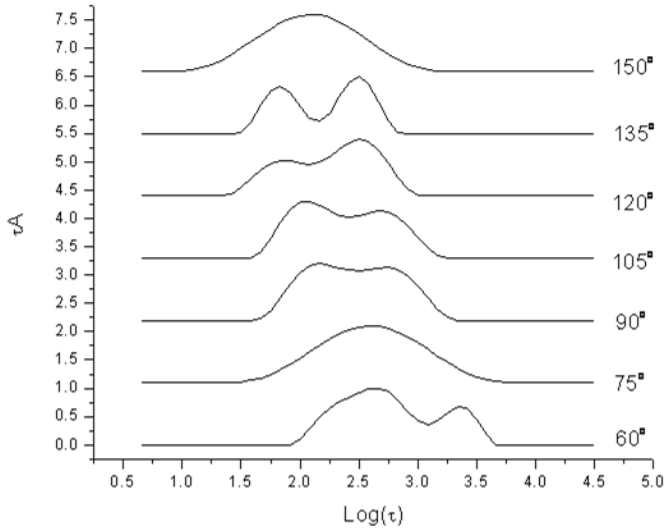

Figure A. 20: Relaxation time distribution functions - 0.1 wt% PEO-b-PNIPAM in 6.95 mM α-CD at 30 °C.

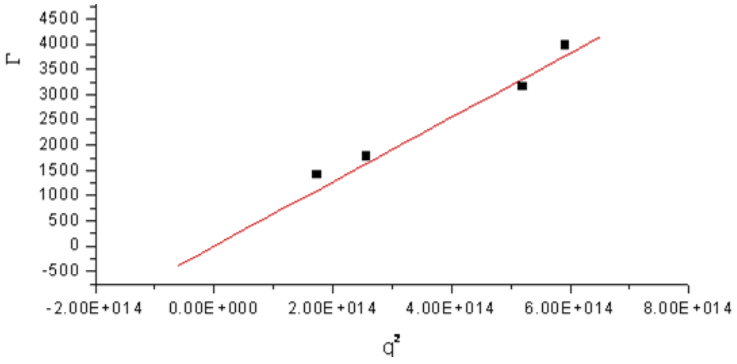

Figure A. 21: Plot of Γ vs. q^2 for 0.1 wt% PEO-b-PNIPAM in 6.95 mM α-CD at 30 °C.

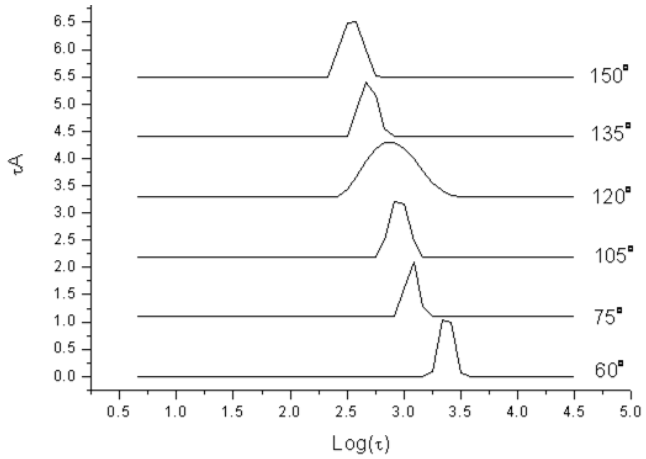

Figure A. 22: Relaxation time distribution functions - 0.005 wt% PEO-b-PNIPAM in 0.35 mM α-CD at 35°C.

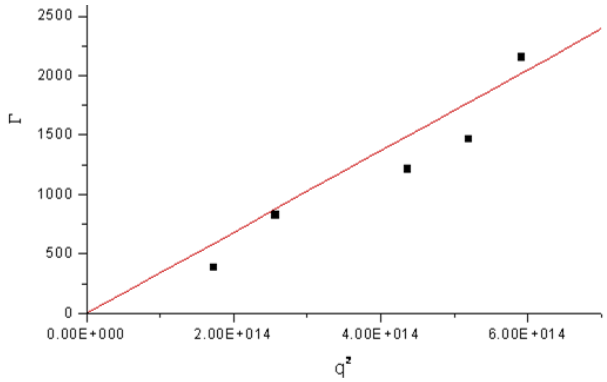

Figure A. 23: Plot of Γ vs. q^2 for 0.005 wt% PEO-b-PNIPAM in 0.35 mM α-CD at 35 °C.

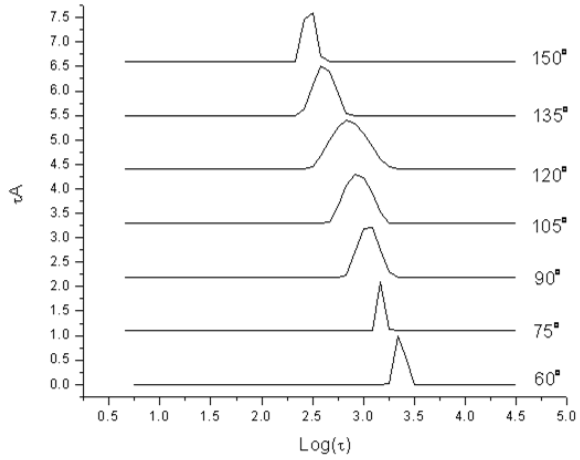

Figure A. 24: Relaxation time distribution functions - 0.005 wt% PEO-b-PNIPAM in 0.35 mM α-CD at 40°C.

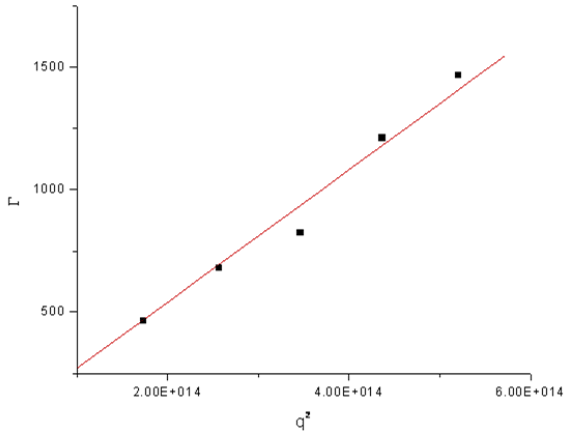

Figure A. 25: Plot of Γ vs. q^2 for 0.005 wt% PEO-b-PNIPAM in 0.35 mM α-CD at 40 °C.

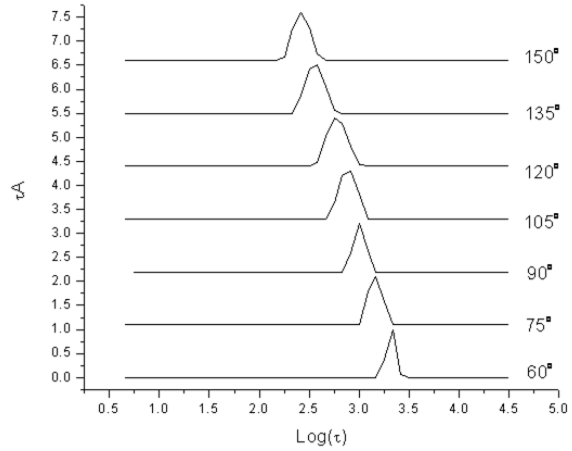

Figure A. 26: Relaxation time distribution functions - 0.005 wt% PEO-b-PNIPAM in 0.35 mM α-CD at 45°C.

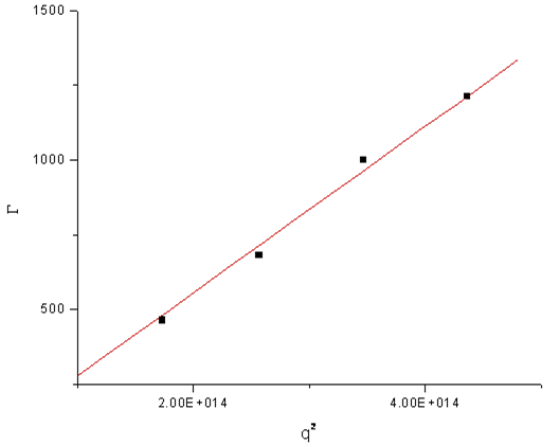

Figure A. 27:Plot of Γ vs. q^2 for 0.005 wt% PEO-b-PNIPAM in 0.35 mM α-CD at 45 °C.

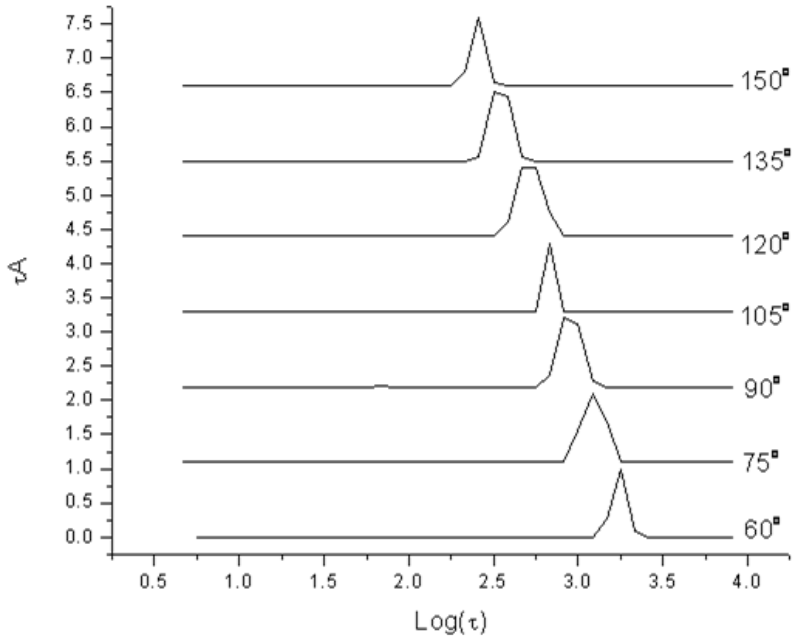

Figure A. 28: Relaxation time distribution functions - 0.005 wt% PEO-b-PNIPAM in 0.35 mM α-CD at 50°C.

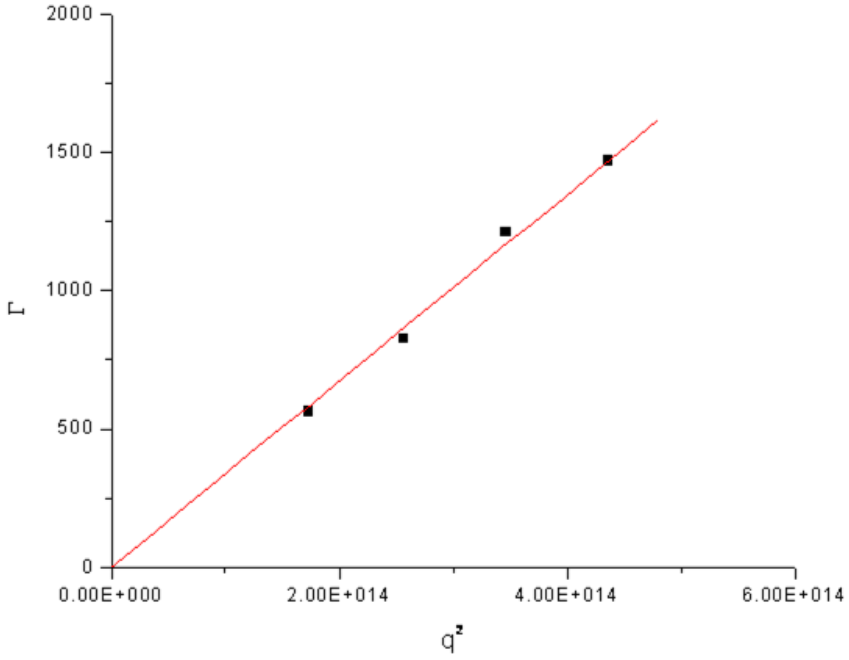

Figure A. 29:Plot of Γ vs. q2 for 0.005 wt% PEO-b-PNIPAM in 0.35 mM α-CD at 50 °C.

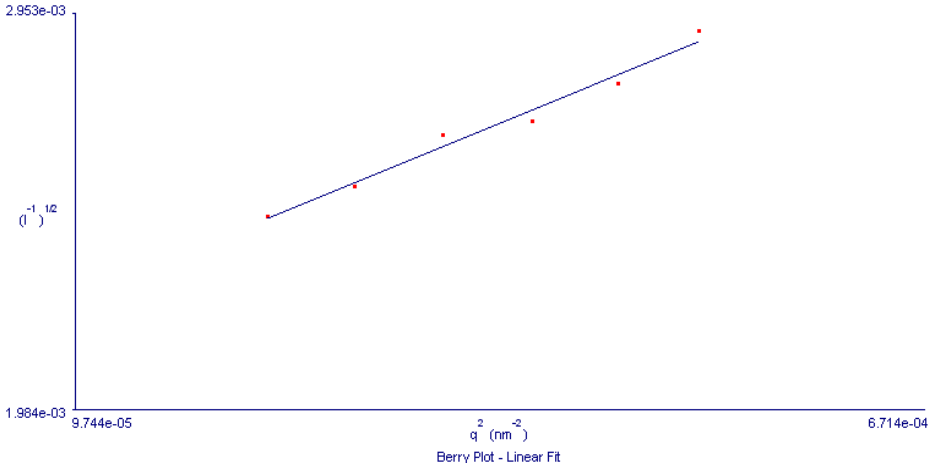

Figure A. 30: SLS results for 0.1 wt% PEO-b-PNIPAM at 35 °C.

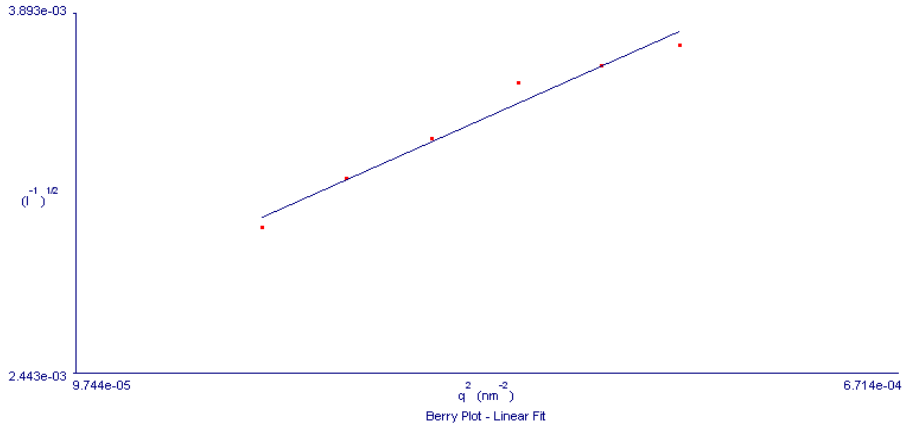

Figure A. 31: SLS results for 0.005 wt% PEO-b-PNIPAM at 40 °C.

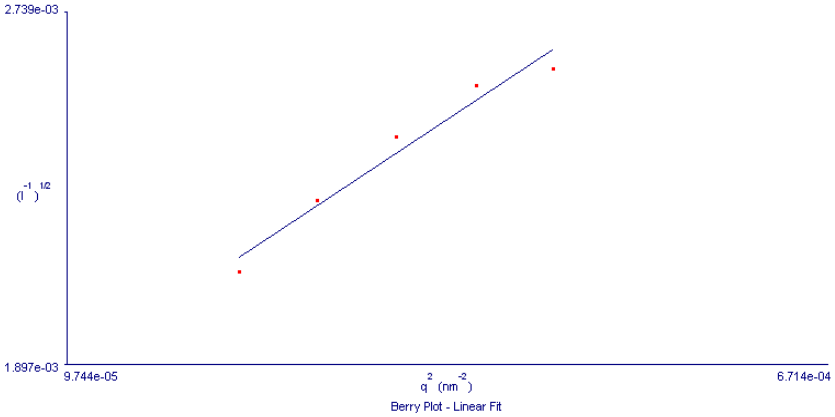

Figure A. 32: SLS results for 0.005 wt% PEO-b-PNIPAM at 45 °C.

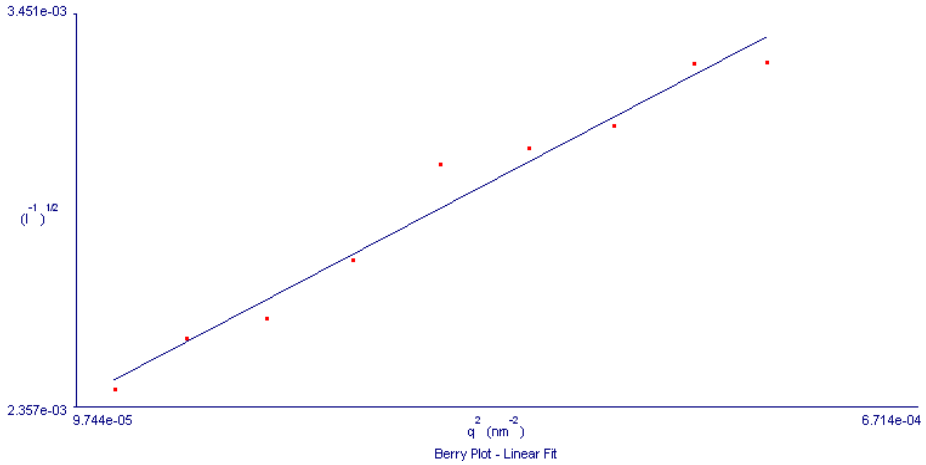

Figure A. 33: SLS results for 0.005 wt% PEO-b-PNIPAM at 50 °C.

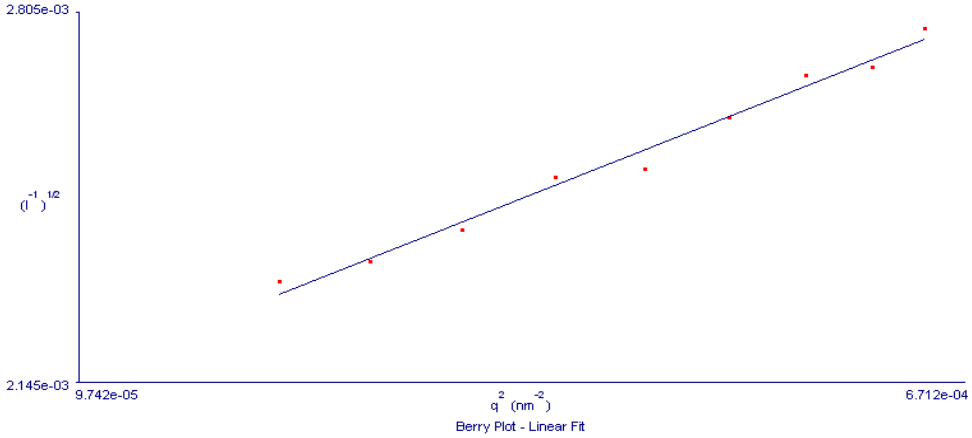

Figure A. 34: SLS results for 0.1 wt% PEO-b-PNIPAM in 6.95 mM α-CD at 10 °C.

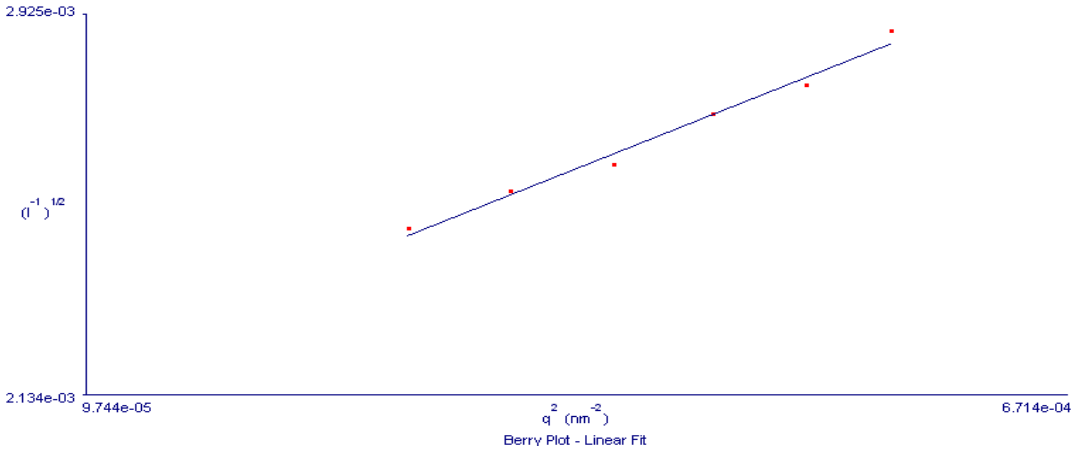

Figure A. 35: SLS results for 0.1 wt% PEO-b-PNIPAM in 6.95 mM α-CD at 15 °C.

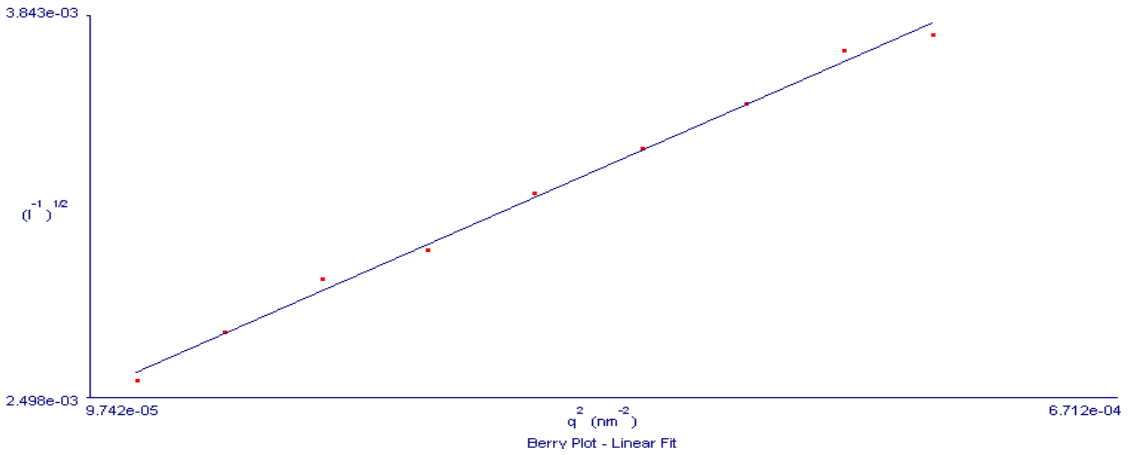

Figure A. 36: SLS results for 0.1 wt% PEO-b-PNIPAM in 6.95 mM α-CD at 20 °C.

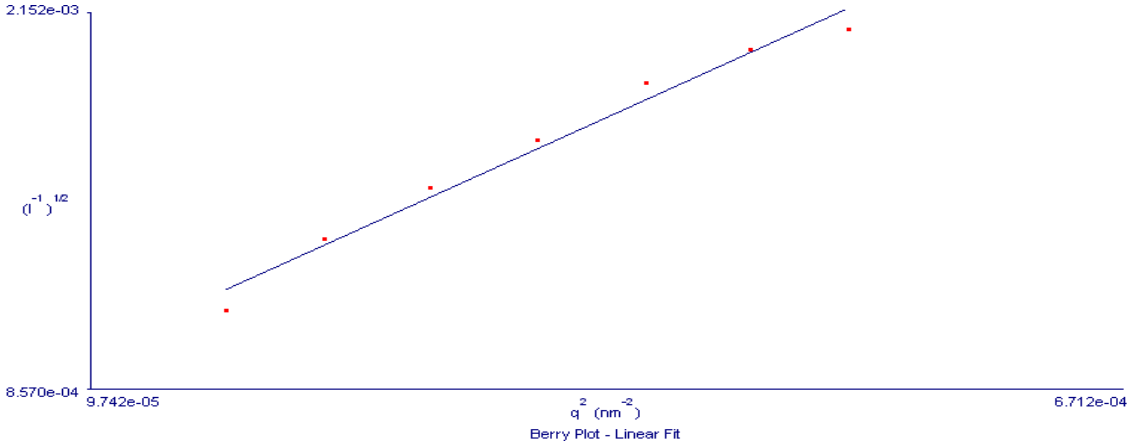

Figure A. 37: SLS results for 0.1 wt% PEO-b-PNIPAM in 6.95 mM α-CD at 25 °C.

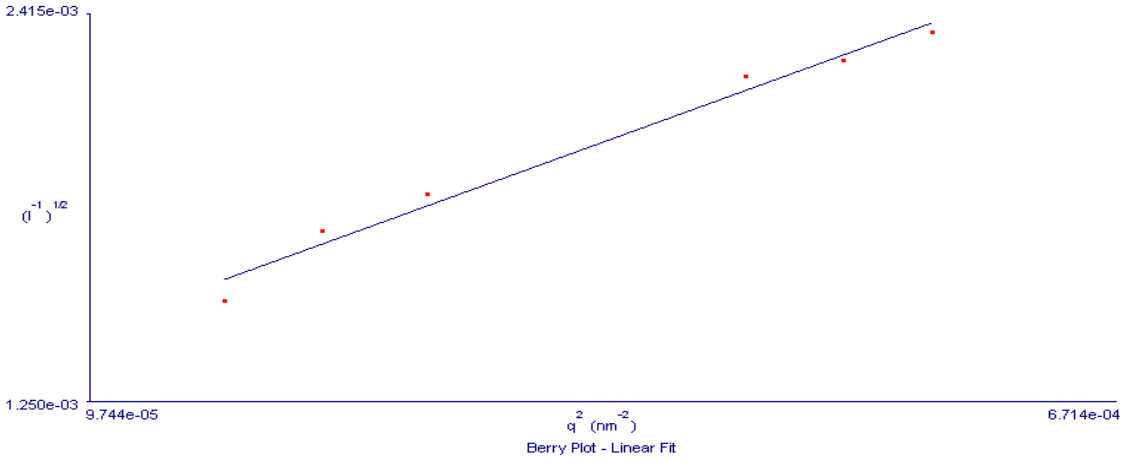

Figure A. 38: SLS results for 0.1 wt% PEO-b-PNIPAM in 6.95 mM α-CD at 30 °C.

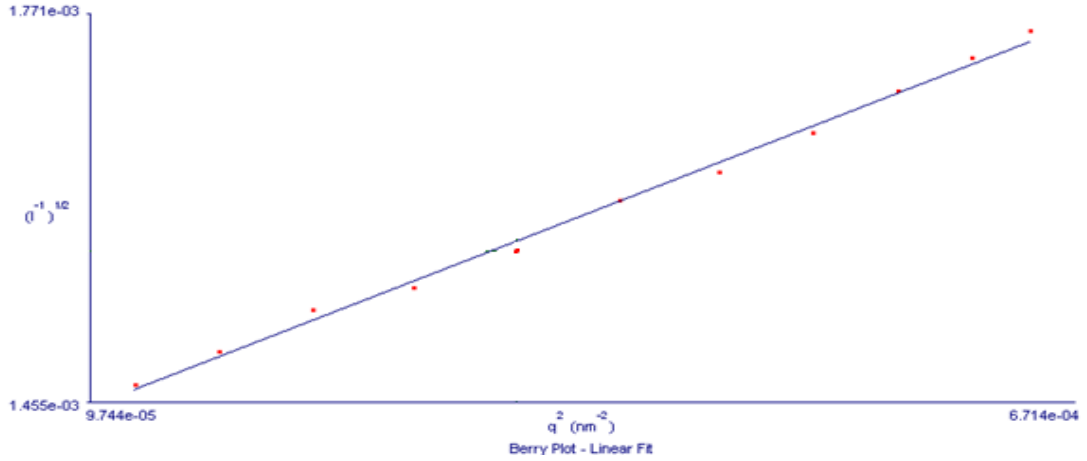

Figure A. 39: SLS results for 0.005 wt% PEO-b-PNIPAM in 0.35 mM α-CD at 35 °C.

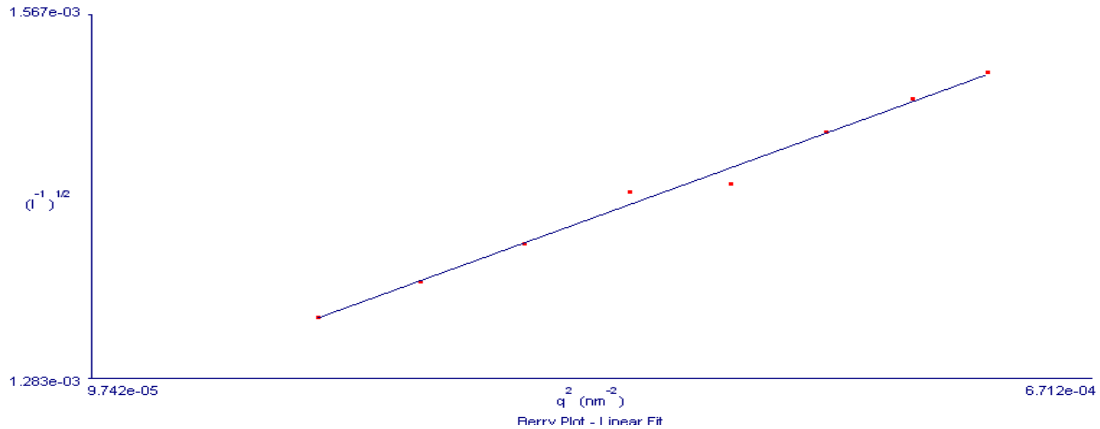

Figure A. 40: SLS results for 0.005 wt% PEO-b-PNIPAM in 0.35 mM α-CD at 40 °C.

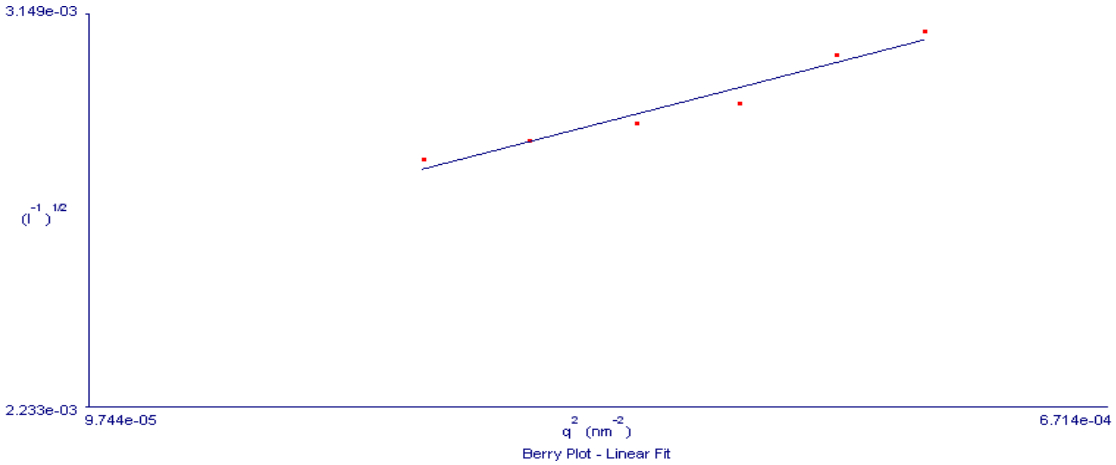

Figure A. 41: SLS results for 0.005 wt% PEO-b-PNIPAM in 0.35 mM α-CD at 45 °C.

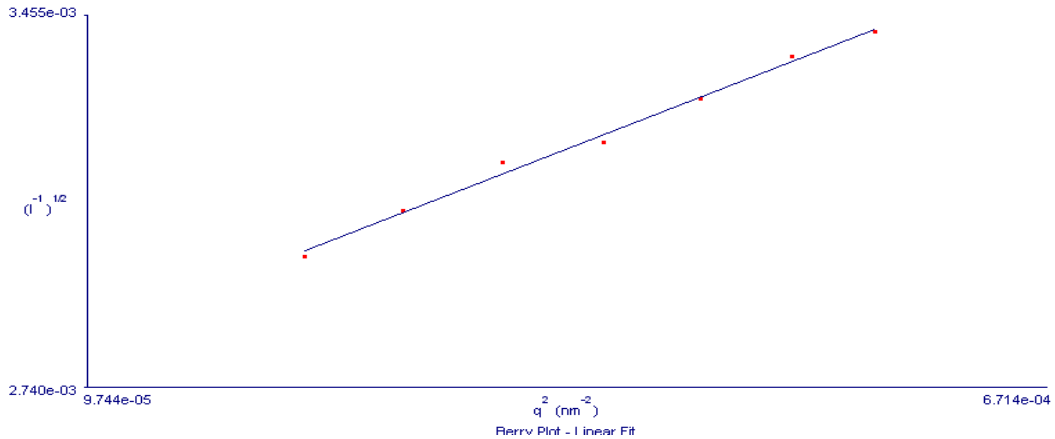

Figure A. 42: SLS results for 0.005 wt% PEO-b-PNIPAM in 0.35 mM α-CD at 50 °C.

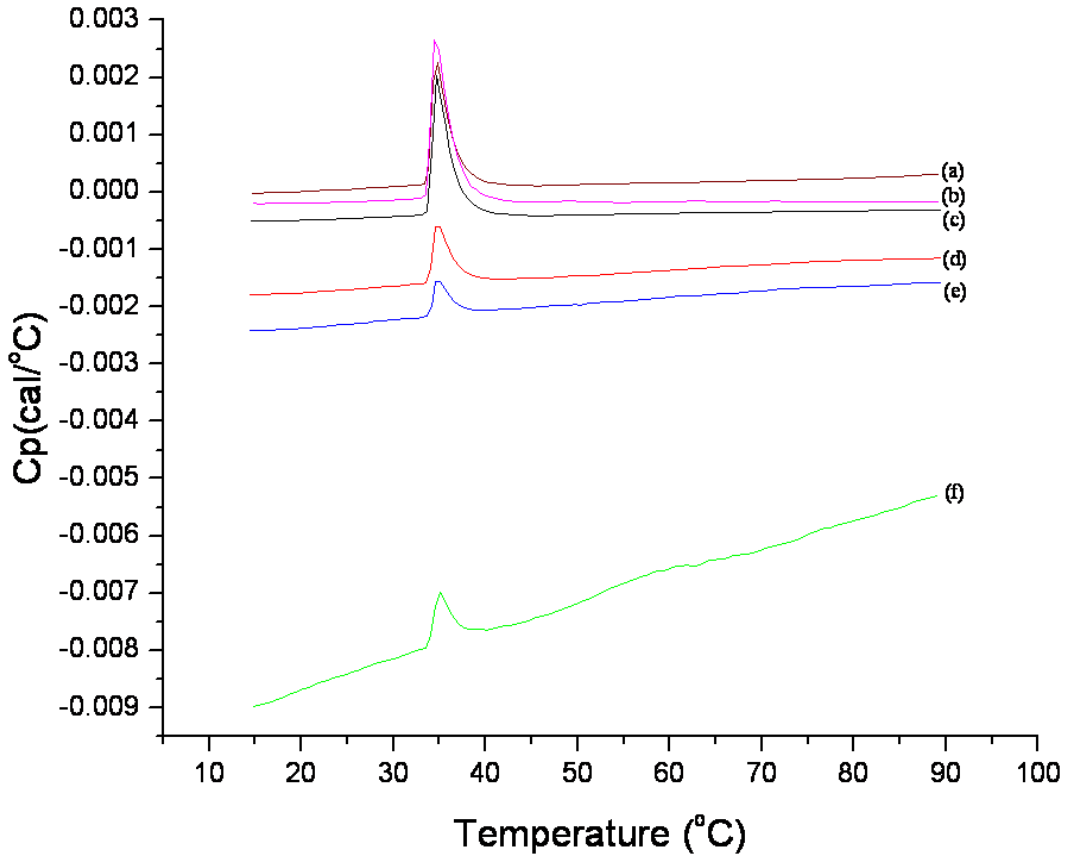

Figure A. 43:DSC Raw Data (a) 0.53, (b) 0, (c) 0.64, (d)2.96, (e)5.93, and (f) 21.26 mole ratio of α-CD to EO.

Appendix B

PPO-b-PMAA – Raw Data

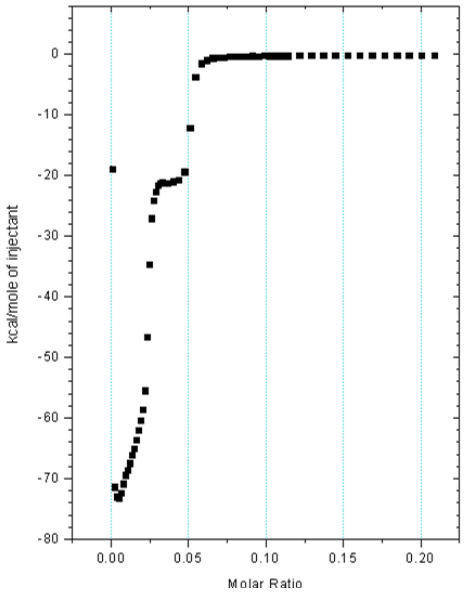

Figure B. 1: ITC results - 0.01 M HCl into pH 10 aqueous solution at 25 °C.

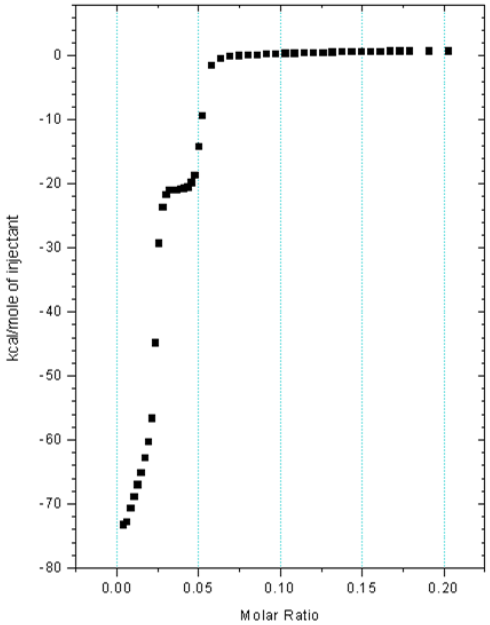

Figure B. 2: ITC results - 0.01 M HCl into pH 10 0.1 wt% PPO-b-PMAA at 25 °C.

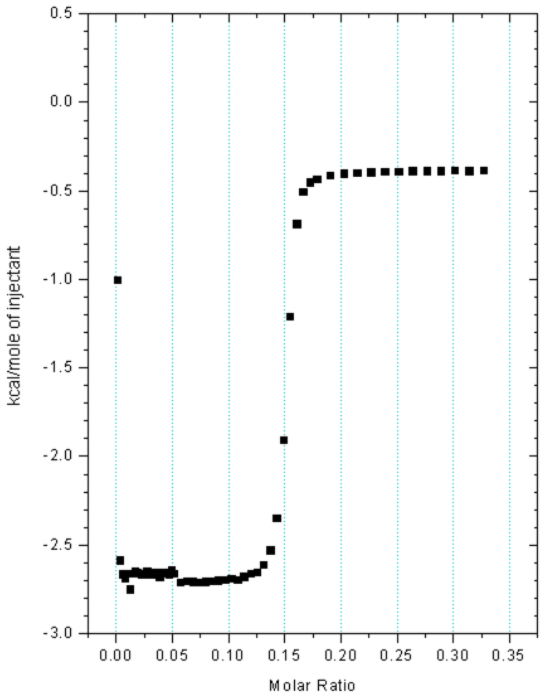

Figure B. 3: ITC results - 0.01 M NaOH into pH 3 aqueous solution at 25 °C.

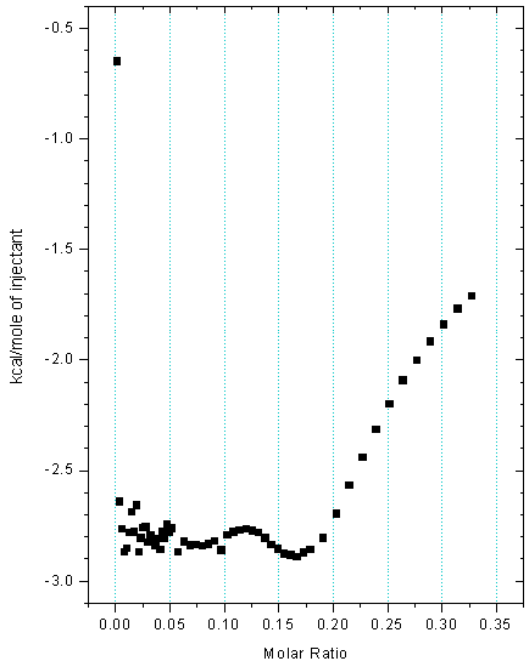

Figure B. 4: ITC results - 0.01 M NaOH into pH 3 0.1 wt% PPO-b-PMAA at 25 °C.

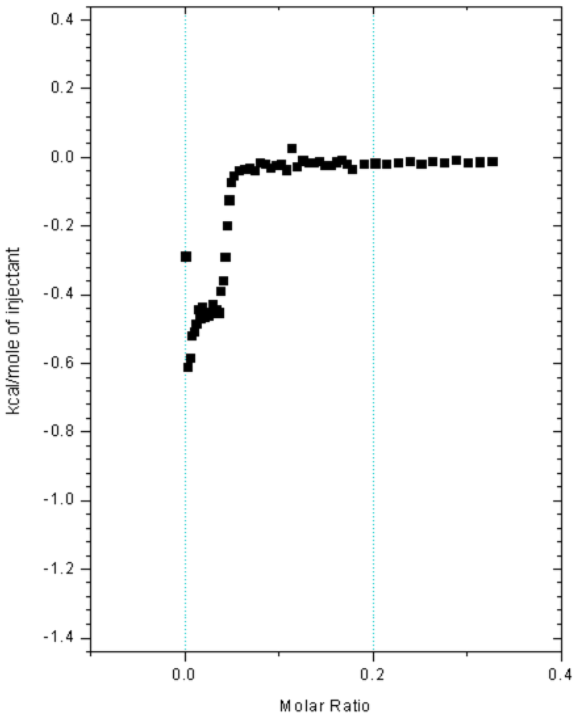

Figure B. 5: 0.01 M HCl into pH 10 aqueous solution at 60 °C.

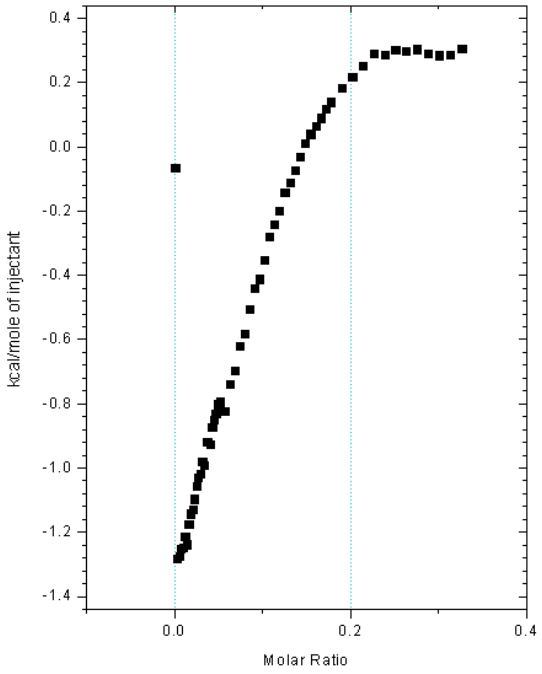

Figure B. 6:0.01 M HCl into pH 10 0.1 wt% PPO-b-PMAA at 60 °C.

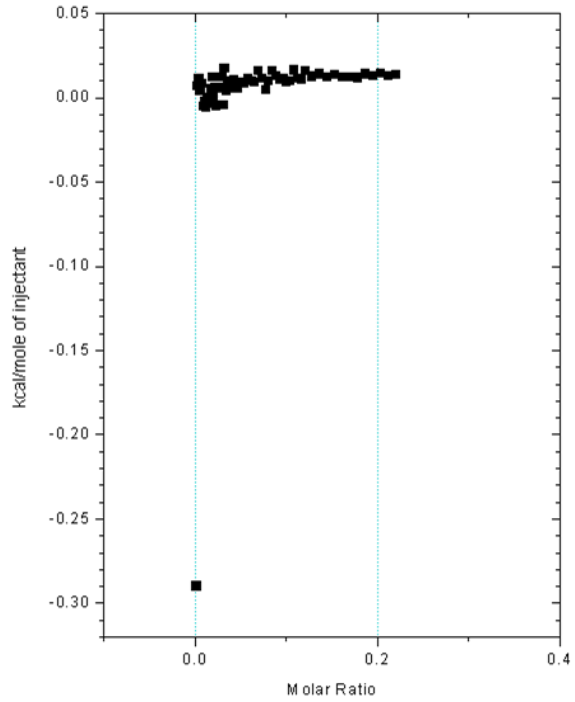

Figure B. 7: 1.85 wt% pH 10 β-CD into pH 10 aqueous solution at 25 °C.

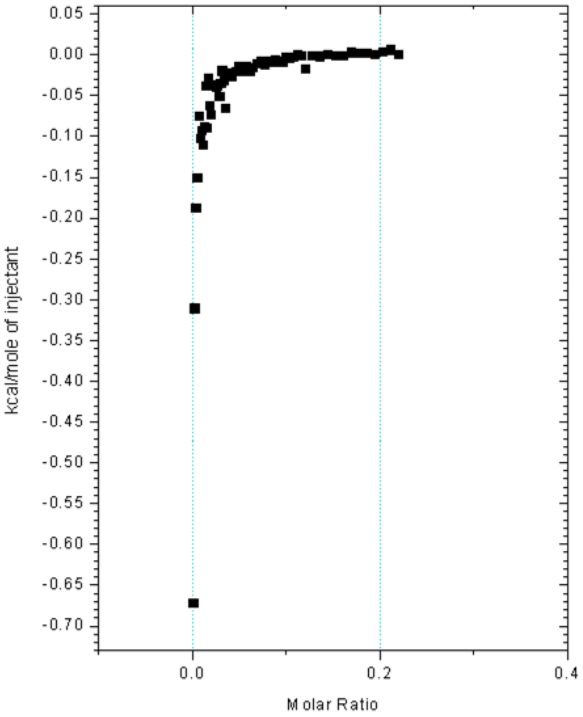

Figure B. 8:1.85 wt% pH 10 β-CD into pH 10 PPO-b-PMAA at 25 °C.

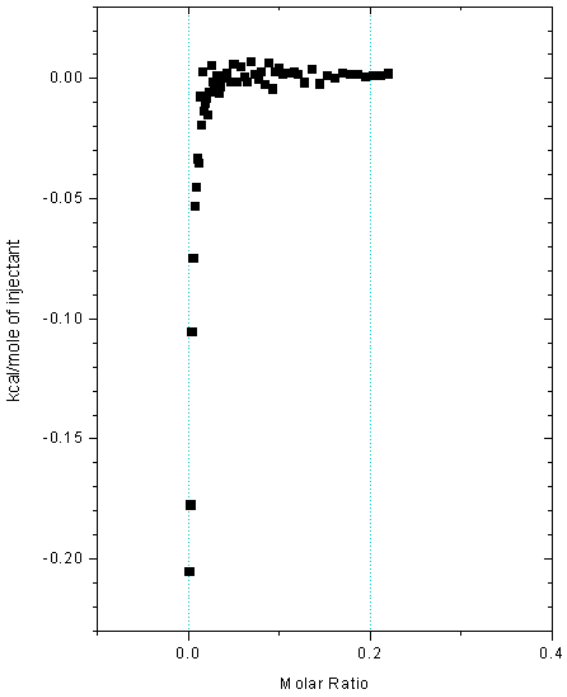

Figure B. 9: 1.85 wt% pH 4 β-CD into pH 4 aqueous solution at 25 °C.

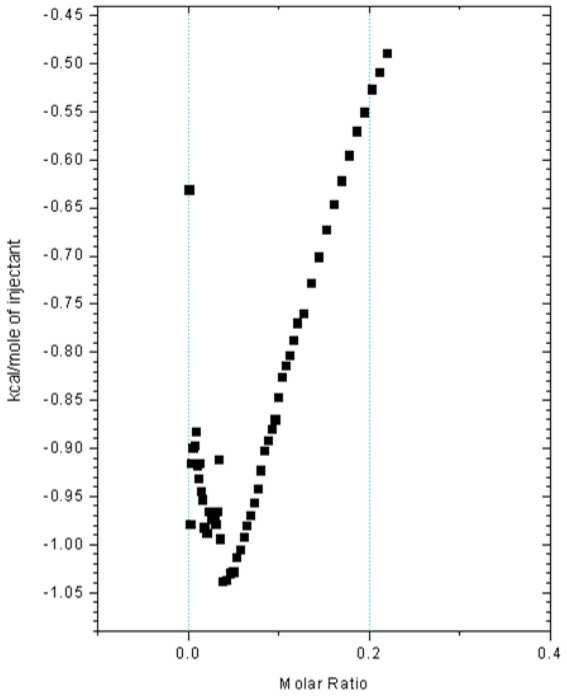

Figure B. 10: 1.85 wt% pH 4 β-CD into pH 4 PPO-b-PMAA at 25 °C.

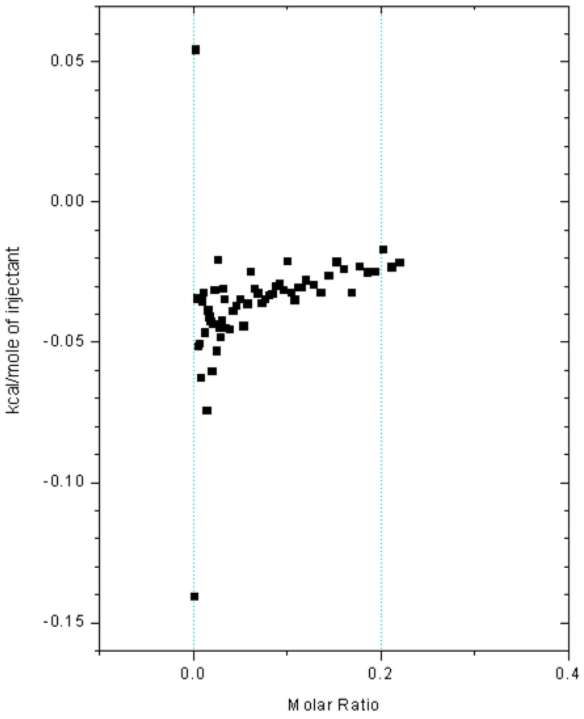

Figure B. 11: 1.85 wt% pH 10 β-CD into pH 10 aqueous solution at 60 °C.

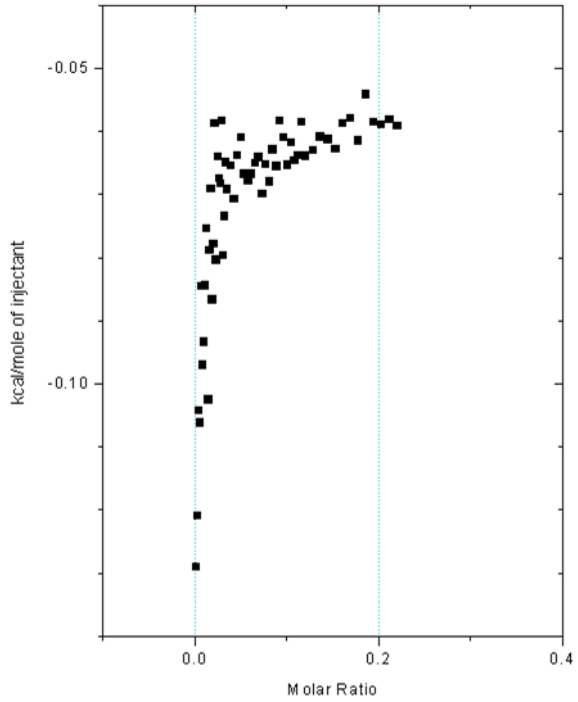

Figure B. 12: 1.85 wt% pH 10 β-CD into pH 10 PPO-b-PMAA at 60 °C.

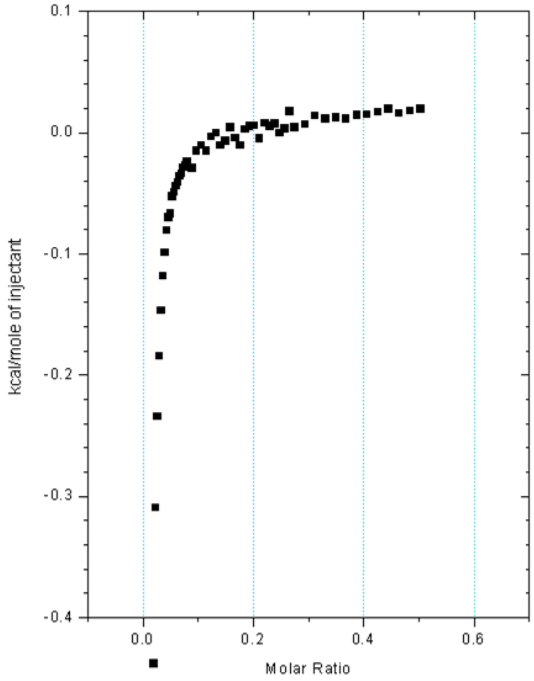

Figure B. 13: 3.625 wt% pH 10 α-CD into pH 10 aqueous solution at 25 °C.

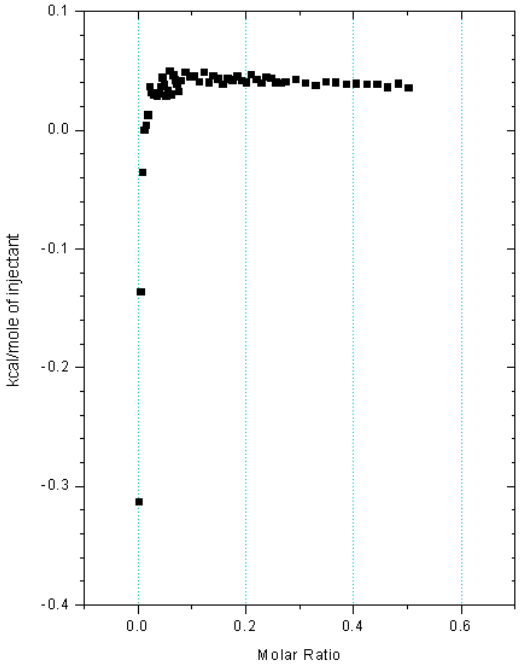

Figure B. 14: 3.625 wt% pH 10 α-CD into pH 10 PPO-b-PMAA at 25 °C.

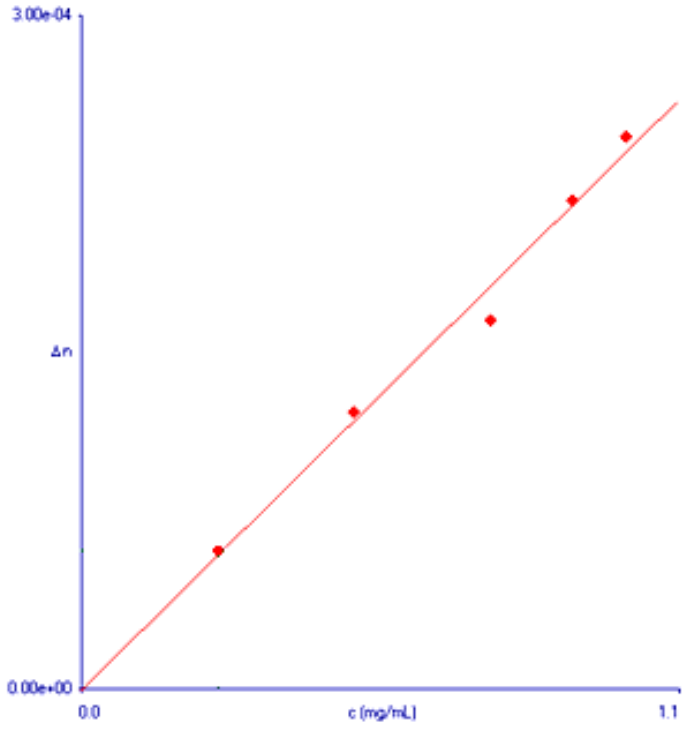

Figure B. 15: Plot of Δn vs. c in the determination of dn/dc of PPO-PMAA at pH 10.

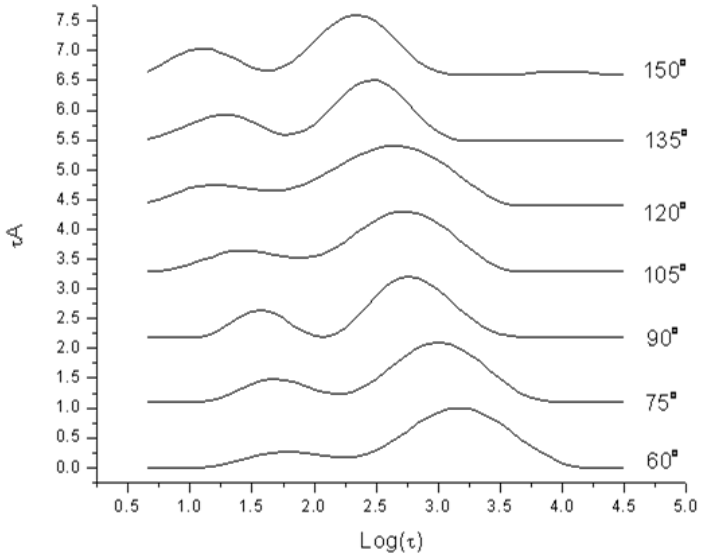

Figure B. 16: Relaxation time distribution functions - 0.1 wt% PPO-b-PMAA at 20 °C.

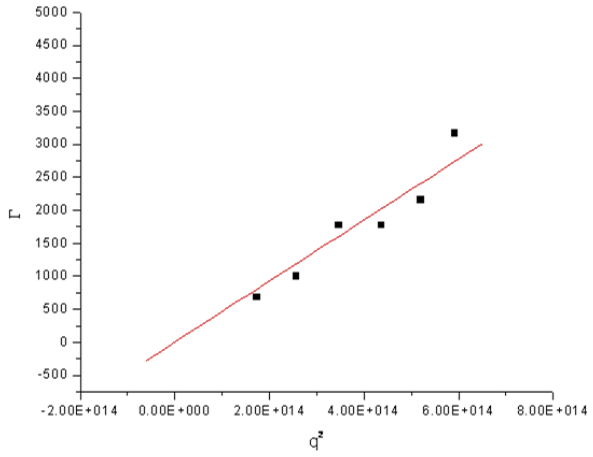

Figure B. 17: Plot of Γ vs. q^2 for 0.1 wt% PPO-MAA at 20 °C – large peak.

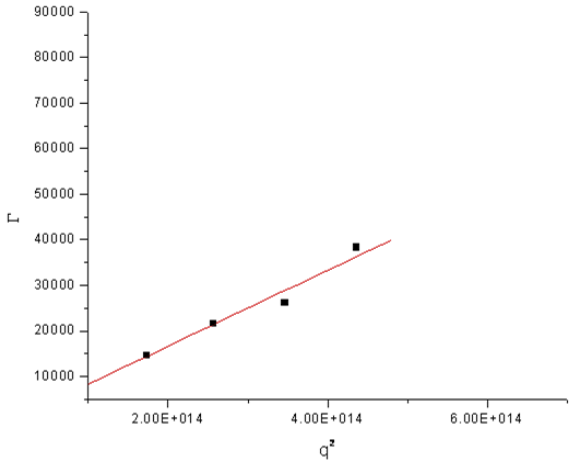

Figure B. 18: Plot of Γ vs. q^2 for 0.1 wt% PPO-MAA at 20 °C – small peak.

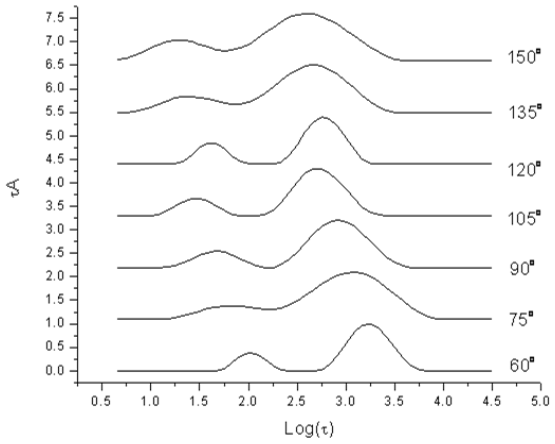

Figure B. 19: Relaxation time distribution functions - 0.1 wt% PPO-b-PMAA at 25 °C.

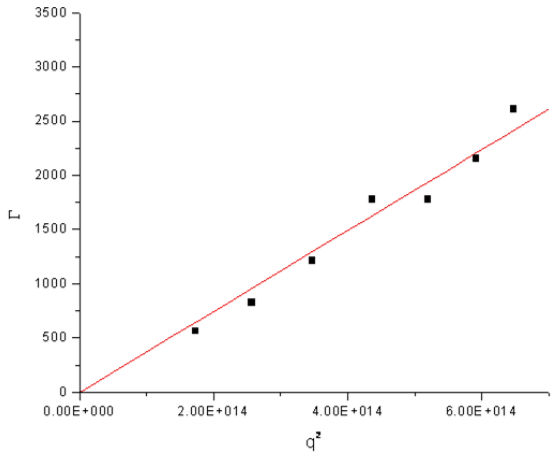

Figure B. 20: Plot of Γ vs. q^2 for 0.1 wt% PPO-MAA at 25 °C – large peak.

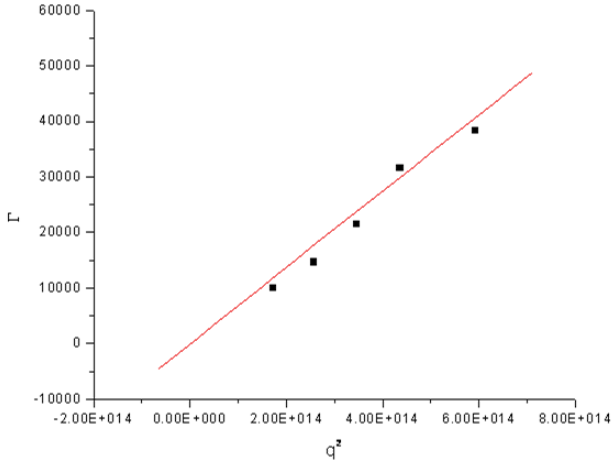

Figure B. 21: Plot of Γ vs. q^2 for 0.1 wt% PPO-MAA at 25 °C – small peak.

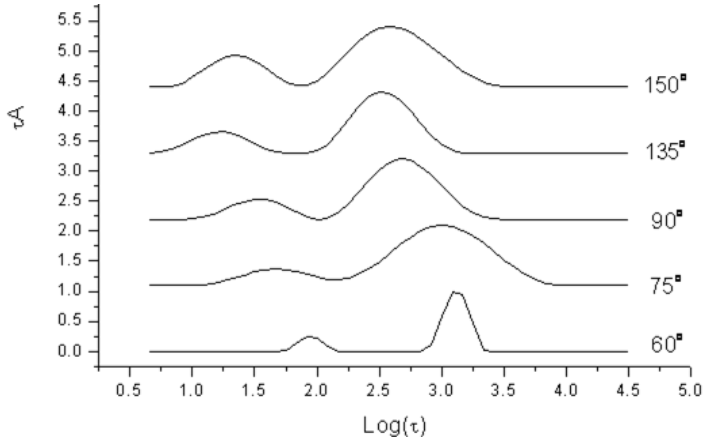

Figure B. 22: Relaxation time distribution functions - 0.1 wt% PPO-b-PMAA at 30 °C.

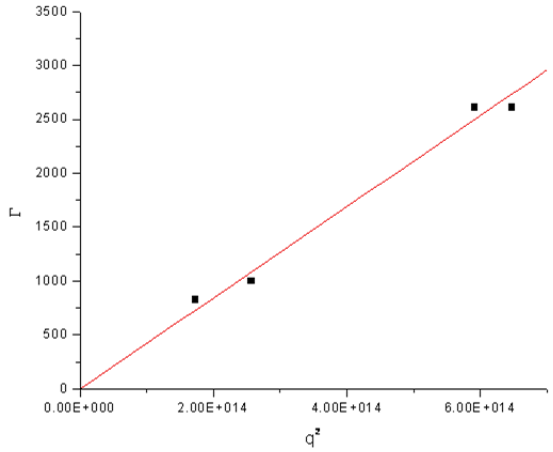

Figure B. 23: Plot of Γ vs. q^2 for 0.1 wt% PPO-MAA at 30 °C – large peak.

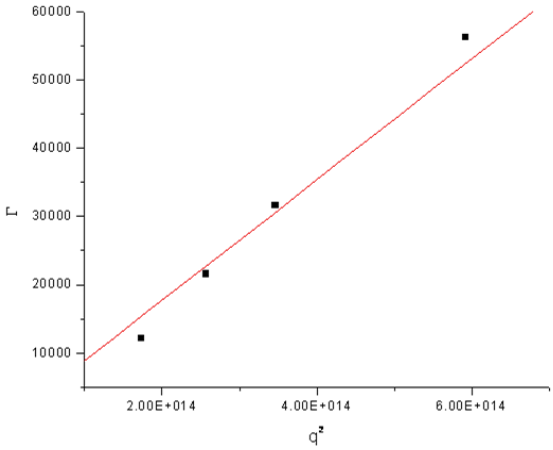

Figure B. 24: Plot of Γ vs. q^2 for 0.1 wt% PPO-MAA at 30 °C – small peak.

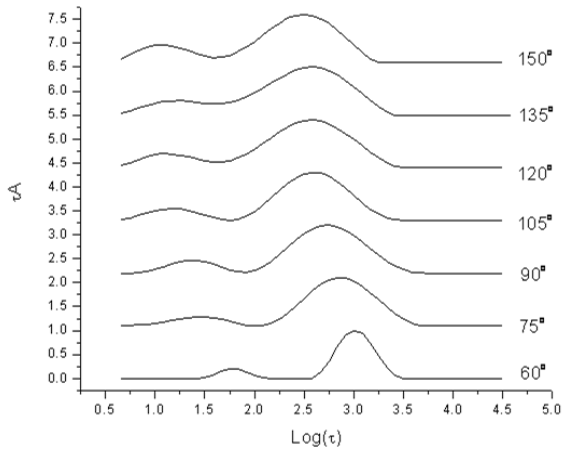

Figure B. 25: Relaxation time distribution functions - 0.1 wt% PPO-b-PMAA at 35 °C.

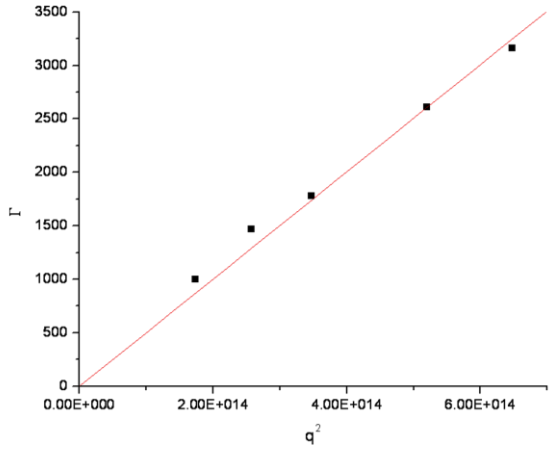

Figure B. 26: Plot of Γ vs. q^2 for 0.1 wt% PPO-MAA at 35 °C – large peak.

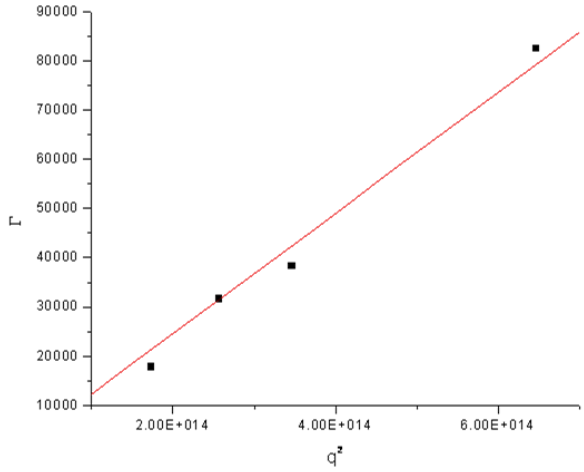

Figure B. 27: Plot of Γ vs. q^2 for 0.1 wt% PPO-MAA at 35 °C – small peak.

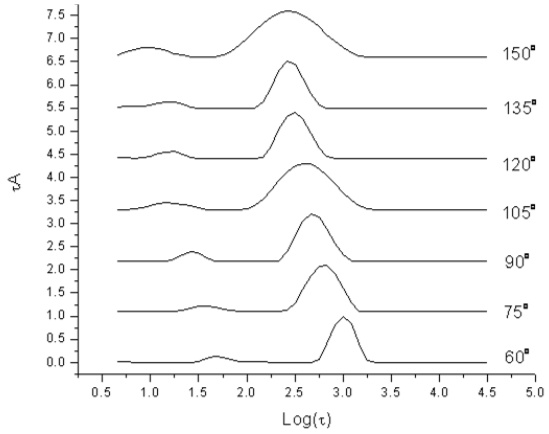

Figure B. 28: Relaxation time distribution functions - 0.1 wt% PPO-b-PMAA at 40 °C.

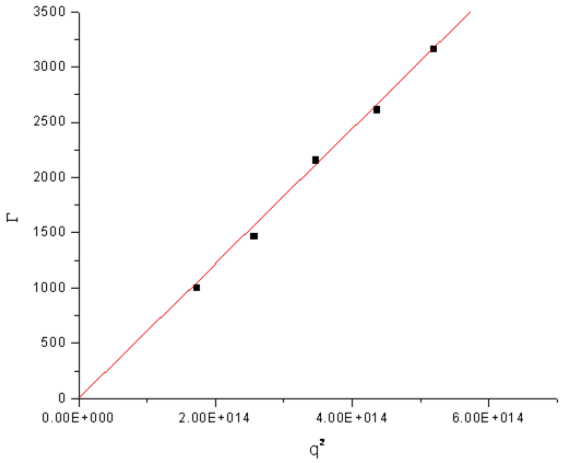

Figure B. 29: Plot of Γ vs. q^2 for 0.1 wt% PPO-MAA at 40 °C – large peak.

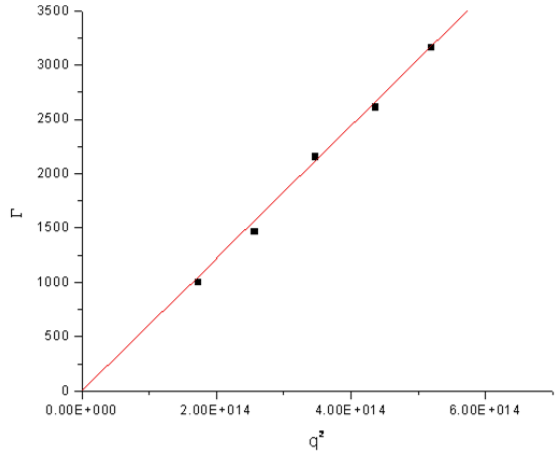

Figure B. 30: Plot of Γ vs. q^2 for 0.1 wt% PPO-MAA at 40 °C – small peak.

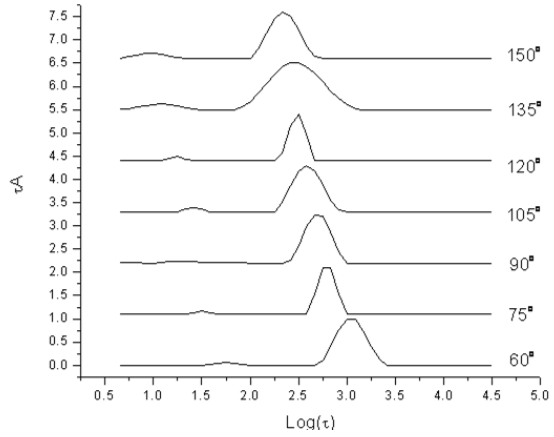

Figure B. 31: Relaxation time distribution functions - 0.1 wt% PPO-b-PMAA at 45 °C.

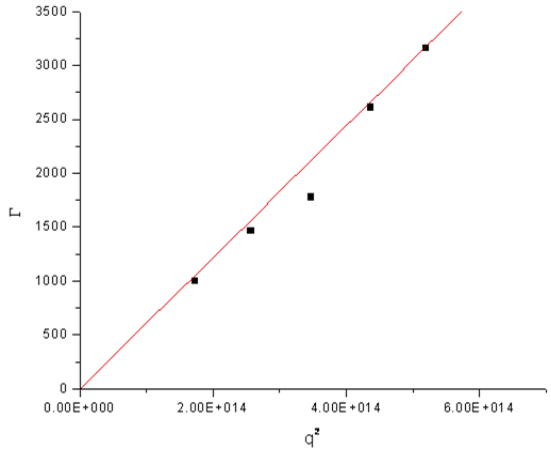

Figure B. 32: Plot of Γ vs. q^2 for 0.1 wt% PPO-MAA at 45 °C.

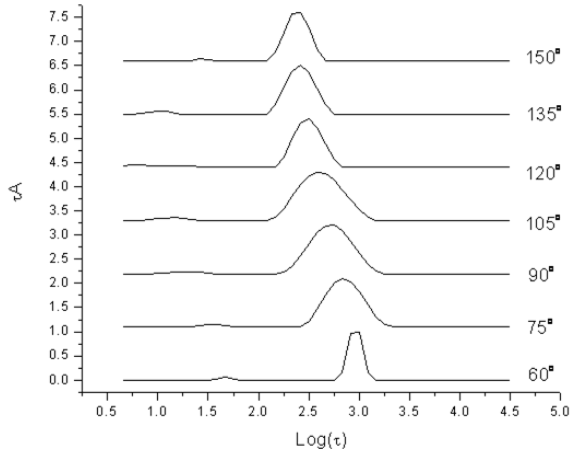

Figure B. 33: Relaxation time distribution functions - 0.1 wt% PPO-b-PMAA at 50 °C.

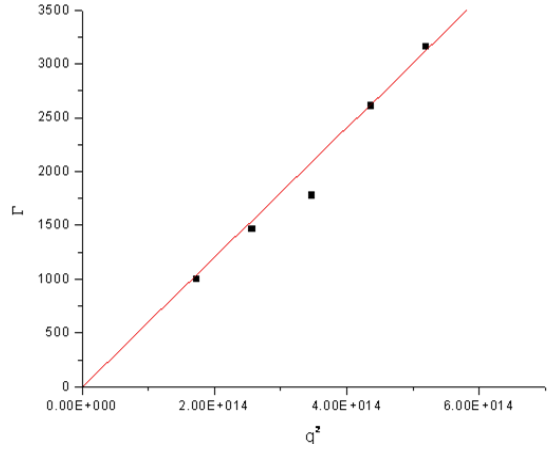

Figure B. 34: Plot of Γ vs. q^2 for 0.1 wt% PPO-MAA at 50 °C.

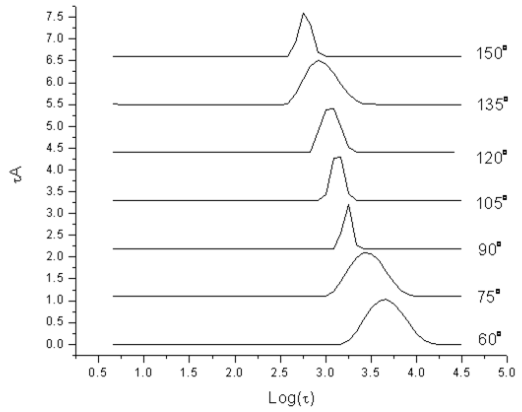

Figure B. 35: Relaxation time distribution functions - 0.1 wt% PPO-b-PMAA in 15.48 mM β-CD at 20 °C.

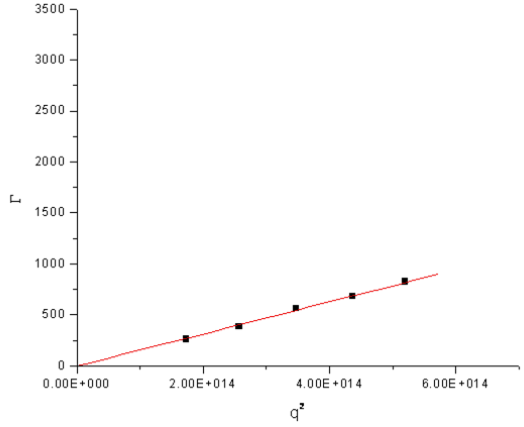

Figure B. 36: Plot of Γ vs. q^2 for 0.1 wt% PPO-MAA in 15.48 mM β-CD at 20 °C.

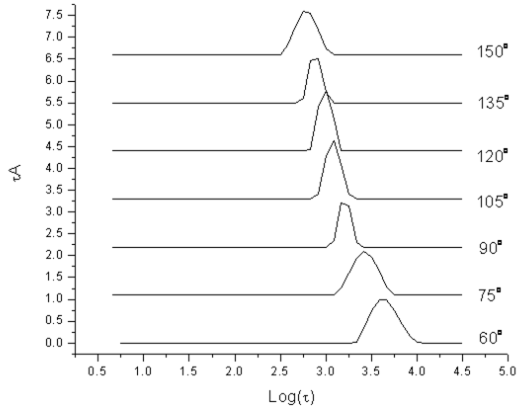

Figure B. 37: Relaxation time distribution functions - 0.1 wt% PPO-b-PMAA in 15.48 mM β-CD at 25 °C.

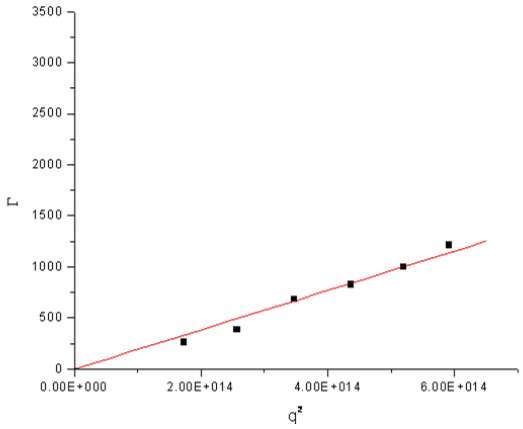

Figure B. 38: Plot of Γ vs. q^2 for 0.1 wt% PPO-MAA in 15.48 mM β-CD at 25 °C.

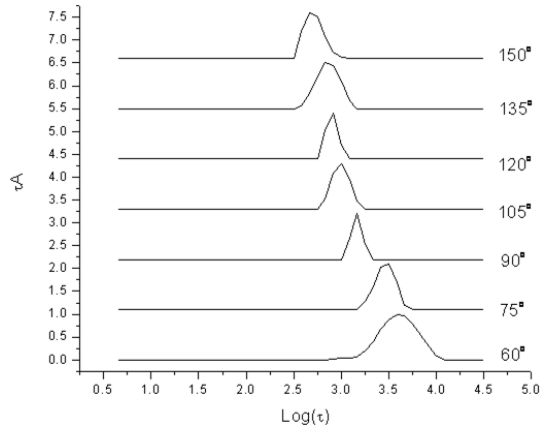

Figure B. 39: Relaxation time distribution functions - 0.1 wt% PPO-b-PMAA in 15.48 mM β-CD at 30 °C.

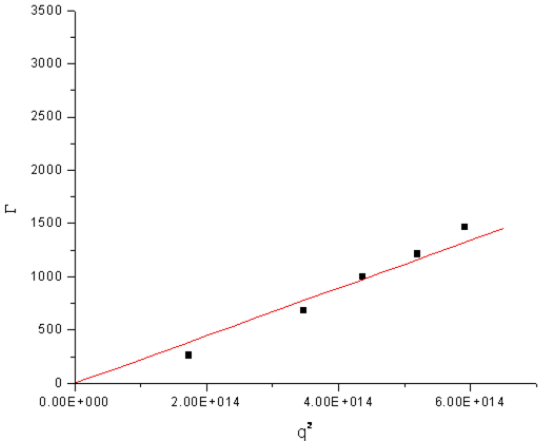

Figure B. 40: Plot of Γ vs. q^2 for 0.1 wt% PPO-MAA in 15.48 mM β-CD at 30 °C.

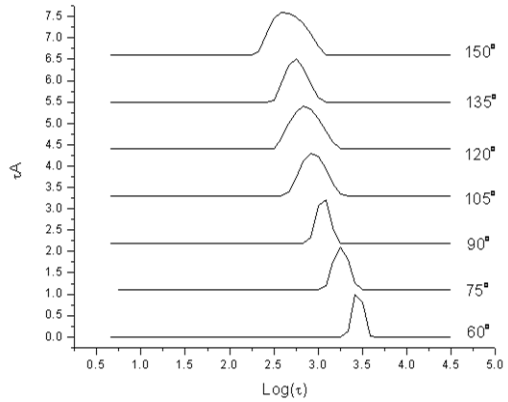

Figure B. 41: Relaxation time distribution functions - 0.1 wt% PPO-b-PMAA in 15.48 mM β-CD at 40 °C.

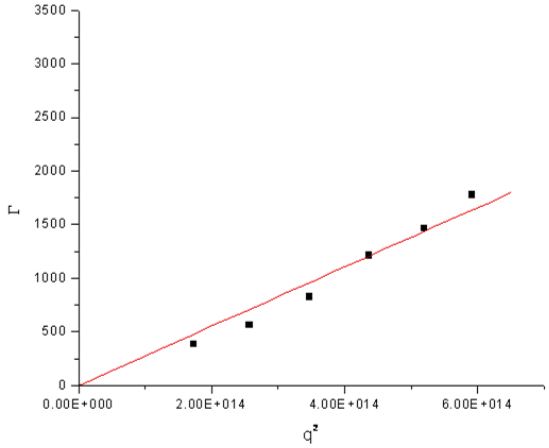

Figure B. 42: Plot of Γ vs. q^2 for 0.1 wt% PPO-MAA in 15.48 mM β-CD at 40 °C.

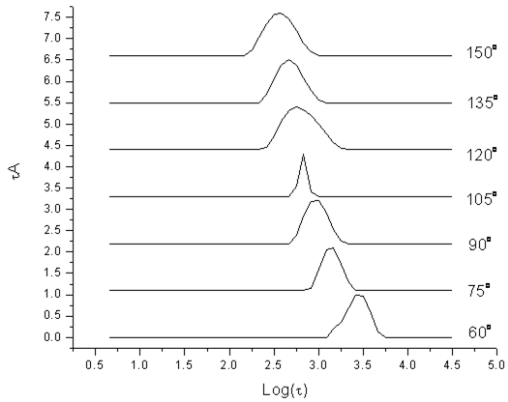

Figure B. 43: Relaxation time distribution functions - 0.1 wt% PPO-b-PMAA in 15.48 mM β-CD at 50 °C.

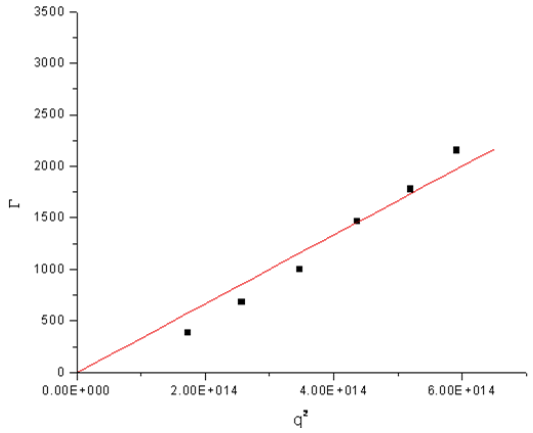

Figure B. 44: Plot of Γ vs. q^2 for 0.1 wt% PPO-MAA in 15.48 mM β-CD at 50 °C.

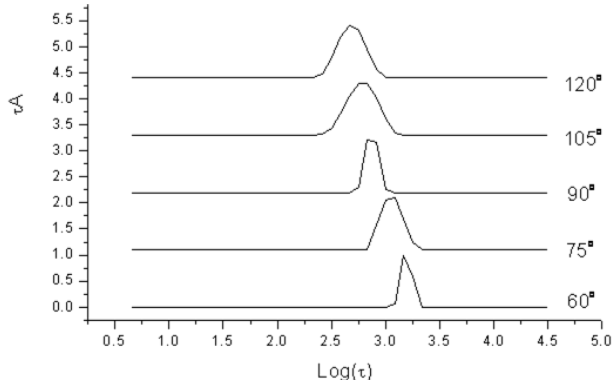

Figure B. 45: Relaxation time distribution functions - 0.1 wt% PPO-b-PMAA in 15.48 mM β-CD at 60 °C.

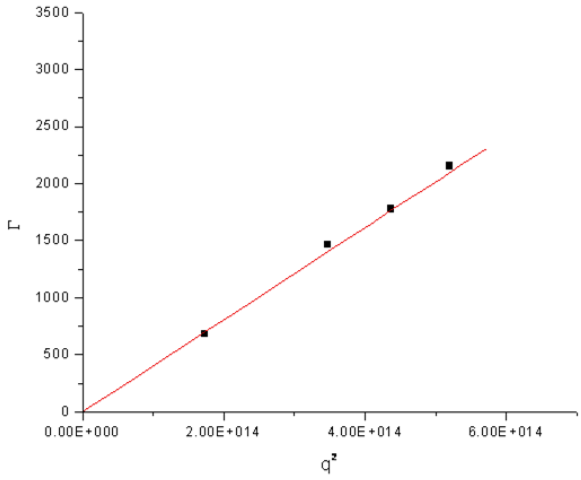

Figure B. 46: Plot of Γ vs. q^2 for 0.1 wt% PPO-MAA in 15.48 mM β-CD at 60 °C.

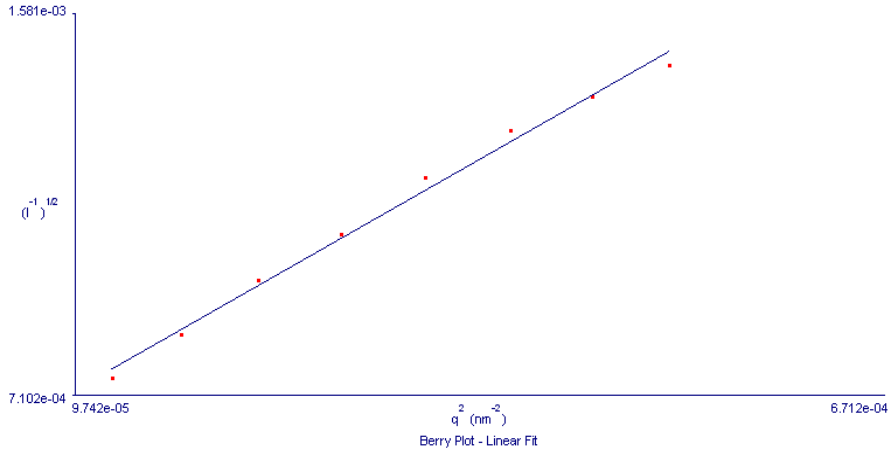

Figure B. 47: SLS results for 0.1 wt% PPO-b-PMAA in 15.48 mM α-CD at 20 °C.

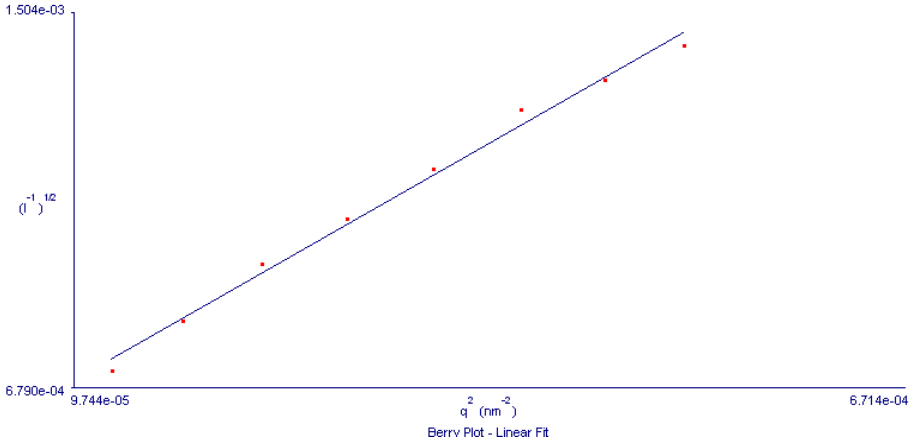

Figure B. 48: SLS results for 0.1 wt% PPO-b-PMAA in 15.48 mM α-CD at 25 °C.

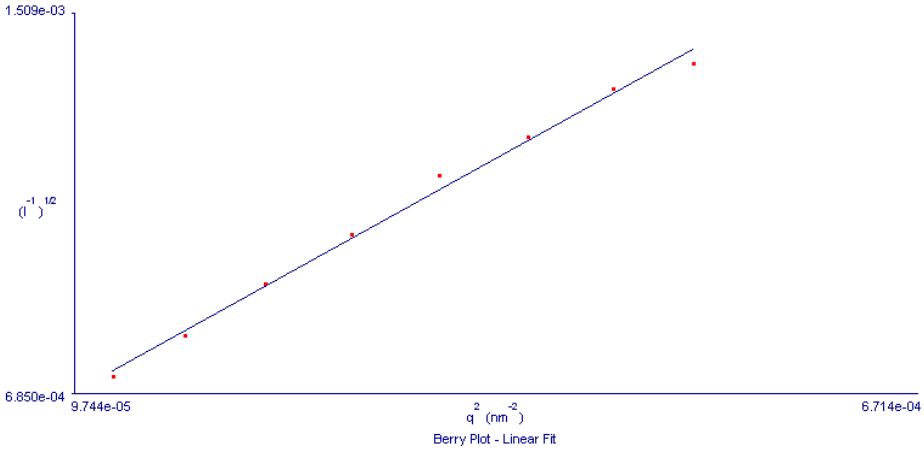

Figure B. 49: SLS results for 0.1 wt% PPO-b-PMAA in 15.48 mM α-CD at 30 °C.

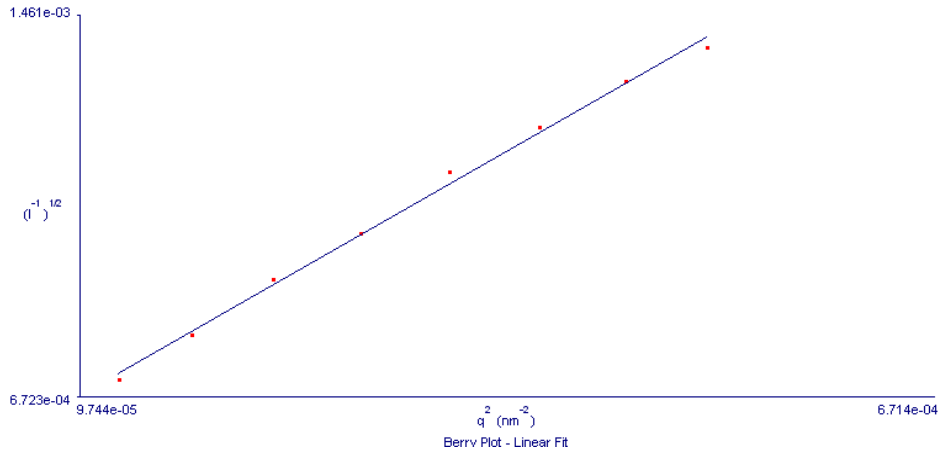

Figure B. 50: SLS results for 0.1 wt% PPO-b-PMAA in 15.48 mM α-CD at 40 °C.

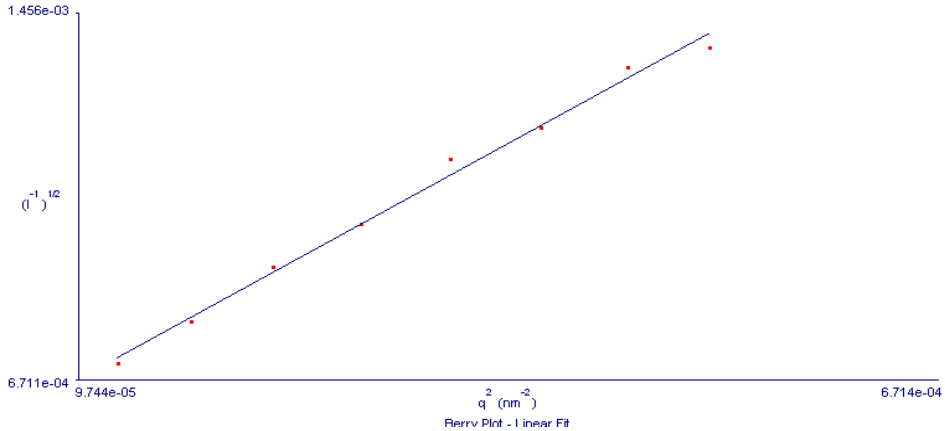

Figure B. 51: SLS results for 0.1 wt% PPO-b-PMAA in 15.48 mM α-CD at 50 °C.

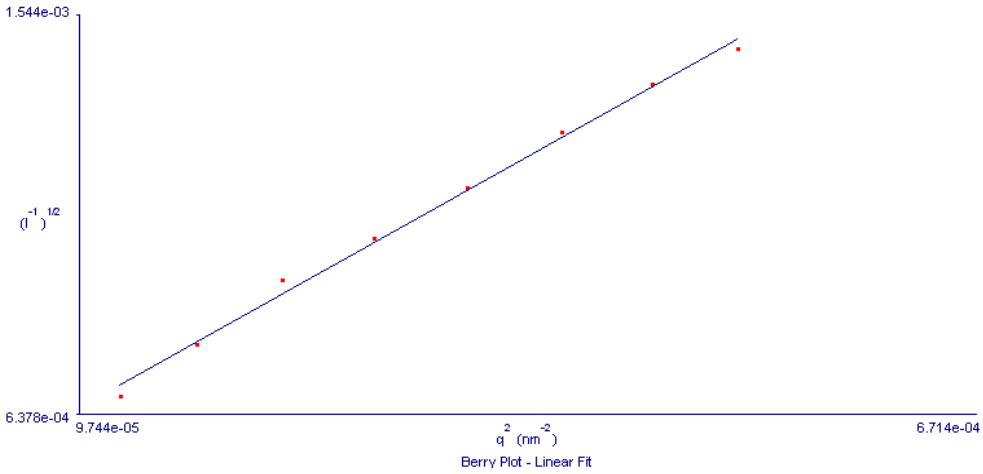

Figure B. 52: SLS results for 0.1 wt% PPO-b-PMAA in 15.48 mM α-CD at 60 °C.

Bibliography

Chapter 2

1. F. J. Xu, J. Li, S. J. Yuan, Z. X. Zhang, E. T. Kang and K. G. Neoh, *Biomacromolecules,* 2008, **9**, 331-339.
2. D. E. Meyer, B. C. Shin, G. A. Kong, M. W. Dewhirst and A. Chilkoti, *Journal of Controlled Release,* 2001, **74**, 213-224.
3. X. Z. Zhang, D. Q. Wu and C. C. Chu, *Biomaterials,* 2004, **25**, 3793-3805.
4. J. E. Chung, M. Yokoyama, M. Yamato, T. Aoyagi, Y. Sakurai and T. Okano, *Journal of Controlled Release,* 1999, **62**, 115-127.
5. A. Chilkoti, M. R. Dreher, D. E. Meyer and D. Raucher, *Advanced Drug Delivery Reviews,* 2002, **54**, 613-630.
6. D. Schmaljohann, *Advanced Drug Delivery Reviews,* 2006, **58**, 1655-1670.
7. N. Shamim, L. Hong, K. Hidajat and M. S. Uddin, *Separation and Purification Technology,* 2007, **53**, 164-170.
8. F. J. M. Hoeben, P. Jonkheijm, E. W. Meijer and A. Schenning, *Chemical Reviews,* 2005, **105**, 1491-1546.
9. D. S. Lawrence, T. Jiang and M. Levett, *Chemical Reviews,* 1995, **95**, 2229-2260.
10. S. Yagai and A. Kitamura, *Chemical Society Reviews,* 2008, **37**, 1520-1529.
11. L. Brunsveld, B. J. B. Folmer, E. W. Meijer and R. P. Sijbesma, *Chemical Reviews,* 2001, **101**, 4071-4097.

12. Y. Liu, D. Y. Zhao, R. J. Ma, D. A. Xiong, Y. L. An and L. Q. Shi, *Polymer*, 2009, **50**, 855-859.

13. P. J. Zheng, X. Hu, X. Y. Zhao, L. Li, K. C. Tam and L. H. Gan, *Macromolecular Rapid Communications*, 2004, **25**, 678-682.

14. X. Y. Chen, B. Gao, J. Kops and W. Batsberg, *Polymer*, 1998, **39**, 911-915.

15. R. L. Xu, M. A. Winnik, F. R. Hallett, G. Riess and M. D. Croucher, *Macromolecules*, 1991, **24**, 87-93.

16. C. L. Zhao, M. A. Winnik, G. Riess and M. D. Croucher, *Langmuir*, 1990, **6**, 514-516.

17. K. Yu and A. Eisenberg, *Macromolecules*, 1998, **31**, 3509-3518.

18. A. V. Kabanov, T. K. Bronich, V. A. Kabanov, K. Yu and A. Eisenberg, *Macromolecules*, 1996, **29**, 6797-6802.

19. S. Dai, P. Ravi, C. Y. Leong, K. C. Tam and L. H. Gan, *Langmuir*, 2004, **20**, 1597-1604.

20. H. W. Park, H. S. Jin, S. Y. Yang and J. D. Kim, *Colloid and Polymer Science*, 2009, **287**, 919-926.

21. A. Suzuki and T. Tanaka, *Nature*, 1990, **346**, 345-347.

22. T. Tanaka, I. Nishio, S. T. Sun and S. Uenonishio, *Science*, 1982, **218**, 467-469.

23. S. Katayama, Y. Hirokawa and T. Tanaka, *Macromolecules*, 1984, **17**, 2641-2643.

24. P. Alexandridis and T. A. Hatton, *Colloids and Surfaces a-Physicochemical and Engineering Aspects*, 1995, **96**, 1-46.

25. T. Tanaka, E. Sato, Y. Hirokawa, S. Hirotsu and J. Peetermans, *Physical Review Letters*, 1985, **55**, 2455-2458.

26. R. Yoshida, K. Uchida, Y. Kaneko, K. Sakai, A. Kikuchi, Y. Sakurai and T. Okano, *Nature*, 1995, **374**, 240-242.

27. S. Juodkazis, N. Mukai, R. Wakaki, A. Yamaguchi, S. Matsuo and H. Misawa, *Nature*, 2000, **408**, 178-181.

28. H. G. Schild, *Progress in Polymer Science*, 1992, **17**, 163-249.

29. M. Arotcarena, B. Heise, S. Ishaya and A. Laschewsky, *Journal of the American Chemical Society*, 2002, **124**, 3787-3793.

30. A. S. Hoffman and A. Afrassiabi, *Abstracts of Papers of the American Chemical Society*, 1986, **191**, 204-POLY.

31. A. Afrassiabi, A. S. Hoffman and L. A. Cadwell, *Journal of Membrane Science*, 1987, **33**, 191-200.

32. Y. H. Bae, T. Okano and S. W. Kim, *Journal of Polymer Science Part B-Polymer Physics*, 1990, **28**, 923-936.

33. R. Yoshida, K. Sakai, T. Okano and Y. Sakurai, *Journal of Biomaterials Science-Polymer Edition*, 1994, **6**, 585-598.

34. X. Zhu, J. DeGraaf, F. M. Winnik and D. Leckband, *Langmuir*, 2004, **20**, 10648-10656.

35. T. Serizawa, K. Wakita and M. Akashi, *Macromolecules*, 2002, **35**, 10-12.

36. J. Kopecek, *European Journal of Pharmaceutical Sciences*, 2003, **20**, 1-16.

37. J. Raula, J. Shan, M. Nuopponen, A. Niskanen, H. Jiang, E. I. Kauppinen and H. Tenhu, *Langmuir*, 2003, **19**, 3499-3504.

38. J. Shan, M. Nuopponen, H. Jiang, E. Kauppinen and H. Tenhu, *Macromolecules*, 2003, **36**, 4526-4533.

39. M. Q. Zhu, L. Q. Wang, G. J. Exarhos and A. D. Q. Li, *Journal of the American Chemical Society*, 2004, **126**, 2656-2657.

40. L. Ying, W. H. Yu, E. T. Kang and K. G. Neoh, *Langmuir*, 2004, **20**, 6032-6040.

41. N. Malmstadt, A. S. Hoffman and P. S. Stayton, *Lab on a Chip*, 2004, **4**, 412-415.

42. D. Bontempo, R. C. Li, T. Ly, C. E. Brubaker and H. D. Maynard, *Chemical Communications*, 2005, , 4702-4704.

43. T. Terada, T. Inaba, H. Kitano, Y. Maeda and N. Tsukida, *Macromolecular Chemistry and Physics*, 1994, **195**, 3261-3270.

44. H. Kitano, T. Hirabayashi, M. Gemmei-Ide and M. Kyogoku, *Macromolecular Chemistry and Physics*, 2004, **205**, 1651-1659.

45. G. H. Chen and A. S. Hoffman, *Nature*, 1995, **373**, 49-52.

46. R. F. S. Freitas and E. L. Cussler, *Chemical Engineering Science*, 1987, **42**, 97-103.

47. S. J. Im, Y. M. Choi, E. Subrarnanyarn, K. M. Huh and K. Park, *Macromolecular Research*, 2007, **15**, 363-369.

48. X. S. Wu, A. S. Hoffman and P. Yager, *Journal of Polymer Science Part a-Polymer Chemistry*, 1992, **30**, 2121-2129.

49. Y. H. Bae, T. Okano and S. W. Kim, *Journal of Controlled Release*, 1989, **9**, 271-279.

50. T. Okano, *Advances in Polymer Science*, 1993, **110**, 179-197.

51. H. Kawaguchi, *Progress in Polymer Science*, 2000, **25**, 1171-1210.

52. L. C. Dong and A. S. Hoffman, *Journal of Controlled Release*, 1991, **15**, 141-152.

53. P. Gupta, K. Vermani and S. Garg, *Drug Discovery Today*, 2002, **7**, 569-579.

54. T. Okano, Y. H. Bae, H. Jacobs and S. W. Kim, *Journal of Controlled Release*, 1990, **11**, 255-265.

55. A. Kikuchi and T. Okano, *Advanced Drug Delivery Reviews*, 2002, **54**, 53-77.

56. J. Zhang and N. A. Peppas, *Macromolecules*, 2000, **33**, 102-107.

57. E. J. Kim, S. H. Cho and S. H. Yuk, *Biomaterials*, 2001, **22**, 2495-2499.

58. Y. Y. Liu, X. D. Fan, H. Hu and Z. H. Tang, *Macromolecular Bioscience*, 2004, **4**, 729-736.

59. Y. Y. Liu and X. D. Fan, *Journal of Applied Polymer Science*, 2003, **89**, 361-367.

60. Y. Y. Liu, X. D. Fan and Q. Zhao, *Journal of Macromolecular Science-Pure and Applied Chemistry*, 2003, **A40**, 1095-1105.

61. Y. Y. Liu, X. D. Fan and L. Gao, *Macromolecular Bioscience*, 2003, **3**, 715-719.

62. A. S. Mathews, C. S. Ha, W. J. Cho and I. Kim, *Drug Delivery*, 2006, **13**, 245-251.

63. Y. K. Son, J. H. Kim, Y. S. Jeon and D. J. Chung, *Macromolecular Research*, 2007, **15**, 527-532.

64. N. Monji and A. S. Hoffman, *Applied Biochemistry and Biotechnology*, 1987, **14**, 107-120.

65. S. H. Qin, Y. Geng, D. E. Discher and S. Yang, *Advanced Materials*, 2006, **18**, 2905-+.

66. X. Li, J. Li and K. W. Leong, *Macromolecules*, 2003, **36**, 1209-1214.

67. G. Wenz, *Angewandte Chemie-International Edition in English*, 1994, **33**, 803-822.

68. C. C. Rusa, T. A. Bullions, J. Fox, F. E. Porbeni, X. W. Wang and A. E. Tonelli, *Langmuir*, 2002, **18**, 10016-10023.

69. L. H. He, J. Huang, Y. M. Chen and L. P. Liu, *Macromolecules*, 2005, **38**, 3351-3355.

70. A. Harada, J. Li and M. Kamachi, *Nature*, 1994, **370**, 126-128.

71. M. Ceccato, P. LoNostro and P. Baglioni, *Langmuir*, 1997, **13**, 2436-2439.

72. S. Loethen, J. M. Kim and D. H. Thompson, *Polymer Reviews*, 2007, **47**, 383-418.

73. J. Szejtli, 2004, **76**, 1825-1845.

74. J. Jeromin and H. Ritter, *Macromolecules*, 1999, **32**, 5236-5239.

75. J. Jeromin, O. Noll and H. Ritter, *Macromolecular Chemistry and Physics*, 1998, **199**, 2641-2645.

76. J. Jeromin and H. Ritter, *Macromolecular Rapid Communications*, 1998, **19**, 377-379.

77. K. Takahashi, *Chemical Reviews*, 1998, **98**, 2013-2033.

78. B. Martel and M. Morcellet, *European Polymer Journal*, 1995, **31**, 1089-1093.

79. K. Uekama, F. Hirayama and T. Irie, *Chemical Reviews*, 1998, **98**, 2045-2076.

80. G. Fundueanu, M. Constantin, D. Mihai, F. Bortolotti, R. Cortesi, P. Ascenzi and E. Menegatti, *Journal of Chromatography B-Analytical Technologies in the Biomedical and Life Sciences*, 2003, **791**, 407-419.

81. J. H. Guo and K. M. Cooklock, *Drug Development and Industrial Pharmacy*, 1995, **21**, 2013-2019.

82. F. Quaglia, G. Varricchio, A. Miro, M. I. La Rotonda, D. Larobina and G. Mensitieri, *Journal of Controlled Release*, 2001, **71**, 329-337.

83. V. J. Stella and R. A. Rajewski, *Pharmaceutical Research*, 1997, **14**, 556-567.

84. D. C. Bibby, N. M. Davies and I. G. Tucker, *International Journal of Pharmaceutics*, 2000, **197**, 1-11.

85. J. Szejtli, *Carbohydrate Polymers*, 1990, **12**, 375-392.

86. M. C. T. Fyfe and J. F. Stoddart, *Accounts of Chemical Research,* 1997, **30**, 393-401.

87. M. M. Conn and J. Rebek, *Chemical Reviews,* 1997, **97**, 1647-1668.

88. J. Szejtli, *Chemical Reviews,* 1998, **98**, 1743-1753.

89. R. Orprecio and C. H. Evans, *Journal of Applied Polymer Science,* 2003, **90**, 2103-2110.

90. D. Plackett, A. Ghanbari-Siahkali and L. Szente, *Journal of Applied Polymer Science,* 2007, **105**, 2850-2857.

91. D. V. Plackett, V. K. Holm, P. Johansen, S. Ndoni, P. V. Nielsen, T. Sipilainen-Malm, A. Sodergard and S. Verstichel, *Packaging Technology and Science,* 2006, **19**, 1-24.

92. R. Li, Z. T. Jiang and R. X. Wang, *Food Analytical Methods,* 2009, **2**, 264-270.

93. S. Fanali and E. Camera, *Journal of Chromatography A,* 1996, **745**, 17-23.

94. Z. Aturki, E. Camera, F. LaTorre and S. Fanali, *Journal of Capillary Electrophoresis,* 1995, **2**, 213-217.

95. S. Fanali, *Journal of Chromatography A,* 1996, **735**, 77-121.

96. S. Fanali and E. Camera, *Chromatographia,* 1996, **43**, 247-253.

97. Y. Xiao, T. T. Ong, T. T. Y. Tan and S. C. Ng, *Journal of Chromatography A,* 2009, **1216**, 994-999.

98. T. T. Ong, W. Tang, W. Muderawan, S. C. Ng and H. S. O. Chan, *Electrophoresis,* 2005, **26**, 3839-3848.

99. A. Lopedota, A. Trapani, A. Cutrignelli, V. Laquintana, N. Denora, M. Franco, G. Trapani and G. Liso, *Journal of Inclusion Phenomena and Macrocyclic Chemistry,* 2007, **57**, 425-432.

100. C. W. Lee, Z. Z. Yuan, Y. B. Kim and S. H. Lee, *Macromolecular Chemistry and Physics*, 2003, **204**, 1989-1993.

101. W. Herrmann, B. Keller and G. Wenz, *Macromolecules,* 1997, **30**, 4966-4972.

102. G. Wenz and B. Keller, *Angewandte Chemie-International Edition in English*, 1992, **31**, 197-199.

103. J. Li, X. P. Ni, Z. H. Zhou and K. W. Leong, *Journal of the American Chemical Society*, 2003, **125**, 1788-1795.

104. H. S. Choi, T. Ooya, S. Sasaki and N. Yui, *Macromolecules*, 2003, **36**, 5342-5347.

105. J. Li, X. Li, K. C. Toh, X. P. Ni, Z. H. Zhou and K. W. Leong, *Macromolecules*, 2001, **34**, 8829-8831.

106. H. Fujita, T. Ooya and N. Yui, *Macromolecules*, 1999, **32**, 2534-2541.

107. T. Ikeda, N. Watabe, T. Ooya and N. Yui, *Macromolecular Chemistry and Physics*, 2001, **202**, 1338-1344.

108. A. Harada, J. Li and M. Kamachi, *Nature*, 1992, **356**, 325-327.

109. A. Harada, J. Li and M. Kamachi, *Journal of the American Chemical Society*, 1994, **116**, 3192-3196.

110. A. Harada, J. Li and M. Kamachi, *Macromolecules,* 1993, **26**, 5698-5703.

111. A. Harada, M. Okada, J. Li and M. Kamachi, *Macromolecules*, 1995, **28**, 8406-8411.

112. A. Harada, T. Nishiyama, Y. Kawaguchi, M. Okada and M. Kamachi, *Macromolecules,* 1997, **30**, 7115-7118.

113. A. Harada and M. Kamachi, *Macromolecules*, 1990, **23**, 2821-2823.

114. J. Huang, L. X. Ren, H. Zhu and Y. M. Chen, *Macromolecular Chemistry and Physics*, 2006, **207**, 1764-1772.

115. H. W. Gibson and H. Marand, *Advanced Materials*, 1993, **5**, 11-21.

116. O. Kornysova, R. Surna, V. Snitka, U. Pyell and A. Maruska, *Journal of Chromatography A*, 2002, **971**, 225-235.

117. M. J. Blanco, M. C. Jimenez, J. C. Chambron, V. Heitz, M. Linke and J. P. Sauvage, *Chemical Society Reviews*, 1999, **28**, 293-305.

118. M. Weickenmeier, G. Wenz and J. Huff, *Macromolecular Rapid Communications*, 1997, **18**, 1117-1123.

119. C. Amiel and B. Sebille, *Advances in Colloid and Interface Science*, 1999, **79**, 105-122.

120. N. M. Gosselet, F. Beucler, E. Renard, C. Amiel and B. Sebille, *Colloids and Surfaces a-Physicochemical and Engineering Aspects*, 1999, **155**, 177-188.

121. K. Akiyoshi, Y. Sasaki, K. Kuroda and J. Sunamoto, *Chemistry Letters*, 1998, , 93-94.

122. H. S. Zhang, T. E. Hogen-Esch, F. Boschet and A. Margaillan, *Langmuir*, 1998, **14**, 4972-4977.

123. L. Karlson, K. Thuresson and B. Lindman, *Carbohydrate Polymers*, 2002, **50**, 219-226.

124. M. Tsianou and P. Alexandridis, *Langmuir*, 1999, **15**, 8105-8112.

125. A. Hashidzume, I. Tomatsu and A. Harada, *Polymer*, 2006, **47**, 6011-6027.

126. H. Bu, S. N. Naess, N. Beheshti, K. Z. Zhu, K. D. Knudsen, A. L. Kjoniksen, A. Elgsaeter and B. Nystrom, *Langmuir*, 2006, **22**, 9023-9029.

127. V. Burckbuchler, A. L. Kjoniksen, C. Galant, R. Lund, C. Amiel, K. D. Knudsen and B. Nystrom, *Biomacromolecules*, 2006, **7**, 1871-1878.

128. C. Galant, A. L. Kjoniksen, G. T. M. Nguyen, K. D. Knudsen and B. Nystrom, *Journal of Physical Chemistry B*, 2006, **110**, 190-195.

129. N. Beheshti, H. Bu, K. Z. Zhu, A. L. Kjoniksen, K. D. Knudsen, R. Pamies, J. G. H. Cifre, de la Torre, J. G. and B. Nystrom, *Journal of Physical Chemistry B*, 2006, **110**, 6601-6608.

130. A. L. Kjoniksen, C. Galant, K. D. Knudsen, G. T. M. Nguyen and B. Nystrom, *Biomacromolecules*, 2005, **6**, 3129-3136.

131. X. H. Guo, A. A. Abdala, B. L. May, S. F. Lincoln, S. A. Khan and R. K. Prud'homme, *Macromolecules*, 2005, **38**, 3037-3040.

132. J. Li, X. P. Ni and K. Leong, *Angewandte Chemie-International Edition*, 2003, **42**, 69-72.

133. K. M. Huh, T. Ooya, W. K. Lee, S. Sasaki, I. C. Kwon, S. Y. Jeong and N. Yui, *Macromolecules*, 2001, **34**, 8657-8662.

134. H. S. Choi, K. Kontani, K. M. Huh, S. Sasaki, T. Ooya, W. K. Lee and N. Yui, *Macromolecular Bioscience*, 2002, **2**, 298-303.

135. A. Harada, J. Li and M. Kamachi, *Nature*, 1993, **364**, 516-518.

136. Y. Okumura and K. Ito, *Advanced Materials*, 2001, **13**, 485-+.

137. S. R. McAlpine and M. A. Garcia-Garibay, *Journal of the American Chemical Society*, 1998, **120**, 4269-4275.

138. R. C. Petter, J. S. Salek, C. T. Sikorski, G. Kumaravel and F. T. Lin, *Journal of the American Chemical Society*, 1990, **112**, 3860-3868.

139. C. W. Tu, S. W. Kuo and F. C. Chang, *Polymer*, 2009, **50**, 2958-2966.

140. M. Hamcerencu, J. Desbrieres, M. Popa and G. Riess, *Biomacromolecules*, 2009, **10**, 1911-1922.

141. L. Moine, C. Amiel, W. Brown and P. Guerin, *Polymer International*, 2001, **50**, 663-676.

142. H. S. Choi, T. Ooya, S. C. Lee, S. Sasaki, M. Kurisawa, H. Uyama and N. Yui, *Macromolecules*, 2004, **37**, 6705-6710.

143. M. Becuwe, F. Cazier, M. Bria, P. Woisel and F. Delattre, *Tetrahedron Letters*, 2007, **48**, 6186-6188.

144. G. Wenz, E. Vonderbey and L. Schmidt, *Angewandte Chemie-International Edition in English*, 1992, **31**, 783-785.

145. Y. K. Joung, T. Ooya, M. Yamaguchi and N. Yui, *Advanced Materials*, 2007, **19**, 396-+.

146. H. S. Choi, S. C. Lee, K. Yamamoto and N. Yui, *Macromolecules*, 2005, **38**, 9878-9881.

147. S. C. Lee, H. S. Choi, T. Ooya and N. Yui, *Macromolecules*, 2004, **37**, 7464-7468.

148. Y. K. Joung, H. S. Choi, T. Ooya and N. Yui, *Journal of Inclusion Phenomena and Macrocyclic Chemistry*, 2007, **57**, 323-328.

149. K. Karaky, C. Brochon, G. Schlatter and G. Hadziioannou, Soft Matter, 2008, **4**, 1165-1168.

150. Y. Y. Liu, X. D. Fan, T. Kang and L. Sun, *Macromolecular Rapid Communications*, 2004, **25**, 1912-1916.

151. R. Auzely-Velty and M. Rinaudo, *Macromolecules*, 2002, **35**, 7955-7962.

152. A. Hashidzume, F. Ito, I. Tomatsu and A. Harada, *Macromolecular Rapid Communications*, 2005, **26**, 1151-1154.

153. Y. Takashima, T. Nakayama, M. Miyauchi, Y. Kawaguchi, H. Yamaguchi and A. Harada, *Chemistry Letters*, 2004, **33**, 890-891.

154. G. Volet and C. Amiel, *European Polymer Journal*, 2009, **45**, 852-862.

155. J. H. Liu, H. R. Sondjaja and K. C. Tam, *Langmuir*, 2007, **23**, 5106-5109.

156. K. M. Huh, T. Ooya, S. Sasaki and N. Yui, *Macromolecules*, 2001, **34**, 2402-2404.

157. K. M. Huh, H. Tomita, T. Ooya, W. K. Lee, S. Sasaki and N. Yui, *Macromolecules*, 2002, **35**, 3775-3777.

158. H. S. Choi, K. M. Huh, T. Ooya and N. Yui, *Journal of Physical Chemistry B*, 2004, **108**, 7646-7650.

159. de Melo, J. S. S., T. Costa, N. Oliveira and K. Schillen, *Polymer International*, 2007, **56**, 882-899.

160. S. Berto, M. C. Bruzzoniti, R. Cavalli, D. Perrachon, E. Prenesti, C. Sarzanini, F. Trotta and W. Tumiatti, *Journal of Inclusion Phenomena and Macrocyclic Chemistry*, 2007, **57**, 631-636.

161. L. M. Landoll, *Journal of Polymer Science Part a-Polymer Chemistry*, 1982, **20**, 443-455.

162. B. Magny, F. Lafuma and I. Iliopoulos, *Polymer*, 1992, **33**, 3151-3154.

163. R. Armat, S. G. Bike, G. B. Chu and F. N. Jones, *Journal of Applied Polymer Science*, 1996, **60**, 1927-1938.

164. K. D. Branham, H. S. Snowden and C. L. McCormick, *Macromolecules*, 1996, **29**, 254-262.

165. Y. Y. Liu and X. D. Fan, *Polymer*, 2002, **43**, 4997-5003.

166. D. S. Liao, S. Dai and K. C. Tam, *Journal of Rheology*, 2009, **53**, 293-308.

167. M. Weickenmeier and G. Wenz, *Macromolecular Rapid Communications*, 1997, **18**, 1109-1115.

168. T. Nozaki, Y. Maeda, K. Ito and H. Kitano, *Macromolecules*, 1995, **28**, 522-524.

169. T. Nozaki, Y. Maeda and H. Kitano, *Journal of Polymer Science Part a-Polymer Chemistry*, 1997, **35**, 1535-1541.

170. T. Hirasawa, Y. Maeda and H. Kitano, *Macromolecules*, 1998, **31**, 4480-4485.

171. H. Ritter, O. Sadowski and E. Tepper, *Angewandte Chemie-International Edition*, 2003, **42**, 3171-3173.

172. M. Yanagioka, H. Kurita, T. Yamaguchi and S. Nakao, *Industrial & Engineering Chemistry Research*, 2003, **42**, 380-385.

173. H. Ohashi, Y. Hiraoka and T. Yamaguchi, *Macromolecules*, 2006, **39**, 2614-2620.

174. M. Yang, L. Y. Chu, R. Xie and C. Wang, *Macromolecular Chemistry and Physics*, 2008, **209**, 204-211.

175. Q. Duan, Y. Miura, A. Narumi, X. Shen, S. Sato, T. Satoh and T. Kakuchi, *Journal of Polymer Science Part a-Polymer Chemistry*, 2006, **44**, 1117-1124.

176. J. Joseph, C. A. Dreiss, T. Cosgrove and J. S. Pedersen, *Langmuir*, 2007, **23**, 460-466.

177. R. Xie, S. B. Zhang, H. D. Wang, M. Yang, P. F. Li, X. L. Zhu and L. Y. Chu, *Journal of Membrane Science*, 2009, **326**, 618-626.

178. J. T. Zhang, S. W. Huang, F. Z. Gao and R. X. Zhuo, *Colloid and Polymer Science*, 2005, **283**, 461-464.

179. Q. F. Wang, S. M. Li, Z. Y. Wang, H. Z. Liu and C. J. Li, *Journal of Applied Polymer Science*, 2009, **111**, 1417-1425.

180. A. S. Mathews, W. J. Cho, I. Kim and C. S. Ha, *Journal of Applied Polymer Science*, 2009, **113**, 1680-1689.

181. S. Yagai, T. Karatsu and A. Kitamura, *Chemistry-a European Journal*, 2005, **11**, 4054-4063.

182. G. Pouliquen, C. Amiel and C. Tribet, *Journal of Physical Chemistry B*, 2007, **111**, 5587-5595.

183. G. Pouliquen and C. Tribet, *Macromolecules*, 2006, **39**, 373-383.

184. C. T. Lee, K. A. Smith and T. A. Hatton, *Macromolecules*, 2004, **37**, 5397-5405.

185. Q. C. Wang, D. H. Qu, J. Ren, K. C. Chen and H. Tian, *Angewandte Chemie-International Edition*, 2004, **43**, 2661-2665.

186. C. A. Stanier, S. J. Alderman, T. D. W. Claridge and H. L. Anderson, *Angewandte Chemie-International Edition*, 2002, **41**, 1769-+.

187. P. J. Zheng, C. Wang, X. Hu, K. C. Tam and L. Li, *Macromolecules*, 2005, **38**, 2859-2864.

188. I. Suzuki, K. Sato, M. Koga, Q. Chen and J. Anzai, *Materials Science & Engineering C-Biomimetic and Supramolecular Systems*, 2003, **23**, 579-583.

189. I. Tomatsu, A. Hashidzume and A. Harada, *Macromolecules*, 2005, **38**, 5223-5227.

190. I. Tomatsu, A. Hashidzume and A. Harada, *Journal of the American Chemical Society*, 2006, **128**, 2226-2227.

191. Y. Inoue, P. Kuad, Y. Okumura, Y. Takashima, H. Yamaguchi and A. Harada, *Journal of the American Chemical Society*, 2007, **129**, 6396-+.

192. L. H. Tong, Z. J. Hou, Y. Inoue and A. Tai, *Journal of the Chemical Society-Perkin Transactions 2*, 1992, , 1253-1257.

193. A. Harada, Y. Kawaguchi and T. Hoshino, 2001, **41**, 115-121.

194. A. Harada, M. Miyauchi and T. Hoshino, 2003, **41**, 3519-3523.

195. Y. Inoue, M. Miyauchi, H. Nakajima, Y. Takashima, H. Yamaguchi and A. Harada, *Macromolecules*, 2007, **40**, 3256-3262.

196. Y. Inoue, M. Miyauchi, H. Nakajima, Y. Takashima, H. Yamaguchi and A. Harada, *Journal of the American Chemical Society*, 2006, **128**, 8994-8995.

197. I. Tomatsu, A. Hashidzume and A. Harada, *Macromolecular Rapid Communications*, 2006, **27**, 238-241.

198. C. A. Nijhuis, J. Huskens and D. N. Reinhoudt, *Journal of the American Chemical Society*, 2004, **126**, 12266-12267.

199. C. A. Nijhuis, F. Yu, W. Knoll, J. Huskens and D. N. Reinhoudt, *Langmuir*, 2005, **21**, 7866-7876.

200. J. Huskens, A. Mulder, T. Auletta, C. A. Nijhuis, M. J. W. Ludden and D. N. Reinhoudt, *Journal of the American Chemical Society*, 2004, **126**, 6784-6797.

201. C. A. Nijhuis, J. K. Sinha, G. Wittstock, J. Huskens, B. J. Ravoo and D. N. Reinhoudt, *Langmuir*, 2006, **22**, 9770-9775.

202. R. Castro, I. Cuadrado, B. Alonso, C. M. Casado, M. Moran and A. E. Kaifer, *Journal of the American Chemical Society*, 1997, **119**, 5760-5761.

203. B. Gonzalez, C. M. Casado, B. Alonso, I. Cuadrado, M. Moran, Y. Wang and A. E. Kaifer, *Chemical Communications*, 1998, , 2569-2570.

204. A. Harada and S. Takahashi, *Journal of the Chemical Society-Chemical Communications*, 1984, , 645-646.

205. A. Harada, Y. Hu, S. Yamamoto and S. Takahashi, *Journal of the Chemical Society-Dalton Transactions*, 1988, , 729-732.

206. Y. Odagaki, K. Hirotsu, T. Higuchi, A. Harada and S. Takahashi, *Journal of the Chemical Society-Perkin Transactions 1*, 1990, , 1230-1231.

207. B. Gonzalez, I. Cuadrado, B. Alonso, C. M. Casado, M. Moran and A. E. Kaifer, *Organometallics*, 2002, **21**, 3544-3551.

208. A. Mirzoian and A. E. Kaifer, *Chemistry-a European Journal*, 1997, **3**, 1052-1058.

209. J. F. Bergamini, M. Jouini, S. Aeiyach, K. I. Chane-Ching, J. C. Lacroix, J. Tanguy and P. C. Lacaze, *Journal of Electroanalytical Chemistry*, 2005, **579**, 125-131.

210. T. Komura, T. Yamaguchi, K. Noda and S. Hayashi, *Electrochimica Acta*, 2002, **47**, 3315-3325.

211. R. Isnin, C. Salam and A. E. Kaifer, *Journal of Organic Chemistry*, 1991, **56**, 35-41.

212. A. E. Kaifer, *Accounts of Chemical Research*, 1999, **32**, 62-71.

213. T. Matsue, D. H. Evans, T. Osa and N. Kobayashi, *Journal of the American Chemical Society*, 1985, **107**, 3411-3417.

214. H. J. Thiem, M. Brandl and R. Breslow, *Journal of the American Chemical Society*, 1988, **110**, 8612-8616.

215. L. A. Godinez, S. Patel, C. M. Criss and A. E. Kaifer, *Journal of Physical Chemistry*, 1995, **99**, 17449-17455.

216. H. S. Choi, K. Yamamoto, T. Ooya and N. Yui, *Chemphyschem*, 2005, **6**, 1081-1086.

217. H. S. Choi, K. M. Huh, T. Ooya and N. Yui, *Journal of the American Chemical Society*, 2003, **125**, 6350-6351.

218. I. Dimitrov, B. Trzebicka, A. H. E. Muller, A. Dworak and C. B. Tsvetanov, *Progress in Polymer Science*, 2007, **32**, 1275-1343.

219. Y. Y. Liu, X. D. Fan and Y. B. Zhao, *Journal of Polymer Science Part a-Polymer Chemistry*, 2005, **43**, 3516-3524.

220. T. Maeda, M. Takenouchi, K. Yamamoto and T. Aoyagi, *Biomacromolecules*, 2006, **7**, 2230-2236.

221. M. W. J. Beulen, J. Bugler, M. R. de Jong, B. Lammerink, J. Huskens, H. Schonherr, G. J. Vancso, B. A. Boukamp, H. Wieder, A. Offenhauser, W. Knoll, F. van Veggel and D. N. Reinhoudt, *Chemistry-a European Journal*, 2000, **6**, 1176-1183.

222. J. Huskens, M. A. Deij and D. N. Reinhoudt, *Angewandte Chemie-International Edition*, 2002, **41**, 4467-+.

223. M. Kurisawa, M. Terano and N. Yui, *Journal of Biomaterials Science-Polymer Edition*, 1997, **8**, 691-708.

224. N. Yamamoto, M. Kurisawa and N. Yui, *Macromolecular Rapid Communications*, 1996, **17**, 313-318.

225. M. Miao, J. T. Cirulis, S. Lee and F. W. Keeley, *Biochemistry*, 2005, **44**, 14367-14375.

226. W. Kutner and K. Doblhofer, *Journal of Electroanalytical Chemistry*, 1992, **326**, 139-160.

227. C. H. Luo, F. Zuo, Z. H. Zheng, X. Cheng, X. B. Ding and Y. X. Peng, *Macromolecular Rapid Communications*, 2008, **29**, 149-154.

228. C. H. Luo, F. Zuo, Z. H. Zheng, X. B. Ding and Y. X. Peng, *Journal of Macromolecular Science Part a-Pure and Applied Chemistry*, 2008, **45**, 364-371.

229. X. C. Yin and H. D. H. Stover, *Macromolecules*, 2003, **36**, 9817-9822.

230. K. Yamamoto, T. Serizawa and M. Akashi, *Macromolecular Chemistry and Physics*, 2003, **204**, 1027-1033.

231. C. H. Luo, F. Zuo, X. B. Ding, Z. H. Zheng, X. Cheng and Y. X. Peng, *Journal of Applied Polymer Science*, 2008, **107**, 2118-2125.

232. D. Kungwatchakun and M. Irie, *Makromolekulare Chemie-Rapid Communications*, 1988, **9**, 243-246.

233. F. Zuo, C. Luo, X. Ding, Z. Zheng, X. Cheng and Y. Peng, *Supramolecular Chemistry*, 2008, **20**, 559-564.

Chapter 3

1. F. M. Winnik, A. R. Davidson, G. K. Hamer and H. Kitano, *Macromolecules,* 1992, **25**, 1876-1880.

2. X. P. Qiu and F. M. Winnik, *Macromolecules,* 2007, **40**, 872-878.

3. X. Lu, L. Zhang, L. Meng and Y. Liu, *Polymer Bulletin,* 2007, **59**, 195-206.

4. C. W. Tu, S. W. Kuo and F. C. Chang, *Polymer,* 2009, **50**, 2958-2966.

5. W. Q. Zhang, L. Q. Shi, K. Wu and Y. G. An, *Macromolecules,* 2005, **38**, 5743-5747.

6. J. S. Wang and K. Matyjaszewski, *Macromolecules*, **28**, 7901-7910.

7. J. Queffelec, S. G. Gaynor and K. Matyjaszewski, *Macromolecules,* 2000, **33**, 8629-8639.

8. A. M. L. Denadai, M. M. Santoro, A. V. Texeira and R. D. Sinisterra, *Materials Science & Engineering C-Materials for Biological Applications,* 2010, **30**, 417-422.

9. A. L. Nielsen, M. B. O. Andersen, T. V. Bugge, C. F. Nielsen, T. B. Nielsen, R. Wimmer, D. Yu and K. L. Larsen, *Journal of Polymer Science Part a-Polymer Chemistry,* 2009, **47**, 6619-6629.

10. H. Mwakibete, R. Cristantino, D. M. Bloor, E. Wynjones and J. F. Holzwarth, *Langmuir,* 1995, **11**, 57-60.

11. H. Q. Bao, L. Li, L. H. Gan and H. B. Zhang, *Macromolecules,* 2008, **41**, 9406-9412.

12. G. Y. Bai, V. Castro, M. Nichifor and M. Bastos, *Journal of Thermal Analysis and Calorimetry,* 2010, **100**, 413-422.

13. M. Fechner, S. Kosmella and J. Koetz, *Journal of Colloid and Interface Science,* 2010, **345**, 384-391.

14. T. Ikeda, W. K. Lee, T. Ooya and N. Yui, *Journal of Physical Chemistry B,* 2003, **107**, 14-19.

15. A. Arnaud and L. Bouteiller, *Langmuir,* 2004, **20**, 6858-6863.

16. P. J. Zheng, C. Wang, X. Hu, K. C. Tam and L. Li, *Macromolecules*, 2005, **38**, 2859-2864.

17. E. Turan, S. Demirci and T. Caykara, *Journal of Polymer Science Part B-Polymer Physics,* 2008, **46**, 1713-1724.

18. T. Hoare and R. Pelton, *Journal of Physical Chemistry B,* 2007, **111**, 1334-1342.

19. R. H. Lambeth, S. Ramakrishnan, R. Mueller, J. P. Poziemski, G. S. Miguel, L. J. Markoski, C. F. Zukoski and J. S. Moore, *Langmuir,* 2006, **22**, 6352-6360.

20. Q. S. Zhang, Y. C. Tang, L. S. Zha, J. H. Ma and B. R. Liang, *European Polymer Journal,* 2008, **44**, 1358-1367.

21. X. De Tang, X. C. Liang and N. F. Han, *Chinese Chemical Letters,* 2009, **20**, 1353-1356.

22. J. Shan, Y. M. Zhao, N. Granqvist and H. Tenhu, *Macromolecules,* 2009, **42**, 2696-2701.

23. B. H. Zimm, *Journal of Chemical Physics,* 1948, **16**, 1093-1099.

24. J. H. Liu, H. R. Sondjaja and K. C. Tam, *Langmuir,* 2007, **23**, 5106-5109.

25. P. Ravi, C. Wang, K. C. Tam and L. H. Gan, *Macromolecules,* 2003, **36**, 173-179.

Chapter 4

1. D. M. Vriezema, M. C. Aragones, J. Elemans, J. Cornelissen, A. E. Rowan and R. J. M. Nolte, *Chemical Reviews,* 2005, **105**, 1445-1489.

2. S. Dai, P. Ravi and K. C. Tam, *Soft Matter*, 2008, **4**, 435-449.

3. H. N. Yow and A. F. Routh, *Soft Matter*, 2006, **2**, 940-949.

4. P. L. Soo and A. Eisenberg, *Journal of Polymer Science Part B-Polymer Physics*, 2004, **42**, 923-938.

5. J. F. Tan, H. P. Too, T. A. Hatton and K. C. Tam, *Langmuir*, 2006, **22**, 3744-3750.

6. X. Y. Xiong, K. C. Tam and L. H. Gan, *Journal of Controlled Release*, 2005, **103**, 73-82.

7. O. C. Farokhzad and R. Langer, *Advanced Drug Delivery Reviews*, 2006, **58**, 1456-1459.

8. T. Betancourt and L. Brannon-Peppas, *International Journal of Nanomedicine*, 2006, **1**, 483-495.

9. L. Brannon-Peppas and J. O. Blanchette, *Advanced Drug Delivery Reviews*, 2004, **56**, 1649-1659.

10. R. Tong and J. J. Cheng, *Polymer Reviews*, 2007, **47**, 345-381.

11. D. E. Bergbreiter, B. L. Case, Y. S. Liu and J. W. Caraway, *Macromolecules*, 1998, **31**, 6053-6062.

12. A. Choucair and A. Eisenberg, *European Physical Journal E*, 2003, **10**, 37-44.

13. W. Q. Zhang, L. Q. Shi, K. Wu and Y. G. An, *Macromolecules*, 2005, **38**, 5743-5747.

14. N. Nishiyama and K. Kataoka, *Pharmacology & Therapeutics*, 2006, **112**, 630-648.

15. A. Lavasanifar, J. Samuel and G. S. Kwon, *Advanced Drug Delivery Reviews*, 2002, **54**, 169-190.

16. D. A. Chiappetta and A. Sosnik, *European Journal of Pharmaceutics and Biopharmaceutics*, 2007, **66**, 303-317.

17. X. Y. Xiong, K. C. Tam and L. H. Gan, *Journal of Nanoscience and Nanotechnology*, 2006, **6**, 2638-2650.

18. S. M. Moghimi and A. C. Hunter, *Trends in Biotechnology*, 2000, **18**, 412-420.

19. K. Nakashima and P. Bahadur, *Advances in Colloid and Interface Science*, 2006, **123**, 75-96.

20. A. Sinaga, T. A. Hatton and K. C. Tam, *Macromolecules*, 2007, **40**, 9064-9073.

21. X. Li, J. Li and K. W. Leong, *Macromolecules*, 2003, **36**, 1209-1214.

22. S. Dai and K. C. Tam, *Journal of Colloid and Interface Science*, 2005, **292**, 79-85.

23. Y. Liu, D. Y. Zhao, R. J. Ma, D. A. Xiong, Y. L. An and L. Q. Shi, *Polymer*, 2009, **50**, 855-859.

24. J. Jakes, *Czechoslovak Journal of Physics*, 1988, **38**, 1305-1316.

25. S. Dai, P. Ravi, K. C. Tam, B. W. Mao and L. H. Gan, *Langmuir*, 2003, **19**, 5175-5177.

Chapter 5

1. D. M. Vriezema, M. C. Aragones, J. Elemans, J. Cornelissen, A. E. Rowan and R. J. M. Nolte, *Chemical Reviews*, 2005, **105**, 1445-1489.

2. S. Dai, P. Ravi and K. C. Tam, *Soft Matter*, 2008, **4**, 435-449.

3. S. H. Qin, Y. Geng, D. E. Discher and S. Yang, *Advanced Materials*, 2006, **18**, 2905-+.

4. E. He, C. Y. Yue and K. C. Tam, *Journal of Pharmaceutical Sciences*, 2010, **99**, 782-793.

5. H. G. Schild and D. A. Tirell, *Journal of Physical Chemistry*, 1990, **94**, 4352.

6. X. Y. Xiong, K. C. Tam and L. H. Gan, *Journal of Nanoscience and Nanotechnology*, 2006, **6**, 2638-2650.

7. C. C. Tsai, W. B. Zhang, C. L. Wang, R. M. Van Horn, M. J. Graham, J. Huang, Y. Chen, M. Guo and Cheng S. Z. D., *Journal of Chemical Physics*, 2010, **132**, 204903.

8. P. Ravi, 2009, *Personal Communication* .

9. J. Y. Rao, Z. Y. Zhu and S. Y. Liu, *Chinese Sci Bull*, 2009, **54**, 1912-1917.

10. L. Leclercq, A. Pollet, M. Morcellet and B. Martel , *European Polymer Journal*, 1999, **35**, 185-193.

11. A. Compostizo, S. M. Cancho, R. G. Rubio and A. Crespo Colin, *Phys. Chem. Chem. Phys.*, 2001, **3**, 1861-1866.

12. J. Jakes, *Czechoslovak Journal of Physics*, 1988, 38, 1305-1316.